UNIVERSITY OF
LIVERPOOL

Low Emittance Tuning Studies for Future Linear Colliders: Design Issues and Practical Techniques

Thesis submitted in accordance with the requirements of
the University of Liverpool for the degree of Doctor in Philosophy

by

Kosmas Grigoriou Panagiotidis

September 2010

To my parents,
the strongest people I know

Abstract

This work is concerned with performance issues related to Linear Colliders, specifically the achievement and maintenance of very low emittance beams. The need for very high quality beams at a large scale calls for the use of special beam storage facilities called damping rings. The quality of a particle beam is characterised by the beam emittance and stability. In this thesis, we investigate the effectiveness of currently employed correction algorithms and their suitability particularly with regards to achieving vertical emittances of order 2 pm in the International Linear Collider (ILC) damping rings. The ILC is a project currently at the planning stage, that would complement the Large Hadron Collider (LHC), acting as a precision machine; it will be able to verify measurements from previously conducted experiments while at the same time shedding light on new physics. We also assess the possible value of novel modeling and tuning techniques, which are based on recent technological advances of the beam position monitors (BPMs).

'Ουδείς ασφαλέστερος εχθρός
του ευεργετηθέντος αχάριστου' [1]

Acknowledgments

Reaching the end of this academic endeavor, I feel obliged to thank all those people that helped me in numerous ways and made the journey as smooth as possible.

Markos Skoulatos and Prof. Christos Touramanis were the first people to introduce me to the physics community and for that I shall always be thankful. Prof. John Dainton and Prof. Neil Marks welcomed me to the (then) newly formed Cockcroft Institute and were very supportive through my very first steps in accelerator physics.

It has been an honour and privilege to work with Dr Andrzej Wolski, who supervised this work. His guidance, insightful comments and technical advise and expertise in the conducted research, have been invaluable as far as the completion of this project is concerned. I am deeply grateful for the countless hours we spent dealing with the idiosyncrasies of "Merlin" and for sharing his knowledge on subtle and difficult (for me anyway) issues of accelerator physics. Most importantly though, Andy has been extremely supportive, especially at times when the encountered difficulties seemed insurmountable.

Lei Zang, Yoel Giboudot, Larissa Malysheva, Antony Scarfe and all the people with whom I shared an office in the Cockcroft Institute deserve my deep appreciation for creating a great and intellectually stimulating working environment.

I wish to extend my warmest gratitude to the following people for making life much more interesting during my stay in Liverpool: Vasillis Ioakeimidis, Kostas Georgakopoulos, and Panagiotis Grammatikopoulos. I especially have to express my allegiance and appreciation to Dr Dimitris Tsovolos, my unofficial roommate and "comedy duo partner" for the last 3 years; he exhibited unusually high levels of tolerance, provided fine dining and

[1] Ancient greek saying loosely translated as "There is no enemy more certain than the benefited ungrateful".

occasionally replaced (literally) the punching bag during training sessions, at the expense of his health and safety.

I would also like to acknowledge the support of STFC, through a studentship provided via the Cockcroft Grant.

Last but not least, I salute all friends and family back home for keeping in touch: Apostolis "Lag" Kountrias, Christos "Mikros" Karaiskos, Christos "Mikros" Koutsarnakis, George "Drago" Dragogiannis, Ioannis "John-John" Panagiotopoulos, George "Sir" Pashos, Dimitris "Jake" Syrivelis and Kostas Aggelis.

Contents

List of Figures

Chapter 1

Introduction

The use of accelerators started, in a sense, with the exploration of the properties of cathode rays, which eventually led to the discovery of the electron by J.J. Thomson in 1897 [54]. The technology has advanced rapidly since then and has made possible the construction of ever more powerful accelerators, dedicated to unveiling the secrets of nature and increasing our knowledge of the physical world. At the same time, accelerator physics has been established as a distinct subject, discovering transverse and longitudinal beam focusing principles, leading to the invention of high power RF sources, characterising the beam dynamics encountered in such machines and eventually establishing beam manipulation schemes.

Currently, the development of accelerators is at a critical point. For reasons that will be explained shortly, the LEP collider at CERN may be the last circular e^+e^- collider built to operate at the energy frontier. The quest for even more powerful accelerators has therefore shifted the focus of research into linear colliders. In this chapter we present the reasons that support the construction of linear accelerators and discuss some of the challenges such designs will be faced with.

1.1 Motivation for Linear Colliders and Low Emittance Tuning

As the specified beam energy for an accelerator system increases, synchrotron radiation effects start to play a very significant role that eventually dictates the accelerator geometry. This becomes immediately apparent from the following equation relating the energy loss per turn for a single electron (or positron) to the beam energy and the radius of the storage ring:

$$\Delta E_{turn} \propto \frac{E^4}{\rho}. \tag{1.1}$$

The energy lost per turn will have to be replaced by the RF systems and this is a major running cost for the collider. Building a ring with a larger radius can decrease the energy loss and therefore the running costs, but the building costs (tunnel excavation, vacuum system, magnets) increase more or less linearly with the circumference. For these reasons, the LEP collider at CERN is generally considered as the last energy-frontier electron-positron storage ring collider, with a circumference of 27 km and an energy maximum of 209 GeV.

The concept of a linear collider dates back as far as 1965 [55] and it provides a more economically viable solution for colliders in the TeV range.

1.1.1 Luminosity

Along with the centre of mass energy, the luminosity of any collider is the critical quantity of interest from the physics point of view since it determines the rate of collisions per unit cross section. A high number of collisions is obviously desirable and it is this requirement that drives many of the design requirements for any collider.

For any collider the luminosity is given by:

$$\mathcal{L} = \frac{f_c N_b^2}{A}, \tag{1.2}$$

where f_c is the bunch collision frequency, N_b is the number of particles per bunch and A is the overlap area of collision at the IP.

For a linear collider with head-on collisions of beams with equal numbers

of particles per bunch the luminosity is given by the equation

$$\mathcal{L} = \frac{H_D N_b^2 f_{rep} n_b}{4\pi \sigma_x^* \sigma_y^*}, \tag{1.3}$$

where $f_c = n_b f_{rep}$ and n_b is the number of bunches per pulse and σ_x^*, σ_y^* are the effective beam sizes (i.e. the rms beam sizes at the IP). H_D is called the "pinch enhancement factor" and is used to take into account the self-focusing (pinch) of the intense beams during collisions (typical value of $\approx$2).

We should note that there are alternative expressions for the luminosity of head-on collisions depending on the bunch configuration of the beams and other validity conditions (e.g. different number of particles per bunch in each beam, different tune shift parameters ξ, etc.). Equation (1.3) is perhaps the most commonly quoted luminosity formula for a linear collider.

Usually, for most experiments, the figure of merit for a collider is the integrated luminosity and not the peak luminosity. To account for down-time, injection, beam lifetimes, etc., one experimental year is taken to be 10^7 s. For example, the expected integrated luminosity of a collider with peak luminosity of $\mathcal{L} = 10^{33}\,\mathrm{cm}^{-2}\mathrm{s}^{-1}$ would be $\mathcal{L}_{integrated} = 10^{40}\,\mathrm{cm}^{-2}$ or $10\,\mathrm{fb}^{-1}$ ($1\mathrm{b} \equiv 10^{-24}\,\mathrm{cm}^{-1}$).

1.1.2 The Need for Low Emittance Tuning (LET)

The average beam power is given by:

$$2P_{beam} = n_b N_b E_{cm} f_{rep}\,. \tag{1.4}$$

Therefore, in terms of power the luminosity equation can be rewritten as:

$$\mathcal{L} = \frac{1}{2\pi}\left(\frac{P_{beam}}{E_{cm}}\right)\left(\frac{N_b}{\sigma_x^*}\right)\left(\frac{1}{\sigma_y^*}\right) H_D\,. \tag{1.5}$$

Consequently, higher luminosity can always be achieved by increasing the beam power. However, this is not a viable option, since higher beam powers are generally constrained by electrical power availability as well as the additional costs and efforts associated with high intensity beams within the machine (machine protection, beam dumps). The availability of power is

further reduced by the RF to beam power conversion efficiency, $\eta_{RF\rightarrow beam}$:

$$P_{beam} = \eta_{RF\rightarrow beam} P_{RF} \,. \tag{1.6}$$

Since a linear collider is by definition a one-pass machine, it is bound to have a much lower collision rate than a storage ring. A large number of bunches per bunch train can recover some of the loss induced by the lower repetition rate but this again impacts negatively on the power consumption. To achieve the very high luminosities intended then in a linear collider, the transverse beam sizes must be significantly reduced. However such a reduction leads to extremely high charge densities of the colliding beams and beam-beam effects become significant:

- instability effects, leading to tighter collision tolerances on the beams;
- a high level of beamstrahlung radiation diluting the luminosity spectrum;
- production of copious quantities of e^+e^- pairs causing background noise in the detectors.

The very high electric fields generated by the beam interact with the opposing bunches causing the particles to deflect. As this deflection occurs, the particles radiate photons. This phenomenon is called **beamstrahlung** and is analogous to synchrotron radiation, although classical synchrotron radiation theory cannot be applied in this high beam intensity regime.

The amount of beamstrahlung radiation gives an indication of the dilution of the luminosity spectrum. The relative energy loss during collision due to beamstrahlung radiation is approximately given by [64]:

$$\delta_{BS} \approx 0.86 \frac{e r_e^3}{2 m_0 c^2} \left(\frac{E_{cm}}{\sigma_z} \right) \frac{N_b^2}{(\sigma_x + \sigma_y)^2} \,. \tag{1.7}$$

Equations (1.7) and (1.5) show that δ_{BS} is a function of the sum of the two beam sizes while luminosity is a function of the product of the two beam sizes. Obviously the goal is to minimize δ_{BS} while simultaneously maximizing the luminosity $\mathcal{L}$; therefore the standard strategy is to collide flat, ribbon-like beams with $\sigma_x \gg \sigma_y$. Then equation (1.7) becomes:

$$\delta_{BS} \approx 0.86 \frac{e r_e^3}{2 m_0 c^2} \left(\frac{E_{cm}}{\sigma_z} \right) \frac{N_b^2}{\sigma_x^2} \,, \tag{1.8}$$

so then the luminosity can increase independently of the beamstrahlung radiation, by making σ_y as small as possible. Combining equations (1.8) and (1.5) a scaling law correlating $\mathcal{L}$ and δ_{BS} can be restated:

$$\mathcal{L} \propto \frac{\eta P_{AC}}{E_{cm}^{3/2}} \frac{\sqrt{\delta_{BS}\sigma_z}}{\sigma_y} . \tag{1.9}$$

Furthermore, if the vertical beam size at the IP is expressed as:

$$\sigma_y = \sqrt{\frac{\beta_y \varepsilon_y}{\gamma}} ; \tag{1.10}$$

then equation (1.9) becomes:

$$\mathcal{L} \propto \frac{\eta P_{AC}}{E_{cm}} \sqrt{\frac{\delta_{BS}}{\varepsilon_y}} H_D . \tag{1.11}$$

Formula (1.11) reveals the fundamental linear collider parameters entering the luminosity scaling, (i.e. power conversion efficiency η, power P_{AC}, beamstrahlung energy loss δ_{BS} and vertical emittance ε_y) and justifies the need for low emittance tuning techniques.

1.2 Linear Collider Designs

Currently there are two international projects concerned with the design and development of linear colliders: the Compact Linear Collider (CLIC) [56, 9] and the International Linear Collider (ILC). There are significant differences in the design specifications between the two designs, however the need for high quality beams is equally important and the issues regarding low-emittance tuning are common. At the time this work began, the ILC design was more developed and therefore it was chosen as the design to use for investigating some of the generic problems related to low-emittance tuning.

1.3 Overview of the ILC

The ILC will collide electrons and positrons in bunches of 5.7 nm vertical size, 554 nm horizontal size, length 6 mm, containing 20 billion particles.

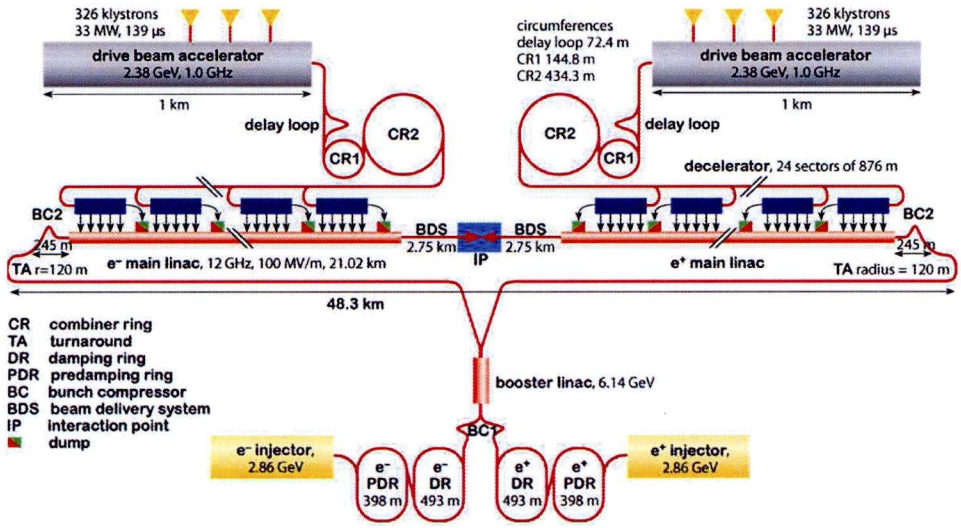

Figure 1.1: Schematic of CLIC layout.

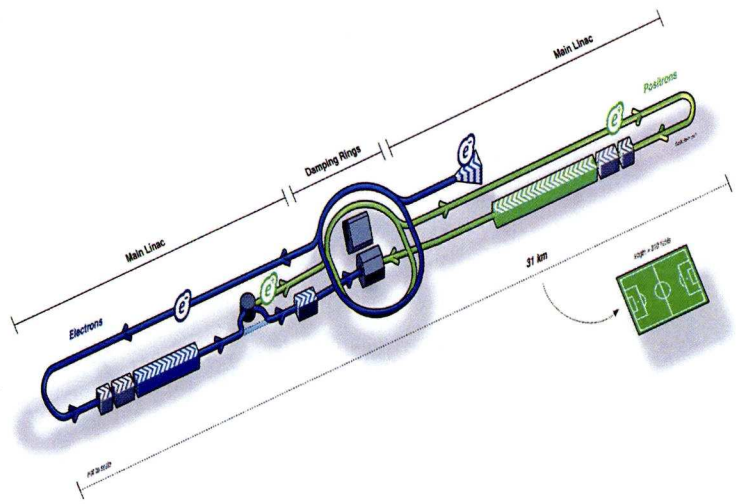

Figure 1.2: Schematic of ILC layout.

Site	To be determined
Peak Luminosity	$34 \times 10^{33}\,\mathrm{cm}^{-2}\mathrm{s}^{-1}$
Energy	Up to 500 GeV with an option to upgrade to 1 TeV
Length	Approximately 31 km
Accelerating Gradient	31.5 MV/m
Number of accelerating structures	16000

Table 1.1: Key ILC parameters [67].

The electron source for the ILC will use laser light pulses to generate electrons from a photocathode. Synchrotron radiation from high energy electrons passing through a helical undulator, interacting with a titanium-alloy wheel target, will then produce positrons; these positrons are collected and accelerated in a separate linac. The electron and positron bunches are then guided into their respective damping rings, where they are accelerated to 5 GeV. The two counter-rotating beams, after extraction from the damping rings, will be sent to the superconducting RF main linacs, each 12 km long, where they will be accelerated to 250 GeV before collision at the Interaction Point (figure 1.2).

Chapter 2

Beam Dynamics

Beam dynamics has been described as the interplay between charged particles and electromagnetic fields. This interplay is of critical importance for the design and operation of any accelerator system. The key problem addressed by beam dynamics is the accurate prediction of the behaviour of a beam of particles under the influence of external electromagnetic fields and electromagnetic fields generated within the bunches.

Although accelerator science and technology are by now well established scientific disciplines (the first accelerator in the form of a *cyclotron* was built in 1931), no single description of the dynamics has yet become standard. This can be quite confusing for the reader, especially in regards to the necessary assumptions that must be made when developing any given formalism and which should be made clear. On the other hand, different approaches are suitable for different problems.

In this chapter we aim to give a brief account of the developed theory of beam dynamics and in particular of those aspects of beam dynamics relevant to low-emittance tuning, neglecting collective effects. Key concepts are highlighted and put into context in relation to the required specifications for future accelerator systems and their design. This leads to an explanation of the research program of Low Emittance Tuning (LET).

2.1 Single Particle Motion

Real beams are collections of particles. Key concepts of beam dynamic theory though, have been developed through the treatment of single particle

motion in an accelerator system. Therefore, this distinction between single and multiple particle motion is necessary for a clearer understanding of the concepts and helps to avoid some common sources of confusion that usually plague relevant presentations of the theory.

Although the charged particles in a bunch will interact with each other, relativistic effects in high energy accelerators mean that a good understanding of beam behaviour can still be obtained by neglecting these interactions as long as the bunch charge is not too large.

In this section we present key beam dynamic concepts for single particle motion; this presentation involves different starting points and attempts to indicate the links between the different approaches.

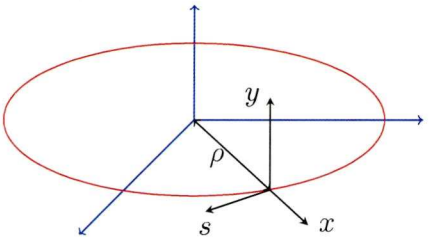

Figure 2.1: Reference system. x and y are collectively known as the transverse axes, individually named "horizontal" and "vertical", respectively; s is the longitudinal coordinate of the particle path while ρ is the bending radius.

2.1.1 Hill's Equation

The coordinate system we will use is shown in figure 2.1. The x and y axes of this coordinate system are collectively known as the transverse axes, individually named "horizontal" and "vertical", respectively; s is the longitudinal coordinate of the particle path while ρ is the bending radius. A certain arrangement of magnets ("optics") defines a trajectory ("orbit"). For the initial design conditions and without magnet errors, the particles move along the *reference trajectory*, indicated by the red circle.

Let us consider a particle passing through a magnetic field with gradient $\partial B_y/\partial x$ over a short distance Δs. The slope of the particle's transverse trajectory will then be altered by an amount:

$$\Delta x' = -\frac{\Delta s}{\rho} = -\Delta s \left(\frac{eB_y}{p}\right) = -\frac{q\Delta s}{p}\frac{\partial B_y}{\partial x}x\,, \tag{2.1}$$

where ρ is the radius of curvature of the trajectory through the magnetic field and $\partial B_y/\partial x$ is the gradient of the magnet.

In equation (2.1) we used the formula:

$$B\rho = \frac{p}{q}\,. \tag{2.2}$$

A particle of charge q moving in a uniform field B with momentum p follows a circular trajectory of radius ρ, given by equation (2.2). The quantity $B\rho$ is called the *beam rigidity* and is often used instead of p/q. The beam rigidity does not refer to a particular strength or radius of curvature of the trajectory and it is useful because it gives a more intuitive way of writing

many formulae without the use of the reference momentum.

The slope $x' = dx/ds$, changes by an amount $\Delta x' = -[\frac{\partial B_y}{\partial x}\Delta s/(B\rho)]x$. Rearranging terms we get

$$\frac{\Delta x'}{\Delta s} = -\frac{1}{B\rho}\frac{\partial B_y}{\partial x}x\,. \tag{2.3}$$

Taking the limit as $\Delta s \to 0$, we obtain a second order differential equation that describes the motion of the particle in the horizontal direction,

$$x'' + \frac{1}{B\rho}\frac{\partial B_y}{\partial x}x = 0 \quad . \tag{2.4}$$

Similarly, for the vertical direction, y, we get

$$y'' - \frac{1}{B\rho}\frac{\partial B_y}{\partial x}y = 0\,. \tag{2.5}$$

In this analysis it is useful to ignore the centripetal term that is inherent in a curvilinear coordinate system. For large accelerators, the centripetal term is usually small in comparison with the gradient term, though it must still be taken into account in the dipole (bending) magnets. Equations (2.4) and (2.5) are known as **Hill's equations**. [1]

2.1.1.1 Solution to Hill's Equation

For $K_y(s) = -[\frac{\partial B_y}{\partial x}/(B\rho)]$ equation (2.5) becomes

$$y'' + K_y(s)y = 0\,. \tag{2.6}$$

In a periodic beamline, with a length of one repeated unit (i.e. one period) and for constant K, we can use the following mathematical result and obtain the solution for equation (2.6)

$$y = \begin{cases} A\cos(\sqrt{K}s + \delta) & K < 0, \\ As + \delta & K = 0, \\ A\cosh(\sqrt{K}s + \delta) & K > 0. \end{cases}$$

[1] Actually, they are special cases of Hill's differential equation.

The integration constants A and δ can be determined by the initial values of y_0 and y'_0. Defining

$$\mathbf{y}(s) = \begin{pmatrix} y(s) \\ y'(s) \end{pmatrix}, \tag{2.7}$$

as the transverse motion state-vector, the solution of equation (2.6) is

$$\mathbf{y}(s) = M(s; s_0)\mathbf{y}(s_0), \tag{2.8}$$

where $M(s; s_0)$ is the transfer matrix. For a constant focusing function K the transfer matrix takes the following forms

$$M(s; s_0) = \begin{cases} \begin{pmatrix} \cos(\sqrt{K}\lambda) & \frac{1}{\sqrt{K}}\sin(\sqrt{K}\lambda) \\ -\sqrt{K}\sin(\sqrt{K}\lambda) & \cos(\sqrt{K}\lambda) \end{pmatrix} & K > 0\text{: vertically focusing quad} \\ \begin{pmatrix} 1 & \lambda \\ 0 & 1 \end{pmatrix} & K = 0\text{: drift space} \\ \begin{pmatrix} \cosh(\sqrt{|K|}\lambda) & \frac{1}{\sqrt{|K|}}\sinh(\sqrt{|K|}\lambda) \\ \sqrt{|K|}\sinh(\sqrt{|K|}\lambda) & \cosh(\sqrt{|K|}\lambda) \end{pmatrix} & K < 0\text{: vertically defocusing quad} \end{cases}$$

and $\lambda = s - s_0$. Following the same line of thought, a transfer matrix for a pure sector dipole [2] with $K_x = 1/\rho^2$ is

$$M_x = \begin{pmatrix} \cos(\theta) & \rho\sin(\theta) \\ -\frac{1}{\rho}\sin(\theta) & \cos(\theta) \end{pmatrix}, \tag{2.9}$$

where $\theta = \lambda/\rho$ is the orbiting angle and ρ is the bending radius.

Having transfer matrices that describe all elements along a length s in the beam line, it is possible to follow the motion of the particle along the length s. If a particle traverses a series of elements having transfer matrices $M_1, M_2, ..., M_n$ then the input and output coordinates of the particle through these elements are related by the matrix

$$M = M_n \cdot M_{n-1} \cdots M_2 \cdot M_1 . \tag{2.10}$$

[2] A sector dipole is one with perpendicular entrance and exit angles to the edge of the dipole field

2.1.1.2 Closed Form Solution and Courant-Snyder Parameterization

The solution of equation (2.6) can also be written in the the form

$$y = Aw(s)\cos[\psi(s) + \delta]\,, \tag{2.11}$$

where $\psi(s) = \sqrt{K}s$. If K is a periodic function of s, then it is possible, subject to certain other constraints, uniquely to determine a function $\omega(s)$ that is also periodic in s (with the same period K). $\psi(s)$ is a monotonically increasing function of s. When K is a periodic function of the longitudinal position s, the solution will differ from that of a simple harmonic oscillator by a factor representing a spatially varying amplitude, $w(s)$ in our case, and a phase which no longer develops linearly with s, $\psi(s)$.

To determine $w(s)$ and $\psi(s)$ we can substitute the general solution into equation (2.6). We then get

$$\begin{aligned} y'' + Ky &= A[2w'\psi' + w\psi'']\sin(\psi + \delta) + \\ &\quad A[w'' - w(\psi')^2 + Kw]\cos(\psi + \delta) = 0\,. \end{aligned} \tag{2.12}$$

Since both functions w and ψ are independent of δ, we will require that the coefficients of the sine and cosine terms individually vanish. Therefore we have

$$\begin{aligned} 2w'\psi' + w\psi'' = 0 \quad &\text{and} \\ w'' - w(\psi')^2 + Kw = 0\,. \end{aligned} \tag{2.13}$$

Now we can establish a relationship between w and ψ. Multiplying the first of equations 2.13 with w we can get the following transformation

$$2ww'\psi' + w^2\psi'' = (w^2\psi')' = 0\,, \tag{2.14}$$

which leads to

$$\psi' = \frac{k}{w^2}\,, \tag{2.15}$$

where k is an arbitrary constant of integration. Using this relationship between w and ψ, for the second of equations (2.13) we form the differential

equation that w must satisfy:

$$w^3(w'' + Kw) = k^2 \,. \tag{2.16}$$

Using a known trigonometric identity, we can rewrite equation (2.11) to take the following form:

$$y = w(s)[A_1 \cos(\psi) + A_2 \sin(\psi)] \,. \tag{2.17}$$

Consequently

$$y' = (A_1 w' + \frac{A_2 k}{w}) \cos(\psi) + (A_2 w' - \frac{A_1 k}{w}) \sin(\psi) \,. \tag{2.18}$$

For the initial conditions x_0, x_0' at $s = s_0$, the constants A_1 and A_2 are

$$A_1 = \frac{y_0}{w}, \qquad A_2 = \frac{y_0' w - x_0 w'}{w} \,. \tag{2.19}$$

Since we require that the function w is periodic over the distance L, the transfer matrix for the propagation of the beam from s_0 to $s_0 + L$ is of the form represented in the following matrix equation of motion

$$\begin{pmatrix} y \\ y' \end{pmatrix}_{s_0+L} =$$

$$= \begin{pmatrix} \cos(\Delta\psi_L) - \frac{ww'}{k} \sin(\Delta\psi_L) & \frac{w^2}{k} \sin(\Delta\psi_L) \\ -\frac{1+(ww'/k)^2}{w^2/k} \sin(\Delta\psi_L) & \cos(\Delta\psi_L) + \frac{ww'}{k} \sin(\Delta\psi_L) \end{pmatrix} \begin{pmatrix} y \\ y' \end{pmatrix}_{s_0} . \tag{2.20}$$

The phase of the particles's oscillation advances through the repetition period by

$$\psi(s_0 \rightarrow s_0 + L) \equiv \Delta\psi_L = \int_{s_0}^{s_0+L} \frac{k}{w^2} ds \,. \tag{2.21}$$

Observation of equation (2.20) reveals that the function $w^2(s)$ and its derivative both scale with the arbitrary constant k. Different values of k lead to different values of $w^2(s)$, scaled by a factor of k. The fundamental importance of w^2 and its derivative to the problem at hand, has led to the definition of a new set of variables, which are termed the **Courant-Snyder**

parameters:

$$\begin{aligned}\beta(s) &\equiv \frac{w^2(s)}{k},\\ \alpha(s) &\equiv -\frac{1}{2}\frac{d\beta(s)}{ds} = -\frac{1}{2}\frac{d}{ds}\left(\frac{w^2(s)}{k}\right),\\ \gamma(s) &\equiv \frac{1+\alpha^2(s)}{\beta}.\end{aligned} \tag{2.22}$$

The function β is also referred to as the amplitude function or beta-function. The previous matrix equation can now be rewritten as

$$\begin{pmatrix} y \\ y' \end{pmatrix}_{s_0+L} =$$

$$= \begin{pmatrix} \cos(\Delta\psi_L) + \alpha\sin(\Delta\psi_L) & \beta\sin(\Delta\psi_L) \\ -\gamma\sin(\Delta\psi_L) & \cos(\Delta\psi_L) - \alpha\sin(\Delta\psi_L) \end{pmatrix} \begin{pmatrix} y \\ y' \end{pmatrix}_{s_0}. \tag{2.23}$$

The phase advance can now be written as

$$\Delta\psi_L = \int_{s_0}^{s_0+L} \frac{ds}{\beta(s)}. \tag{2.24}$$

As well as indicating variations in the local amplitude, β gives the local wavelength of the oscillation (divided by 2π). For a circular machine, a very important concept can now be defined. The number of oscillations per turn,

$$\nu \equiv \frac{1}{2\pi}\oint \frac{ds}{\beta(s)}, \tag{2.25}$$

is called the tune of the accelerator. There exist different tunes for the horizontal and vertical direction. Longitudinally, the RF cavities provide focusing in a similar way that quadrupoles provide transverse focusing.

2.1.2 Hamiltonian Formalism

Hamiltonian mechanics provides a framework especially suited for the problems posed in accelerator physics. The development of mathematical techniques for such systems is especially helpful for accelerators since any deviations, due to nonlinear restoring forces, can be treated as perturbations of the harmonic oscillation.

There exists a function $H(x_i, p_i; t)$, called the Hamiltonian, that defines the dynamics of a system. Given the Hamiltonian, the equations of motion are derived in the the following manner:

$$\begin{aligned} \frac{dx_i}{dt} &= \frac{\partial H}{\partial p_i}, \\ \frac{dp_i}{dt} &= -\frac{\partial H}{\partial x_i}, \end{aligned} \tag{2.26}$$

where p_i are the momenta conjugate to the coordinates x_i. The conjugate momentum and the Hamiltonian depend on the Lagrangian L:

$$L = T - V, \tag{2.27}$$

where T is the kinetic energy and V is the potential energy of the system, and can be derived as follows:

$$p_i = \frac{\partial L}{\partial \dot{x}_i}, \tag{2.28}$$

$$H = \sum_i \dot{x}_i p_i - L, \tag{2.29}$$

with

$$\dot{x}_i = \frac{dx_i}{dt}. \tag{2.30}$$

For many cases the Hamiltonian can be expressed as the total energy of the system. In the simple case of a particle with one degree of freedom with kinetic energy T and potential energy V:

$$T = \frac{p_x^2}{2m} \qquad V = \frac{1}{2} m\omega^2 x^2, \tag{2.31}$$

where ω is a constant, the Hamiltonian would be written as:

$$H = T + V = \frac{p_x^2}{2m} + \frac{1}{2} m\omega^2 x^2. \tag{2.32}$$

It should be noted that in Hamiltonian mechanics the "state" of the system at any time is defined by specifying values for the coordinates x_i and the canonical momentum p_i, defined by equation (2.28). Using Hamilton's equations of motion (2.26) and the Hamiltonian (2.32), we get the equations

of motion:

$$\frac{dx}{dt} = \frac{p_x}{m}, \tag{2.33}$$

$$\frac{dp_x}{dt} = -m\omega^2 x\,. \tag{2.34}$$

If we consider the case of a particle of fixed mass, moving in one degree of freedom and subject to a force F given by:

$$F = -m\omega^2 x\,, \tag{2.35}$$

where ω is a constant,then, according to Newtonian mechanics, the equation of motion is given by:

$$\frac{d}{dt}m\dot{x} = F(x, \dot{x}; t)\,, \tag{2.36}$$

and therefore:

$$\begin{aligned} m\frac{d}{dt}\dot{x} &= -m\omega^2 x \\ \therefore \quad \frac{d^2x}{dt^2} &= -\omega^2 x\,. \end{aligned} \tag{2.37}$$

The solution to the latter equation is found to be:

$$x(t) = x_0 \sin(\omega t + \phi_0)\,. \tag{2.38}$$

The dynamics in this case is defined by the force F and given the function that describes F one can derive the equations of motion. H defines the dynamics in Hamiltonian mechanics in the same way that F defines the dynamics in Newtonian mechanics.

One important aspect of the Hamiltonian formalism is the fact that the equations of motion for a particular system can be easier to solve. For example, in Lagrangian Formalism the Euler-Lagrange equations will give n second-order differential equations, Hamilton's equations give $2n$ first-order differential equations. Avoiding the higher-order equations has certain advantages concerning linear methods, stability analysis, etc.

2.1.2.1 The Relativistic Hamiltonian

Einstein tells us that the equation relating the energy E and mechanical momentum p of a particle with rest mass m is:

$$E^2 = p^2c^2 + m^2c^4 \,. \tag{2.39}$$

The Hamiltonian can often take the form:

$$H = T + V \,, \tag{2.40}$$

where T is the kinetic energy and V is the potential energy, making the Hamiltonian the total energy of the system expressed in canonical variables. Using equation (2.39) the relativistic Hamiltonian, in the absence of an electromagnetic field, becomes:

$$H = \sqrt{p^2c^2 + m^2c^4} \,, \tag{2.41}$$

p now being the canonical momentum. Adding an electromagnetic field into the system with a potential energy of:

$$V = q\phi \,, \tag{2.42}$$

where ϕ is a scalar function of position and q is the particle's charge, the relativistic Hamiltonian becomes:

$$H = \sqrt{(\vec{p} - q\vec{A})^2c^2 + m^2c^4} + q\phi \,, \tag{2.43}$$

where $\vec{A}$ is the vector potential. From this Hamiltonian, Hamilton's first equation, (2.26), will give:

$$\frac{dx}{dt} = \frac{\partial H}{\partial p_x} = \frac{(p_x - qA_x)}{\sqrt{(\vec{p} - q\vec{A})^2 + m^2c^2}} \,. \tag{2.44}$$

Rearranging the last equation gives:

$$\begin{aligned} \vec{p} - q\vec{A} &= \vec{\beta}\gamma mc \\ \therefore \quad \vec{p} &= \vec{\beta}\gamma mc + q\vec{A} \,. \end{aligned} \tag{2.45}$$

Equation (2.45) gives the canonical momentum.

Hamilton's second equation, gives:

$$\begin{aligned}\frac{dp_x}{dt} &= -\frac{\partial H}{\partial x} = \frac{qc}{\sqrt{(\vec{p}-q\vec{A})^2+m^2c^2}} \times \\ &\left[(p_x - qA_x)\frac{\partial A_x}{\partial x} + (p_y - qA_y)\frac{\partial A_y}{\partial x} + (p_z - qA_z)\frac{\partial A_z}{\partial x}\right] \\ &-q\frac{\partial \phi}{\partial x}\,. \end{aligned} \tag{2.46}$$

If we use equation (2.45) then we get the more compact form

$$\frac{dp_x}{dt} = q\left(\dot{x}\frac{\partial A_x}{\partial x} + \dot{y}\frac{\partial A_y}{\partial x} + \dot{z}\frac{\partial A_z}{\partial x}\right) - q\frac{\partial \phi}{\partial x}\,. \tag{2.47}$$

Equation (2.47) can be rewritten, in the form:

$$\begin{aligned}\frac{d}{dt}(\vec{p}-q\vec{A}) &= q(\vec{E}+\vec{u}\times\vec{B}) \\ \therefore \quad \frac{d}{dt}\beta\gamma mc &= q(\vec{E}+\vec{u}\times\vec{B})\,, \end{aligned} \tag{2.48}$$

where $\vec{u} = (\dot{x}, \dot{y}, \dot{z})$. Equation (2.48) is equivalent to the Lorentz force equation:

$$\vec{F} = q(\vec{E}+\vec{u}\times\vec{B})\,. \tag{2.49}$$

All the components comprising an accelerator, such as the magnets, RF cavities and other components are at defined locations along the reference trajectory. As a result the longitudinal position of a particle arriving, for example, at a magnet is known but not necessarily the time at which it arrives. Therefore it is more convenient in accelerator physics to work with the path length s of the reference trajectory as the independent variable than the time t.

Such a change in the independent variable can be accommodated with recourse to the Principle of Least Action. The Euler-Lagrange equations define a path in a plot of $\dot{x}$ vs x for which the action S is minimum:

$$\delta S = \delta\left[\int_{t_0}^{t_1} L dt\right] = 0\,. \tag{2.50}$$

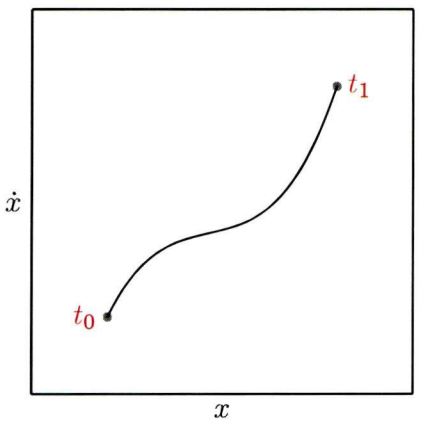

Figure 2.2: Path followed by a particle in phase-space between time t_0 and time t_1. The Euler-Lagrange equations define the path for which the action S is minimum.

In terms of the Hamiltonian this equation becomes:

$$S = \int_{t_0}^{t_1} (p_x \dot{x} + p_y \dot{y} + p_s \dot{s} - H) dt \,. \tag{2.51}$$

At this point we can choose our coordinates so that the s axis defines the reference trajectory. If we change the variable of integration from the time t to the path length s, the action becomes:

$$S = \int_{z_0}^{z_1} (p_x x' + p_y y' + p_s - H t') dz \,, \tag{2.52}$$

where the prime indicates derivatives with respect to s. A comparison between equations (2.51) and (2.52) indicates that in order to describe the Hamiltonian in terms of the path length s as the independent variable, the appropriate canonical variables are:

$$(x, p_x), \qquad (y, p_y) \qquad (-t, E) \,, \tag{2.53}$$

and also use for the Hamiltonian $H = -p_s$. Rearranging equation (2.43) and identifying the Hamiltonian with the energy E we can derive an expression

for p_s:

$$H = -p_s = -\sqrt{\frac{(E - q\phi)^2}{c^2} - m^2c^2 - (p_x - qA_x)^2 - (p_y - qA_y)^2} - qA_s \,. \tag{2.54}$$

It is very helpful to work with variables whose values remain small as the particle moves through the accelerator because one can make useful approximations. We therefore introduce the reference momentum P_0 which can be chosen freely but is usually given a value close to the nominal momentum of particles in the accelerator. So if we make the substitution:

$$p_i \rightarrow \widetilde{p}_i = \frac{p_i}{P_0} \,, \tag{2.55}$$

then Hamilton's equations remain unchanged as long as the substitution:

$$H \rightarrow \widetilde{H} = \frac{H}{P_0} \,, \tag{2.56}$$

takes place simultaneously. Accordingly, we can now write:

$$\widetilde{H} = -\sqrt{\frac{(E - q\phi)^2}{P_0^2 c^2} - \frac{m^2c^2}{P_0^2} - (\widetilde{p}_x - \alpha_x)^2 - (\widetilde{p}_y - \alpha_y)^2} - \alpha_z \,, \tag{2.57}$$

where the normalized vector potential $\vec{\alpha}$ is defined by:

$$\vec{\alpha} = q\frac{\vec{A}}{P_0} \,. \tag{2.58}$$

The transverse normalized momenta p_x, p_y will now be small but the longitudinal normalized momentum E/P_0 will generally be close to the speed of light, c. A canonical transformation can be made using a generating function of the second kind [21]:

$$F_2(x, P_x, y, P_y, -t, \delta, s) = xP_x + yP_y + \left(\frac{s}{\beta_0} - ct\right)\left(\frac{1}{\beta_0} + \delta\right) \,, \tag{2.59}$$

where P_x, P_y and δ are the new momentum variables, and β_0 is the normalized velocity of a particle with the reference momentum P_0. With the help of equations:

$$\widetilde{p}_i = \frac{\partial F_2}{\partial q_i} \,, \quad Q_i = \frac{\partial F_2}{\partial P_i} \,, \quad K = \widetilde{H} + \frac{\partial F_2}{\partial z} \,, \tag{2.60}$$

we find that the transverse variables remain unchanged,

$$\begin{aligned} \widetilde{p}_x &= P_x \qquad X = x \\ \widetilde{p}_y &= P_y \qquad Y = y\,. \end{aligned} \tag{2.61}$$

The new Hamiltonian K is then:

$$K = \frac{\delta}{\beta_0} - \sqrt{\left(\frac{1}{\beta_0} + \delta - \frac{q\phi}{P_0 c}\right)^2 - (P_x - \alpha_x)^2 - (P_y - a_y)^2 - \frac{m^2c^2}{P_0^2}} - \alpha_s\,, \tag{2.62}$$

where δ is a new dynamical variable called the "energy deviation" and is given by:

$$\delta = \frac{E}{P_0 c} - \frac{1}{\beta_0}\,. \tag{2.63}$$

With an appropriate choice for P_0, δ is then a small value. Reverting to the original notation through:

$$K \to H, \qquad P_i \to p_i = \frac{\gamma m \dot{x} + q\vec{A}_i}{P_0}, \qquad Z \to z\,, \tag{2.64}$$

we get the so-called "Accelerator Hamiltonian":

$$H = \frac{\delta}{\beta_0} - \sqrt{\left(\frac{1}{\beta_0} + \delta - \frac{q\phi}{P_0 c}\right)^2 - (p_x - \alpha_x)^2 - (p_y - \alpha_y)^2 - \frac{1}{\gamma_0^2 \beta_0^2}} - \alpha_s\,, \tag{2.65}$$

and

$$\vec{u} = (\dot{x}, \dot{y}, \dot{s}), \qquad \vec{\beta} = \frac{\vec{u}}{c}, \qquad \gamma = \frac{1}{\sqrt{1 - \vec{\beta}^2}}\,. \tag{2.66}$$

In a field free region equation (2.65) becomes:

$$H = \frac{\delta}{\beta_0} - \sqrt{\left(\frac{1}{\beta_0} + \delta\right)^2 - p_x^2 - p_y^2 - \frac{1}{\beta_0^2 \gamma_0^2}}\,. \tag{2.67}$$

In a drift space of length L there is no dependence on the coordinates and therefore the momenta are constant, i.e.

$$\Delta p_x = 0\,, \qquad \Delta p_y = 0\,, \qquad \Delta\delta = 0\,. \tag{2.68}$$

The transverse coordinates then will change as:

$$\frac{\Delta x}{L} = \frac{p_x}{\sqrt{\left(\frac{1}{\beta_0}+\delta\right)^2 - p_x^2 - p_y^2 - \frac{1}{\beta_0^2\gamma_0^2}}}, \tag{2.69}$$

$$\frac{\Delta y}{L} = \frac{p_y}{\sqrt{\left(\frac{1}{\beta_0}+\delta\right)^2 - p_x^2 - p_y^2 - \frac{1}{\beta_0^2\gamma_0^2}}}. \tag{2.70}$$

The change in the longitudinal coordinates is given by

$$\frac{\Delta s}{L} = \frac{1}{\beta_0} - \frac{\frac{1}{\beta_0}+\delta}{\sqrt{\left(\frac{1}{\beta_0}+\delta\right)^2 - p_x^2 - p_y^2 - \frac{1}{\beta_0^2\gamma_0^2}}}. \tag{2.71}$$

The set of equations (2.68), (2.69), (2.70) and (2.71) are a dynamical map for the drift space. Knowing the values of the dynamical variables at the entrance of the drift space we can calculate the values at the exit. This dynamical map is nonlinear and that prevents us from writing directly this dynamical map as a transfer matrix. It is possible though that Taylor expansions are made for the changes in the coordinates (2.69), (2.70) and (2.71). For small values of the canonical momenta (that is where the reference momentum comes into use), first order approximations provide acceptable accuracy for some applications.

2.1.2.2 The Paraxial Approximation

All the elements in an accelerator system are not linear. When, however, we refer to "linear" elements, we refer to those elements whose principle effects on the beam may be obtained by expanding the Hamiltonian to second order in the dynamical variables. This approximation is known as the "paraxial approximation".

The magnetic field inside a normal quadrupole is given by:

$$B_x = b_2\frac{y}{\rho_0}, \quad B_y = b_2\frac{x}{\rho_0}, \quad B_s = 0, \tag{2.72}$$

where the coefficient b_2 describes the strength of the quadrupole field. The

above field components can be derived from the potential:

$$A_x = 0\,, \quad A_y = 0\,, \quad A_s = -\frac{1}{2}\frac{b_2}{2\rho_0}(x^2 - y^2)\,. \tag{2.73}$$

.

The Hamiltonian describing the motion inside a quadrupole, using the usual accelerator variables, is:

$$H = \frac{\delta}{\beta_0} - \sqrt{\left(\frac{1}{\beta_0} + \delta\right)^2 - p_x^2 - p_y^2 - \frac{1}{\gamma_0^2\beta_0^2}} - \alpha_s\,, \tag{2.74}$$

where the longitudinal component α_s of the normalised vector potential is:

$$\alpha_s = q\frac{A_s}{P_0} = -\frac{q}{P_0} = -\frac{1}{2}\frac{q}{P_0}\frac{b_2}{\rho_0}(x^2 - y^2)\,. \tag{2.75}$$

If we define the *normalised quadrupole gradient* as:

$$k_1 = \frac{q}{P_0}\frac{b_2}{\rho_0}\,, \tag{2.76}$$

then the Hamiltonian can be rewritten as:

$$H = \frac{\delta}{\beta_0} - \sqrt{\left(\frac{1}{\beta_0} + \delta\right)^2 - p_x^2 - p_y^2 - \frac{1}{\gamma_0^2\beta_0^2}} - \frac{1}{2}k_1(x^2 - y^2)\,. \tag{2.77}$$

Expanding the Hamiltonian of equation (2.77) to second order in the dynamical variables (making the paraxial approximation) we construct the Hamiltonian:

$$H_2 = \frac{1}{2}p_x^2 + \frac{1}{2}p_y^2 + \frac{1}{2}k_1x^2 - \frac{1}{2}k_1y^2 + \frac{1}{2\gamma_0^2\beta_0^2}\delta^2\,. \tag{2.78}$$

Equation (2.78) looks much like the harmonic oscillator equation; for $k_1 \gg 0$ we have a "focusing" potential in x and a defocusing potential in y. There is no focusing in the longitudinal direction. The transfer map obtained from

(2.78) can be written as a matrix:

$$R = \begin{pmatrix} \cos\omega L & \frac{\sin\omega L}{\omega} & 0 & 0 & 0 & 0 \\ -\omega\sin\omega L & \cos\omega L & 0 & 0 & 0 & 0 \\ 0 & 0 & \cosh\omega L & \frac{\sinh\omega L}{\omega} & 0 & 0 \\ 0 & 0 & \omega\sinh\omega L & \cosh\omega L & 0 & 0 \\ 0 & 0 & 0 & 0 & 1 & \frac{L}{\gamma_0^2\beta_0^2} \\ 0 & 0 & 0 & 0 & 0 & 1 \end{pmatrix} \tag{2.79}$$

2.1.2.3 Canonical Variables

The concept of canonical (or conjugate, or canonically conjugate) variables is of major importance. They always occur in complementary pairs, such as spatial location x and linear momentum p, angle ϕ and angular momentum L, and energy E and time t.

For the case of Hamiltonian dynamics, the canonical variables consist of a set of coordinates and their conjugate momenta defined by equation (2.28), rather than coordinates and velocities used in the Lagrangian formalism.

2.1.2.4 Action-Angle Variables

In order to specify the location of a particle in phase-space we need to know the coordinate x and the conjugate momentum p_x. An alternative way for this specification is to give the action J_x and the position or angle ϕ_x around the phase-space ellipse. The action J_x and angle ϕ_x can be defined so that:

$$\begin{aligned} x &= \sqrt{2\beta_x J_x}\cos\phi_x\,, \\ p_x &= -\sqrt{\frac{2J_x}{\beta_x}}(\sin\phi_x + \alpha_x\cos\phi_x)\,. \end{aligned} \tag{2.80}$$

Therefore for angle ϕ_x , we get:

$$\tan\phi_x = -\alpha_x - \beta_x\frac{p_x}{x}\,, \tag{2.81}$$

and

$$2J_x = \gamma_x x^2 + 2\alpha_x x p_x + \beta_x p_x^2\,. \tag{2.82}$$

It is possible to see that (ϕ_x, J_x) form a canonical pair of variables, by

deriving them as new variables from the generating function:

$$F_1 = F_1(x, \phi_x) = -\frac{x^2}{2\beta_x}(\tan\phi_x + \alpha_x)\,. \tag{2.83}$$

Since the action is constant:

$$\frac{dJ_x}{ds} = -\frac{\partial H}{\partial \phi_x} = 0\,, \tag{2.84}$$

the Hamiltonian must be independent of ϕ_x. We also know (again from section 2.1.1.2) that:

$$\frac{d\phi_x}{ds} = \frac{1}{\beta_x}\,. \tag{2.85}$$

Equations (2.84) and (2.85) may be derived from Hamilton's equations, using the Hamiltonian:

$$H = \frac{J_x}{\beta_x}\,. \tag{2.86}$$

Equation (2.86) provides a simple approximation for uncoupled linear dynamics in an accelerator.

2.1.3 Matrix Formalism

The solutions to Hamilton's equations of motion can be expressed in terms of symplectic transformations. In a linear beamline, these transformations can be approximated as symplectic matrices (using the paraxial approximation). Symplectic transfer matrices can be written down explicitly for all elements in an accelerator (e.g. drift, dipole, quadrupole, RF cavity, etc.). The tracking of a particle is then possible using equation (2.10). The 2×2 transfer matrix in one degree of freedom can be written for one periodic section, quite generally, as;

$$R_2 = I\cos(\mu_x) + S_2 \cdot A_2 \sin(\mu_x)\,, \tag{2.87}$$

where

$$S_2 = \begin{pmatrix} 0 & 1 \\ -1 & 0 \end{pmatrix}, \tag{2.88}$$

and A_2 is a symmetric 2×2 matrix and I is the identity matrix. The right hand side of equation (2.87) has 4 parameters corresponding to the three independent components of matrix A_2 and the parameter μ_x. The values of the components of the symmetric matrix A_2 and the parameter μ_x can then be determined from the values of the four components of R_2.

If we consider the horizontal motion of a particle we can write A_2 as:

$$A_2 = \begin{pmatrix} \gamma_x & \alpha_x \\ \alpha_x & \beta_x \end{pmatrix}. \tag{2.89}$$

Symplecticity is a very important concept in the formalism developed to describe the the dynamics in an accelerator system. A symplectic matrix M is defined as a matrix that satisfies the equation:

$$M^T \cdot S \cdot M = S\,, \tag{2.90}$$

where M^T denotes the transpose of matrix M. The implications of symplecticity are analysed in section 2.2.1. If we were to make a classical analogy, we would say that a symplectic transport of a particle is transport with no "friction" forces.

The symplectic condition for the general form of a transfer matrix, R_2,

applied in equation (2.87) gives the condition:

$$\beta_x \gamma_x - \alpha_x^2 = 1 \,. \tag{2.91}$$

If R_2 is symplectic, then we find from (2.91) that:

$$R_2^T \cdot A_2 \cdot R_2 = A_2 \,. \tag{2.92}$$

Therefore, the matrix A_2 is invariant under a transformation representing the transport through a cell. A_2 is defined in terms of a single set of Twiss parameters. Therefore, it is defined at a single point in a beamline. This implies that we are dealing with a *periodic* beamline.

The invariance of this particular transformation can help us in defining a very important concept in beam dynamics, that of *action*. If we construct the quantity J_x :

$$J_x = \frac{1}{2} \begin{pmatrix} x & p_x \end{pmatrix} \cdot A_2 \cdot \begin{pmatrix} x \\ p_x \end{pmatrix} , \tag{2.93}$$

where p_x is the momentum canonically conjugate to x, then under transport through a cell :

$$\begin{pmatrix} x \\ p_x \end{pmatrix} \mapsto R_2 \cdot \begin{pmatrix} x \\ p_x \end{pmatrix} , \tag{2.94}$$

and then:

$$J_x \to \frac{1}{2} \begin{pmatrix} x & p_x \end{pmatrix} \cdot R_2^T \cdot A_2 \cdot R_2 \cdot \begin{pmatrix} x \\ p_x \end{pmatrix} = J_x \,. \tag{2.95}$$

We observe that J_x is also invariant under transport through a cell. We can write:

$$J_x = \frac{1}{2} (\gamma_x x^2 + 2\alpha_x x p_x + \beta_x p_x^2) \,. \tag{2.96}$$

J_x defined in this way is usually called the **action of the particle**. It is the same quantity that was defined in equation (2.96) in section 2.82.

The components of A_2 are functions only of the components of the transfer matrix for a complete periodic cell. Consequently, the parameters α_x, β_x and γ_x characterize the beamline rather than the motion of a particular

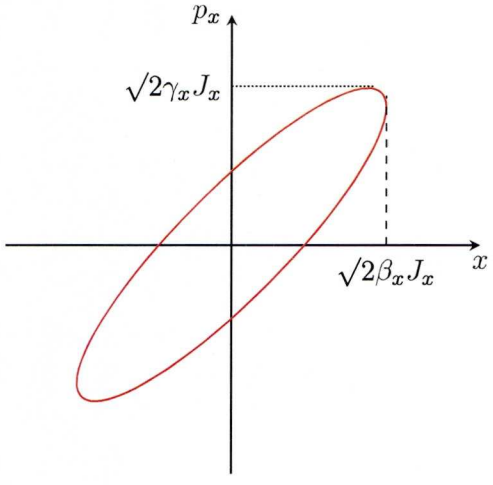

Figure 2.3: Ellipse describing particle motion in horizontal phase-space (Horizontal momentum-vs horizontal coordinate). A particle moving through a periodic lattice will, after each period, move in steps around the ellipse. The parameters β_x and γ_x describe the shape of the ellipse, and are functions of position in the lattice, with the same periodicity as the lattice. The action J_x describes the amplitude of the betatron oscillation: the area of the ellipse is πJ_x.

particle and they are usually called the **Twiss parameters** [3]; the same parameters we encountered in 2.1.1.2. Obviously, there exist corresponding Twiss parameters for the vertical and longitudinal motion.

If the canonical variables x and p_x of a single particle at the same position of every periodic cell are plotted on a phase-space diagram, then an ellipse is formed, the shape of which is determined by the Twiss parameters and with area equal to $2\pi J_x$, figure 2.3. Under the assumption of linear symplectic transport, the action is a conserved quantity. When transported through a periodic cell, a set of particles with a given action will move round an ellipse in phase-space. If we take "snapshots" of this set of particles in phase-space at corresponding points in different periodic cells, then these "snapshots" will look identical. Should the distribution of particles be not properly matched to the lattice, then the ellipse will appear to "rotate" from one periodic cell to the next.

[3]There is an interesting story behind the naming; it turns out out that Prof. Twiss had nothing to do with the introduction of the these parameters

2.1.4 Linear Coupled Motion

Under the assumption of uncoupled motion the transverse motion of particles in an accelerator can be treated independently for the horizontal and vertical plane. Proper selection, design and alignment procedures can be implemented to ensure that uncoupled bunches will be transported through the lattice. In reality though, errors in fabrication and alignment tolerances will inevitably introduce coupling between the two transverse planes of motion, i.e. the motion in each plane in no longer independent of the motion in the other planes. The major sources of coupling are solenoid fields, vertical alignment errors of sextupoles and rotated quadrupoles, which are two of the most generally used magnets in accelerator systems. Restricting the sources of coupling to these three sources one defines the regime of linear coupling.

2.1.4.1 Matrix Formalisms

In the presence of coupling, the single-turn transfer matrix will not be block diagonal, i.e it will contain non-zero elements in locations other that the block-diagonal. A global decoupling involves a transformation that will lead to a block-diagonal transfer matrix. This is the approach introduced by Edwards and Teng [18]. A number of approaches to characterize the betatron coupling in an accelerator system have been published in the literature [19, 47, 11, 34] and this is a subject of continuing research. Here we present two of the different descriptions for the betatron coupling.

Sagan and Rubin description

Sagan and Rubin have described the construction of the $\bar{C}$ matrix to describe the betatron coupling [48].

In a circular accelerator the linear 4×4 one-turn transfer matrix T for the two-dimensional phase spase (x, x', y, y') can be described by four 2×2 sub-matrices, M, m, n and N,

$$T = \begin{pmatrix} M & m \\ n & N \end{pmatrix} \tag{2.97}$$

where M and N are the standard transfer matrices for the (x, x') and (y, y') phase space, respectively. Off-diagonal sub-matrices m, n represent the cou-

pling between the two transverse planes. In a perfect accelerator system with no coupling present, $m = n = 0$.

Equation (2.97) can be further decomposed into normal modes as:

$$T = VUV^{-1} \tag{2.98}$$

where V is a symplectic matrix:

$$V = \begin{pmatrix} \gamma I & C \\ -\bar{C} & \gamma I \end{pmatrix}, \tag{2.99}$$

with γ defined via the symplecticity condition as:

$$\gamma^2 + ||C|| = 1\,. \tag{2.100}$$

U has the form:

$$U = \begin{pmatrix} A & 0 \\ 0 & B \end{pmatrix}, \tag{2.101}$$

and A is the single-turn transfer matrix for one of the normal modes and is given by the standard formula [30]:

$$A = \begin{pmatrix} \cos 2\pi\nu_A + \alpha_\alpha \sin 2\pi\nu_A & \beta_\alpha \sin 2\pi\nu_A \\ -\gamma_\alpha \sin 2\pi\nu_A & \cos 2\pi\nu_A - \alpha_A \sin 2\pi\nu_A \end{pmatrix}. \tag{2.102}$$

A similar formula holds for B, associated with the other normal mode.

The symplectic conjugate C^+ is equal to:

$$\bar{C} = \begin{pmatrix} c_{11} & c_{12} \\ -c_{21} & c_{22} \end{pmatrix}. \tag{2.103}$$

The components of $\bar{C}$ are parameters based on the elements of the single-turn transfer matrix and characterize how the normal modes are related to the horizontal and vertical motion. The following relations have been derived for these components [5]:

$$\bar{C}_{12} = \gamma\sqrt{\frac{\beta_A}{\beta_B}}\left(\frac{y}{x}\right)_A \sin\Delta\phi_A; \qquad \bar{C}_{22} = -\gamma\sqrt{\frac{\beta_A}{\beta_B}}\left(\frac{y}{x}\right)_A \cos\Delta\phi_A\,. \tag{2.104}$$

Similarly, if only mode B is excited:

$$\bar{C}_{12} = \gamma\sqrt{\frac{\beta_B}{\beta_A}}\left(\frac{x}{y}\right)_B \sin\Delta\phi_B; \qquad \bar{C}_{22} = -\gamma\sqrt{\frac{\beta_B}{\beta_A}}\left(\frac{x}{y}\right)_B \cos\Delta\phi_B\,, \tag{2.105}$$

where $(x/y)_B$ is the ratio of the x amplitude to the y amplitude for the B mode and $\Delta\phi_B$ the phase difference between the two motions. It is therefore possible to determine the components of $\bar{C}$ through the measurable quantities $(x/y)_B, (y/x)_A, \Delta\phi_A$ and $\Delta\phi_B$.

Geometrical representation of $\bar{C}$

The real-space ellipse traced out by a single particle during successive turns when only one normal mode is excited can be written as:

$$x = x_{amp}\cos\phi\,, \tag{2.106}$$

$$y = y_{amp}\cos\left(\phi + \Delta\phi\right). \tag{2.107}$$

Such a representation defines an ellipse with major axes d and f that is tilted by an angle θ with respect to the x and y axes. In the case of weak coupling, where $|\bar{C}_{ij}|^2 \ll 1$ and $\gamma \approx 1$ we find:

$$\theta_A \approx \bar{C}_{22}\sqrt{\frac{\beta_B}{\beta_A}}\,, \tag{2.108}$$

$$d_A \approx \epsilon_A\sqrt{\beta_A}\,, \tag{2.109}$$

$$f_A \approx \epsilon_A|\bar{C}_{12}|\sqrt{\beta_B}\,. \tag{2.110}$$

In such an approximation and with the appropriate scaling by the root beta functions, $\bar{C}_{22}$ is interpreted as the tilt angle of the ellipse and $\bar{C}_{12}$ as the ratio of the lengths of the major and minor axis of the ellipse.

Since $\Delta\phi_A$ is the difference in phase between the horizontal and vertical motion, the term $\bar{C}_{22}$ is a measure of the component of vertical motion that is in phase with the horizontal motion. Similarly, the term $\bar{C}_{12}$ is a measure of the component of vertical motion that has a phase difference of 90° with respect to the horizontal motion.

Local Coupling Description

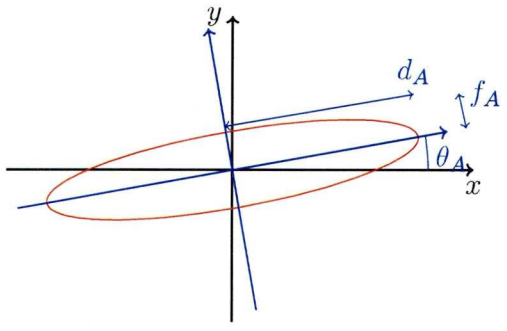

Figure 2.4: Real-space ellipse with major axes d and f tilted by an angle θ with respect to the x and y axes. In the case of weak coupling the components of the $\bar{C}$ matrix, $\bar{C}_{22}$ and $\bar{C}_{12}$ can be interpreted as the tilt angle of the ellipse and the ratio of the lengths of the major and minor axis of the ellipse, respectively.

Wolski [70] has proposed the following description of coupled linear optics. This approach can easily be adapted to three degrees of freedom, whereas the more conventional descriptions (e.g. Sagan and Rubin) deal only with two degrees of freedom (coupling between the two transverse planes). However, in an accelerator, the coupling between transverse and longitudinal motion is often not negligible. The key concept is to derive the lattice functions for the optics of coupled bunches. This approach uses a general 6×6 formalism, making no assumptions on the presence or absence of coupling.

If the linear single-turn transfer matrix M is symplectic, then it has six eigenvalues that can be arranged in reciprocal pairs

$$\lambda_{-k}\lambda_k = 1\,. \tag{2.111}$$

where k = I,II,III, corresponding to each of the three degrees of freedom. The eigenvectors $e_{\pm k}$ of M are defined as:

$$Me_{\pm k} = \lambda_{\pm k}e_{\pm k}\,. \tag{2.112}$$

These eigenvectors can be normalized and arranged in such a way that they form a matrix E such that:

$$E^T \cdot S \cdot E = iS\,. \tag{2.113}$$

A matrix Q is then defined as:

$$Q = \frac{1}{\sqrt{2}} \begin{pmatrix} 1 & i \\ -1 & i \end{pmatrix} . \tag{2.114}$$

Using matrix Q the normalising matrix N can be constructed as:

$$N = E \cdot Q \,, \tag{2.115}$$

where E is now the matrix of eigenvectors of R, the transfer matrix for one periodic cell of a beamline. Then N has the following property:

$$N^{-1} \cdot R \cdot N = \tilde{R}(\mu_{\mathrm{I}}, \mu_{\mathrm{II}}, \mu_{\mathrm{III}}) \,. \tag{2.116}$$

$\tilde{R}$ is a block-diagonal rotation matrix with rotation angles μ_k:

$$\tilde{R}_2(\mu_k) = \begin{pmatrix} \cos\mu_k & \sin\mu_k \\ -\sin\mu_k & \cos\mu_k \end{pmatrix} . \tag{2.117}$$

Since E is a matrix of the eigenvectors of R with appropriate ordering, it can diagonalize R , with the eigenvalues being the elements of the diagonal:

$$E^{-1} \cdot R \cdot E = \begin{pmatrix} e^{-i\mu_{\mathrm{I}}} & & & & & \\ & e^{i\mu_{\mathrm{I}}} & & & & \\ & & e^{-i\mu_{\mathrm{II}}} & & & \\ & & & e^{i\mu_{\mathrm{II}}} & & \\ & & & & e^{-i\mu_{\mathrm{III}}} & \\ & & & & & e^{i\mu_{\mathrm{III}}} \end{pmatrix} . \tag{2.118}$$

We can also write

$$Q^{-1} \cdot E^{-1} \cdot R \cdot E \cdot Q = \tilde{R}(\mu_{\mathrm{I}}, \mu_{\mathrm{II}}, \mu_{\mathrm{III}}) \,, \tag{2.119}$$

where

$$\tilde{R}(\mu_{\mathrm{I}}, \mu_{\mathrm{II}}, \mu_{\mathrm{III}}) = \begin{pmatrix} \tilde{R}_2(\mu_{\mathrm{I}}) & & \\ & \tilde{R}_2(\mu_{\mathrm{II}}) & \\ & & \tilde{R}_2(\mu_{\mathrm{III}}) \end{pmatrix} . \tag{2.120}$$

With the help of equation (2.115) we can write

$$N^{-1} \cdot R \cdot N = \tilde{R}(\mu_{\rm I}, \mu_{\rm II}, \mu_{\rm III}) \,. \tag{2.121}$$

It can be proved that matrix N is symplectic. Starting from the definition of N,

$$N^T \cdot S \cdot N = Q^T \cdot E^T \cdot S \cdot E \cdot Q \,, \tag{2.122}$$

and using equation (2.113) we get

$$N^T \cdot N = iQ^T \cdot S \cdot Q \,. \tag{2.123}$$

From the definition of matrix Q,[eq.(2.114)], it follows that:

$$N^T \cdot S \cdot N = S \,. \tag{2.124}$$

Thus, matrix N is symplectic.

Using the normalizing matrix N it is possible to define a vector $\vec{J}$ with new dynamical variables:

$$\vec{J} = N^{-1} \cdot \vec{x} \,, \tag{2.125}$$

where

$$\vec{J} = \begin{pmatrix} X_{\rm I} \\ P_{\rm I} \\ X_{\rm II} \\ P_{\rm II} \\ X_{\rm III} \\ P_{\rm III} \end{pmatrix} \,, \qquad \vec{x} = \begin{pmatrix} x \\ p_x \\ y \\ p_y \\ z \\ \delta \end{pmatrix} \,. \tag{2.126}$$

The new pairs of variables (X_k, P_k), etc. are canonically conjugate since they are derived from the original variables (x, p_x), that form canonically conjugate pairs themselves, by a symplectic transformation (N^{-1}) [70]. With the help of a generating function of the 1st kind :

$$F_1(X_k, \phi_k) = -\frac{1}{2} \sum_{k={\rm I,II,III}} X_k^2 \tan\phi_k \,, \tag{2.127}$$

and its appropriate derivatives:

$$X_k = \frac{\partial F_1}{\partial P_k} \,, \qquad J_k = -\frac{\partial F_1}{\partial \phi_k} \,, \tag{2.128}$$

it is possible to derive the pair of new canonical variables (ϕ_k, J_k):

$$J_k = \frac{1}{2}(X_k^2 + P_k^2)\,, \qquad \tan\phi_k = -\frac{P_k}{X_k}\,. \tag{2.129}$$

Using equation (2.129) the action vector $\vec{J}$ is constructed:

$$\vec{J} = \begin{pmatrix} \sqrt{2J_{\rm I}}\cos\phi_{\rm I} \\ -\sqrt{2J_{\rm I}}\sin\phi_{\rm I} \\ \sqrt{2J_{\rm II}}\cos\phi_{\rm II} \\ -\sqrt{2J_{\rm II}}\sin\phi_{\rm II} \\ \sqrt{2J_{\rm III}}\cos\phi_{\rm III} \\ -\sqrt{2J_{\rm III}}\sin\phi_{\rm III} \end{pmatrix}\,. \tag{2.130}$$

For a transformation $R = R(s_0, s_1)$ across one complete periodic cell from point s_0 to point s_1 we have:

$$\vec{x}(s_1) = R \cdot \vec{x}(s_0)\,. \tag{2.131}$$

Accordingly:

$$\begin{aligned} \vec{J}(s_1) &= N^{-1} \cdot \vec{x}(s_1) \\ &= N^{-1} \cdot R \cdot \vec{x}(s_0) \\ &= N^{-1} \cdot R \cdot N \cdot N^{-1} \cdot \vec{x}(s_0) \\ &= N^{-1} \cdot R \cdot N \cdot \vec{J}(s_0)\,. \end{aligned} \tag{2.132}$$

Using equation (2.116) in (2.132) it then becomes:

$$\vec{J}(s_1) = \tilde{R}(\mu_{\rm I}, \mu_{\rm II}, \mu_{\rm III}) \cdot \vec{J}(s_0)\,. \tag{2.133}$$

Taking into account that $\tilde{R}(\mu_{\mathrm{I}}, \mu_{\mathrm{II}}, \mu_{\mathrm{III}})$ is a rotation matrix, the latter equation becomes:

$$\tilde{R}(\mu_{\mathrm{I}}, \mu_{\mathrm{II}}, \mu_{\mathrm{III}}) \cdot \begin{pmatrix} \sqrt{2J_{\mathrm{I}}}\cos\phi_{\mathrm{I}} \\ -\sqrt{2J_{\mathrm{I}}}\sin\phi_{\mathrm{I}} \\ \sqrt{2J_{\mathrm{II}}}\cos\phi_{\mathrm{II}} \\ -\sqrt{2J_{\mathrm{II}}}\sin\phi_{\mathrm{II}} \\ \sqrt{2J_{\mathrm{III}}}\cos\phi_{\mathrm{III}} \\ -\sqrt{2J_{\mathrm{III}}}\sin\phi_{\mathrm{III}} \end{pmatrix} = \begin{pmatrix} \sqrt{2J_{\mathrm{I}}}\cos(\phi_{\mathrm{I}} + \mu_{\mathrm{I}}) \\ -\sqrt{2J_{\mathrm{I}}}\sin(\phi_{\mathrm{I}} + \mu_{\mathrm{I}}) \\ \sqrt{2J_{\mathrm{II}}}\cos(\phi_{\mathrm{II}} + \mu_{\mathrm{II}}) \\ -\sqrt{2J_{\mathrm{II}}}\sin(\phi_{\mathrm{II}} + \mu_{\mathrm{II}}) \\ \sqrt{2J_{\mathrm{III}}}\cos(\phi_{\mathrm{III}} + \mu_{\mathrm{III}}) \\ -\sqrt{2J_{\mathrm{III}}}\sin(\phi_{\mathrm{III}} + \mu_{\mathrm{III}}) \end{pmatrix} . \tag{2.134}$$

Therefore the action-angle variables for a single periodic cell will transform, under the action of the relevant transfer matrix R, as:

$$J_k \rightarrow J_k \qquad \phi_k \rightarrow \phi_k + \mu_k \,. \tag{2.135}$$

The sigma matrix is defined as the average over all particles in the bunch of the outer product of the phase-space variables:

$$\Sigma = \langle \vec{x} \cdot \vec{x}^T \rangle \,. \tag{2.136}$$

With the help of equation (2.125) the latter equation becomes:

$$\Sigma = N \cdot \langle \vec{J} \cdot \vec{J}^T \rangle \cdot N^T \,. \tag{2.137}$$

If the angle variables are uncorrelated so that:

$$\langle \sin\phi_j \sin\phi_k \rangle = \langle \cos\phi_j \cos\phi_k \rangle = \frac{1}{2}\delta_{jk} \,, \tag{2.138}$$

where δ_{jk} is the Kronecker delta, and:

$$\langle \sin\phi_j \cos\phi_k \rangle = 0 \,, \tag{2.139}$$

then the sigma matrix can be written as:

$$\Sigma = \sum_{k=\mathrm{I,II,III}} B^k \varepsilon_k \,, \tag{2.140}$$

where the matrices B^k are defined as:

$$B^k = N \cdot T^k \cdot N^T , \tag{2.141}$$

and the emittances ε_k are given by:

$$\varepsilon_k = \langle J_k \rangle . \tag{2.142}$$

The matrices T^k have the following form:

$$T^{\mathrm{I}} = \begin{pmatrix} 1 & & & & & \\ & 1 & & & & \\ & & 0 & & & \\ & & & 0 & & \\ & & & & 0 & \\ & & & & & 0 \end{pmatrix}$$

$$T^{\mathrm{II}} = \begin{pmatrix} 0 & & & & & \\ & 0 & & & & \\ & & 1 & & & \\ & & & 1 & & \\ & & & & 0 & \\ & & & & & 0 \end{pmatrix}$$

$$T^{\mathrm{III}} = \begin{pmatrix} 0 & & & & & \\ & 0 & & & & \\ & & 0 & & & \\ & & & 0 & & \\ & & & & 1 & \\ & & & & & 1 \end{pmatrix} . \tag{2.143}$$

The components β_{ij}^k of the matrices B^k are the generalizations of the Twiss parameters for the case of coupled optics. They may be referred to as the *coupled lattice functions* or the *generalized Twiss parameters*. In the case of a block diagonal single-turn transfer matrix, the motion is uncoupled and the coordinate in every plane is determined only by its relative action. Identifying $k = \mathrm{I}$ with the horizontal and $k = \mathrm{II}$ with the vertical plane, the following relationships between the components β_{ij}^k and the familiar Twiss

parameters are established; in the horizontal plane:

$$\beta_x = \beta^{\mathrm{I}}_{11}\,, \tag{2.144}$$
$$\alpha_x = -\beta^{\mathrm{I}}_{12}\,, \tag{2.145}$$
$$\gamma_x = \beta^{\mathrm{I}}_{22}\,, \tag{2.146}$$

and in the vertical plane:

$$\beta_y = \beta^{\mathrm{II}}_{33}\,, \tag{2.147}$$
$$\alpha_y = -\beta^{\mathrm{II}}_{34}\,, \tag{2.148}$$
$$\gamma_y = \beta^{\mathrm{II}}_{44}\,. \tag{2.149}$$

The usual case for a storage ring involves a single-turn transfer matrix that is not block-diagonal. In that case motion from the longitudinal plane is coupled to the transverse planes through the mechanism of dispersion, so for the horizontal coordinate we have:

$$x = \sqrt{2\beta_x J_x}\cos\phi_x + \eta_x\delta\,. \tag{2.150}$$

It follows that:

$$\langle x\delta\rangle = \eta_x\langle\delta^2\rangle\,. \tag{2.151}$$

In terms of the β^k_{ij} components as defined in equation (2.141):

$$\langle x\delta\rangle = \beta^{\mathrm{III}}_{16}\varepsilon_{\mathrm{III}}\,, \tag{2.152}$$
$$\langle\delta^2\rangle = \beta^{\mathrm{III}}_{66}\varepsilon_{\mathrm{III}}\,. \tag{2.153}$$

It then follows that the horizontal and similarly the vertical dispersion are given by:

$$\eta_x = \frac{\beta^{\mathrm{III}}_{16}}{\beta\mathrm{III}_{66}}\,, \qquad \eta_y = \frac{\beta^{\mathrm{III}}_{36}}{\beta\mathrm{III}_{66}}\,. \tag{2.154}$$

In the sigma matrix definition (2.140), there is also the assumption that the distribution is matched in the sense that the sigma matrix is invariant under transport from one periodic cell to the next:

$$R\cdot\Sigma\cdot R^T = \Sigma\,. \tag{2.155}$$

The eigenvalues of $\Sigma \cdot S$ are equal to $\pm i\varepsilon_k$, where ε_k are the emittances of the beam. The eigenvectors of $\Sigma \cdot S$ are contained in the same matrix E that contains the eigenvectors for the transfer matrix R. Multiplying both sides of equation(2.140) we have:

$$\Sigma \cdot S = \sum_{k=\mathrm{I,II,III}} B^k \cdot S\varepsilon_k \,. \tag{2.156}$$

But for the matrices B^k we have:

$$\begin{aligned} B^k \cdot S &= N \cdot T^k \cdot N^T \cdot S \quad (N \text{ is symplectic}) \\ \therefore B^k \cdot S &= N \cdot T^k \cdot S \cdot N^{-1} \,. \end{aligned} \tag{2.157}$$

With the help of definition (2.115) it follows that:

$$\begin{aligned} B^k \cdot S &= E \cdot Q \cdot T^k \cdot S \cdot Q^{-1} \cdot E^{-1} \\ \therefore E^{-1} \cdot B^k \cdot S \cdot E &= Q \cdot T^k \cdot S \cdot Q^{-1} \,. \end{aligned} \tag{2.158}$$

Performing the multiplications for the right hand side of equation (2.158), where the matrices are constant:

$$E^{-1} \cdot B^k \cdot S \cdot E = -i\tilde{T}^k \tag{2.159}$$

where now the $\tilde{T}^k$ matrices have the form:

$$\tilde{T}^{\mathrm{I}} = \begin{pmatrix} 1 & & & & & \\ & -1 & & & & \\ & & 0 & & & \\ & & & 0 & & \\ & & & & 0 & \\ & & & & & 0 \end{pmatrix} \tag{2.160}$$

$$\tilde{T}^{\mathrm{II}} = \begin{pmatrix} 0 & & & & & \\ & 0 & & & & \\ & & 1 & & & \\ & & & -1 & & \\ & & & & 0 & \\ & & & & & 0 \end{pmatrix} \tag{2.161}$$

$$\tilde{T}^{\mathrm{III}} = \begin{pmatrix} 0 & & & & & \\ & 0 & & & & \\ & & 0 & & & \\ & & & 0 & & \\ & & & & 1 & \\ & & & & & -1 \end{pmatrix}. \tag{2.162}$$

From equations (2.156) and (2.159) it turns out that:

$$E^{-1}(\Sigma S)E = \begin{pmatrix} \varepsilon_{\mathrm{I}} & & & & & \\ & -\varepsilon_{\mathrm{I}} & & & & \\ & & \varepsilon_{\mathrm{II}} & & & \\ & & & -\varepsilon_{\mathrm{II}} & & \\ & & & & \varepsilon_{\mathrm{III}} & \\ & & & & & -\varepsilon_{\mathrm{III}} \end{pmatrix}. \tag{2.163}$$

The components of the diagonal are the eigenvalues of the $\Sigma \cdot S$ matrix, where ε_k comes from equation (2.142).

One of the goals of such a description is to know how the coupled lattice functions transform with respect to position in an accelerator. The coordinates of each particle from position s_0 to position s_1 transform under the

action of a transfer matrix $R = R(s_0, s_1)$ as:

$$\vec{x}(s_1) = R \cdot \vec{x}(s_0)\,. \tag{2.164}$$

Equation (2.136) provides then the transformation of the sigma matrix as:

$$\begin{aligned} \Sigma(s_1) &= R \cdot \Sigma(s_0) \cdot R^T \\ \therefore \Sigma(s_1) \cdot S &= R \cdot \Sigma(s_0) \cdot R^T \cdot S \quad (R \text{ is symplectic}) \\ \therefore &= R \cdot \Sigma(s_0) \cdot S \cdot R^{-1}\,. \end{aligned} \tag{2.165}$$

It is known that for any matrices U, V, the eigenvalues of V are equal to the eigenvalues of $U \cdot V \cdot U^{-1}$. Therefore, the eigenvalues of $\Sigma(s_1) \cdot S$ are the same as the eigenvalues of $\Sigma(s_0) \cdot S$. As a result, the bunch emittances (i.e. the eigenvalues) are conserved under linear symplectic trasportation. Knowing that the sigma matrix is related to the coupled lattice functions through equation (2.140), the coupled lattices will transform in the same way as the sigma matrix:

$$B^k(s_1) = R \cdot B^k(s_0) \cdot R^T\,. \tag{2.166}$$

It is important to note that in this transformation of the coupled lattice functions R can be any symplectic transfer matrix, irrespective of periodicity regarding the lattice structure. Therefore, if one can determine the initial lattice functions for the bunch distribution at the start of the beam line, then it is possible to calculate their propagation using the appropriate symplectic transfer matrices.

In the case of a storage ring, if the single-turn transfer matrix R, starting at a some point, is known, then it is possible to calculate the matched coupled lattice functions B^k at that point (i.e. the lattice functions that describe a distribution that remains invariant after one turn). Knowing also the emittances at that point allows for the calculation of the sigma matrix at that point. In that case the square of the horizontal beam size is given by:

$$\langle x^2 \rangle = \beta_{11}^{\mathrm{I}} \varepsilon_{\mathrm{I}} + \beta_{11}^{\mathrm{II}} \varepsilon_{\mathrm{II}} + \beta_{11}^{\mathrm{III}} \varepsilon_{\mathrm{III}}\,. \tag{2.167}$$

The square of the horizontal beam size may also be written as:

$$\sigma_x^2 = \beta_x \varepsilon_x + \eta_x^2 \sigma_\delta^2 \,, \tag{2.168}$$

where

$$\sigma_x^2 = \langle x^2 \rangle \,, \tag{2.169}$$

$$\sigma_\delta^2 = \langle \delta^2 \rangle \,. \tag{2.170}$$

However, for equation (2.168) to be true a number of assumptions must be made. Assuming that there is no coupling between the two transverse planes, then $\beta_{11}^{\mathrm{II}} = 0$. Furthermore, if the coupling is weak between the horizontal and the longitudinal plane (small horizontal dispersion), then the approximation:

$$\beta_{11}^{\mathrm{I}} \approx \beta_x \,, \tag{2.171}$$

is valid. At the same time, if the longitudinal motion is slow, so that the energy deviation δ of each particle can be considered as a constant, the horizontal position of a particle with zero betatron amplitude at that point in the storage ring is:

$$x = \eta_x \delta \,. \tag{2.172}$$

Additionally, the angle variables ϕ_x of all particles must be uncorrelated and the energy deviation δ is uncorrelated with the horizontal variables J_x or ϕ_x.

2.1.4.2 Perturbation Theory for Coupled Motion

To describe betatron coupling for a single particle in Hamiltonian mechanics, we start from the Hamiltonian which is a function of the particle's angles and actions and, generally, time or distance along the reference trajectory:

$$H = H(\phi_x, J_x, \phi_y, J_y; s)\,. \tag{2.173}$$

The equations of motion derived from equation (2.173) are then:

$$\begin{aligned} \frac{dJ_x}{ds} &= -\frac{\partial H}{\partial \phi_x}\,, & \frac{dJ_y}{ds} &= -\frac{\partial H}{\partial \phi_y}\,, \\ \frac{d\phi_x}{ds} &= -\frac{\partial H}{\partial J_x}\,, & \frac{d\phi_y}{ds} &= -\frac{\partial H}{\partial J_y}\,. \end{aligned} \tag{2.174}$$

The Hamiltonian, for a particle moving along a linear, uncoupled beamline can be written as:

$$H = \frac{J_x}{\beta_x} + \frac{J_y}{\beta_y}\,. \tag{2.175}$$

A Hamiltonian describing the betatron coupling in a skew quadrupole, in cartesian coordinates, has the form:

$$H = \frac{1}{2}p_x^2 + \frac{1}{2}p_y^2 - k_s xy\,, \tag{2.176}$$

where

$$k_s = \frac{1}{B\rho}\frac{\partial B_x}{\partial x}\,. \tag{2.177}$$

The equations of motion, then, in a skew-quadrupole can be written, as:

$$\begin{aligned} \frac{dp_x}{ds} &= k_s y\,, & \frac{dp_y}{ds} &= k_s x\,, \\ \frac{dx}{ds} &= p_x\,, & \frac{dy}{ds} &= p_y\,. \end{aligned} \tag{2.178}$$

In the case of a number of skew quadrupoles distributed around a storage ring, the "focusing" effect of a skew quadrupole is represented by a term in the Hamiltonian:

$$k_s xy = 2k_s\sqrt{\beta_x\beta_y}\sqrt{J_x J_y}\cos\phi_x\cos\phi_y\,. \tag{2.179}$$

Therefore, the Hamiltonian can now be written as:

$$H = \frac{J_x}{\beta_x} + \frac{J_y}{\beta_y} - 2k_s\sqrt{\beta_x\beta_y}\sqrt{J_xJ_y}\cos\phi_x\cos\phi_y\,. \tag{2.180}$$

The beta functions and the skew quadrupole strength are functions of position, s; the solution of the equations of motion becomes cumbersome. We can, however, simplify the problem, by "averaging" the Hamiltonian [30], thus:

$$H = \omega_x J_x + \omega_y J_y - 2\kappa\cos\phi_x\cos\phi_y\,, \tag{2.181}$$

where

$$\omega_{x,y} = \frac{1}{C}\int_0^C \frac{ds}{\beta_{x,y}}\,, \tag{2.182}$$

is a constant term and C is the circumference of the ring.

If we rewrite the coupling term in the Hamiltonian, we get:

$$H = \omega_x J_x + \omega_y J_y - \kappa_-\sqrt{J_xJ_y}\cos\left(\phi_x - \phi_y\right) - \kappa_+\sqrt{J_xJ_y}\cos\left(\phi_x + \phi_y\right). \tag{2.183}$$

The constants $\kappa_\pm$ represent the skew quadrupole strength averaged around the ring; we have to take into account though that the "kick" from a skew quadrupole depends on the betatron phase:

$$\kappa_\pm e^{i\chi} = \frac{1}{C}\int_0^C e^{i(\mu_x \pm \mu_y)}k_s\sqrt{\beta_x\beta_y}ds\,. \tag{2.184}$$

If we suppose that $\kappa_- \gg \kappa_+$, then the Hamiltonian simplifies to:

$$H = \omega_x J_x + \omega_y J_y - \kappa_-\sqrt{J_xJ_y}\cos\left(\phi_x - \phi_y\right). \tag{2.185}$$

The equations of motion from the simplified Hamiltonian are:

$$\begin{aligned}
\frac{dJ_x}{ds} &= -\frac{\partial H}{\partial\phi_x} = \kappa_-\sqrt{J_xJ_y}\sin\left(\phi_x - \phi_y\right),\\
\frac{dJ_y}{ds} &= -\frac{\partial H}{\partial\phi_y} = -\kappa_-\sqrt{J_xJ_y}\sin\left(\phi_x - \phi_y\right),\\
\frac{d\phi_x}{ds} &= -\frac{\partial H}{\partial J_x} = \omega_x + \frac{\kappa_-}{2}\sqrt{\frac{J_y}{J_x}}\cos\left(\phi_x - \phi_y\right),\\
\frac{d\phi_y}{ds} &= -\frac{\partial H}{\partial J_y} = \omega_y + \frac{\kappa_-}{2}\sqrt{\frac{J_x}{J_y}}\cos\left(\phi_x - \phi_y\right).
\end{aligned} \tag{2.186}$$

From equations (2.186) it follows (in general) that:

$$\begin{aligned} & \frac{dJ_x}{ds} + \frac{dJ_y}{ds} = 0 \\ \therefore \quad & \frac{d}{dx}(J_x + J_y) = 0 \\ \therefore \quad & J_x + J_y = \text{constant}\,. \end{aligned} \tag{2.187}$$

Furthermore, if:

$$\phi_x = \phi_y\,, \tag{2.188}$$

then:

$$\frac{dJ_x}{ds} = \frac{dJ_y}{ds} = 0\,. \tag{2.189}$$

This result implies that if we can find a solution to the equations of motion with $\phi_x = \phi_y$ for all s, then the actions will remain constant. If:

$$\phi_x = \phi_y \tag{2.190}$$

and

$$\frac{d\phi_x}{ds} = \frac{d\phi_y}{ds}\,, \tag{2.191}$$

then:

$$\frac{J_y}{J_x} = \frac{\sqrt{1 + \kappa_-^2/\Delta\omega^2} - 1}{\sqrt{1 + \kappa_-^2/\Delta\omega^2} + 1}\,. \tag{2.192}$$

Making the substitution $J_x + J_y = J_0$, where J_0 is a constant, we get the *fixed point solution*:

$$\begin{aligned} J_x &= \frac{1}{2}\left(1 + \frac{1}{\sqrt{1 + \kappa_-^2/\Delta\omega^2}}\right) J_0\,, \\ J_y &= \frac{1}{2}\left(1 - \frac{1}{\sqrt{1 + \kappa_-^2/\Delta\omega^2}}\right) J_0\,. \end{aligned} \tag{2.193}$$

If we identify $\langle J_0 \rangle$ with the natural emittance in a storage ring (determined by synchrotron radiation effects, see section 2.2.2.1), then $\langle J_x \rangle$ and $\langle J_y \rangle$ may be identified with the equilibrium horizontal and vertical emittances respectively.

2.2 Collection of Particles

Tracking individual particles is important but in practice we need to describe the behaviour (e.g. variation of size) of a collection of particles, a "bunch", usually containing of order 10^{10} particles or more. In this analysis, we assume that particles move independently, considering only the effects of external electromagnetic fields.

2.2.1 Symplectic Transport

Symplecticity is a very important concept in the formalism developed to describe the the dynamics in an accelerator system. As a starting point we define a symplectic matrix M, a $2n \times 2n$ matrix that satisfies the equation:

$$M^T \cdot S \cdot M = S\,, \tag{2.194}$$

where M^T denotes the transpose of matrix M and S is a $2n \times 2n$ matrix with block diagonals:

$$S_2 = \begin{pmatrix} 0 & 1 \\ -1 & 0 \end{pmatrix}. \tag{2.195}$$

Equations (2.26) can be written in the form:

$$\frac{d}{dt}\vec{x} = S \cdot \nabla_{\vec{x}} H\,, \tag{2.196}$$

where

$$\vec{x} = \begin{pmatrix} x \\ p_x \\ y \\ p_y \\ \vdots \end{pmatrix} \quad \text{and} \quad \nabla_{\vec{x}} = \begin{pmatrix} \partial_x \\ \partial_{p_x} \\ \partial_y \\ \partial_{p_y} \\ \vdots \end{pmatrix}. \tag{2.197}$$

In the paraxial approximation, the Hamiltonian describing the dynamics of a particle in an electromagnetic field can be shown to be of second-order in the dynamical variables. This leads, as we have mentioned, to linear equations of motion. For a general second-order Hamiltonian we can write:

$$\nabla_{\vec{x}} H = J \cdot \vec{x}\,, \tag{2.198}$$

where J is a symmetric matrix, i.e. $J^T = J$ (J in this context should not be confused with the action). Combining equations (2.198) and (2.196) we get:

$$\frac{d}{dt}\vec{x} = S \cdot J \cdot \vec{x}\,. \tag{2.199}$$

The solution to the equation (2.199) is:

$$\vec{x}(t) = M(t) \cdot \vec{x}(0)\,, \tag{2.200}$$

where matrix M is given by:

$$M(t) = \exp(tS \cdot J)\,. \tag{2.201}$$

The matrix exponential is defined as:

$$\exp(A) = \sum_{n=0}^{\infty} \frac{A^n}{n!}\,, \tag{2.202}$$

following the similar definition for the exponential function as a power series in the form of a Taylor series expansion. Taking into account that J is symmetric and S antisymmetric:

$$J^T = J \qquad S^T = -S\,, \tag{2.203}$$

and some useful properties such as:

$$\exp(A) \cdot \exp(-A) = I\,, \tag{2.204}$$

and

$$S \cdot \exp(tS \cdot J) = \exp(tJ \cdot S) \cdot S\,, \tag{2.205}$$

we can show that the transfer matrix M is symplectic, i.e.

$$\begin{aligned} M^T(t) \cdot S \cdot M(t) &= \exp(-tJ \cdot S) \cdot S \cdot \exp(tS \cdot J) && (2.206)\\ &= \exp(-tJ \cdot S) \cdot \exp(tJ \cdot S) \cdot S && (2.207)\\ &= S\,. && (2.208) \end{aligned}$$

2.2.1.1 Emittance

If we consider bunches consisting of a very large number of particles, then we need to describe the average of some quantity over all particles in the bunch (usually, this quantity is a dynamical variable). The notation for this description is $\langle \bullet \rangle$, e.g. $\langle x \rangle$ is the average horizontal coordinate of the particles in the bunch. This is the value that would be recorded by a horizontal Beam Position Monitor (BPM) as the bunch goes past.

The quantities $\langle x_i \rangle$, where x_i $(1 \leq i \leq 6)$ is one of the dynamical variables $(x, p_x, y, p_y, z, \delta)$, are usually called the *first order moments* of the bunch distribution. Collectively, the first order moments of the bunch distribution

are also called the bunch *centroid.*

The quantities:

$$\Sigma_{ij} = \langle (x_i - \langle x_i \rangle)(x_j - \langle x_j \rangle) \rangle = \langle x_i x_j \rangle - \langle x_i \rangle \langle x_j \rangle \,, \tag{2.209}$$

are called the *second order moments* of the bunch distribution. The first order moments describe the position of the bunch, while the second order moments describe the size of the bunch.

A symmetric matrix Σ can be formed by the second order moments Σ_{ij}, usually referred to as the *sigma matrix.* The diagonal components of the sigma matrix are the variances of the dynamical variables over all particles in the bunch, for example:

$$\Sigma_{11} = \langle x^2 \rangle - \langle x \rangle^2 = \sigma_x^2 \,.$$

The term *coupling* is usually used to describe situations where motion of particles in one plane affect the motion in another. It is important here to distinguish between the terms of a coupled/uncoupled bunch and a coupled/uncoupled beamline.

An uncoupled bunch distribution is one for which all the components of the sigma matrix outside the 2×2 block diagonals are zero. In any other case the distribution is said to be coupled. The same conditions for components of the transport matrix define a coupled or uncoupled beamline. An uncoupled distribution travelling down an uncoupled beamline will stay uncoupled. If however, an uncoupled bunch distribution travels through a coupled beamline then coupling will be introduced to the bunch.

For the special case of an uncoupled bunch distribution of first order moments $\langle x_i \rangle$ all equal to zero, the horizontal part of the sigma matrix can be written as:

$$\Sigma_2 = \begin{pmatrix} \langle x^2 \rangle & \langle x p_x \rangle \\ \langle x p_x \rangle & \langle p_x^2 \rangle \end{pmatrix} . \tag{2.210}$$

The eigenvalues of $\Sigma_2 \cdot S_2$ are $\lambda_\pm$ as follows

$$\lambda_\pm = \pm i \varepsilon_x \,, \tag{2.211}$$

where

$$\varepsilon_x = \sqrt{\langle x^2 \rangle \langle p_x^2 \rangle - \langle x p_x \rangle^2} \,, \tag{2.212}$$

with S_2 being equal to:

$$S_2 = \begin{pmatrix} 0 & 1 \\ -1 & 0 \end{pmatrix}.$$

The quantity ε_x defined by (2.212) is known as the horizontal **emittance**. Obviously, similar expressions can be written down for the vertical and longitudinal emittances.

Knowing the transfer matrix $R = R(s_0, s_1)$ from a point s_0 to a point s_1 along the reference trajectory, we can calculate how the sigma matrix transforms. In matrix form this can be written simply as:

$$\Sigma(s_1) = R \cdot \Sigma(s_0) \cdot R^T. \tag{2.213}$$

From the sigma matrix Σ, we can construct the matrix $\Sigma \cdot S$. S is the matrix used to define the symplectic condition for a matrix M (equation (2.194)). For a symplectic transfer matrix $R = R(s_0, s_1)$, the matrix $\Sigma \cdot S$ can be transformed as:

$$\Sigma \cdot S \rightarrow R \cdot \Sigma \cdot R^T \cdot S = R \cdot \Sigma \cdot S \cdot R^{-1}. \tag{2.214}$$

For any matrices M and N, we can observe that the eigenvalues of $N \cdot M \cdot N^{-1}$ are the same as the eigenvalues of M. Therefore the eigenvalues of $\Sigma \cdot S$ are conserved under symplectic, linear transport represented by a symplectic transfer matrix R. The latter statement leads to the conclusion that the beam emittances for an uncoupled distribution, defined by (2.212) and similar expressions for the vertical and longitudinal degrees of freedom, are also conserved. It is important to note here that emittances defined this way are only conserved for uncoupled bunches.

Generalization of the definition of the emittances to coupled distributions is possible. For a periodic beamline, any bunch distribution for which the sigma matrix remains invariant under transport through one periodic cell is known as a matched distribution. If R is the transfer matrix for one periodic cell and the sigma matrix Σ satisfies the condition:

$$\Sigma = R \cdot \Sigma \cdot R^T, \tag{2.215}$$

then Σ is a matched distribution. The Twiss parameters are defined by the

transfer matrix for a single periodic cell :

$$R_2 = \begin{pmatrix} \cos\mu_x + \alpha_x \sin\mu_x & \beta_x \sin\mu_x \\ -\gamma_x \sin\mu_x & \cos\mu_x - \alpha_x \sin\mu_x \end{pmatrix} . \tag{2.216}$$

Given the Twiss parameters, it is possible to express x and p_x in terms of J_x and ϕ_x:

$$\begin{pmatrix} x \\ p_x \end{pmatrix} = \begin{pmatrix} \sqrt{\beta_x} & 0 \\ -\frac{\alpha_x}{\sqrt{\beta_x}} & \frac{1}{\sqrt{\beta_x}} \end{pmatrix} \cdot \begin{pmatrix} \sqrt{2J_x}\cos\phi_x \\ -\sqrt{2J_x}\sin\phi_x \end{pmatrix} . \tag{2.217}$$

Assuming that the angle variables of all particles in the bunch are uniformly distributed:

$$\langle \sin\phi_x \rangle = \langle \cos\phi_x \rangle = 0 ,$$

and using equation (2.217) and

$$\beta_x \gamma_x - \alpha_x^2 = 1 , \tag{2.218}$$

which comes from the symplectic condition for matrix R_2 (equation (2.216)), we arrive at the following

$$\langle x^2 \rangle = \beta_x \langle J_x \rangle , \tag{2.219}$$

$$\langle x p_x \rangle = -\alpha_x \langle J_x \rangle , \tag{2.220}$$

$$\langle p_x^2 \rangle = \gamma_x \langle J_x \rangle . \tag{2.221}$$

From equations (2.219), (2.220), (2.221) and (2.218) we find:

$$\langle x^2 \rangle \langle p_x^2 \rangle - \langle x p_x \rangle^2 = \langle J_x \rangle^2 . \tag{2.222}$$

If we compare the latter equation with equation (2.212) we get:

$$\varepsilon_x = \langle J_x \rangle . \tag{2.223}$$

Thus the horizontal emittance of a bunch is simply the average of the horizontal actions over every particle in the bunch. The latter derivation is consistent with the fact that both the emittance and the action are conserved under linear symplectic transport.

So now, equations (2.219), (2.220), (2.221) can be rewritten as:

$$\begin{aligned} \langle x^2 \rangle &= \beta_x \varepsilon_x \,, \\ \langle x p_x \rangle &= -\alpha_x \varepsilon_x \,, \\ \langle p_x^2 \rangle &= \gamma_x \varepsilon_x \,. \end{aligned}$$

Therefore, the size of the bunch is given by the Twiss parameters combined with the emittance. The Twiss parameters give the local variation in the size of the bunch, while the emittance represents an *invariant* size of the bunch.

Geometric and Normalized Emittance

In these considerations regarding the emittance of a beam we have assumed that the reference momentum P_0 remains fixed, which is appropriate for damping rings (accelerating cavities in damping rings exist to replenish the energy lost by particles due to synchrotron radiation). In a linear accelerator, consisting of a number of accelerating cavities, the energy of each particle is increased significantly. Therefore each cavity affects the energy deviation δ of each particle. When this energy deviation becomes large enough, then the linear approximations on which the derivation of the transport matrices was based are no longer valid.

To maintain δ at a small value in a linac, we can adjust the reference momentum. The transverse coordinates x and y are independent of the reference momentum. The conjugate momentum p_x though is defined as:

$$p_x = \frac{\gamma m \dot{x} + q A_x}{P_0} \,, \tag{2.224}$$

where $\dot{x}$ is the transverse velocity, γ is the relativistic factor for the particle, m the rest mass of the particle, q the electric charge and A_x the horizontal component of the magnetic vector potential. A change in the reference momentum, will result in the following transformations:

$$P_0 \mapsto P_0' \,, \qquad x \mapsto x \,, \qquad p_x \mapsto \frac{P_0}{P_0'} p_x \,. \tag{2.225}$$

The transformations the dynamical variables undergo in equation (2.225) are **not** symplectic. As a result the emittance of the beam will not be

conserved under a change in reference momentum. We can however define a new quantity that is conserved under changes in reference momentum. We observe from equations (2.225) and (2.212) that the horizontal emittance transforms as:

$$P_0 \rightarrow P_0', \qquad \varepsilon_x \rightarrow \varepsilon_x' = \frac{P_0}{P_0'}\varepsilon_x \Rightarrow P_0'\varepsilon_x' = P_0\varepsilon_x \,. \tag{2.226}$$

Since $P_0 = \beta_0\gamma_0 mc$ we can write:

$$\beta_0'\gamma_0'\varepsilon_x' = \beta_0\gamma_0\varepsilon_x \,. \tag{2.227}$$

This new quantity is called **normalized emittance**, $\varepsilon_{x,N}$ and is defined as:

$$\varepsilon_{x,N} = \beta_0\gamma_0\varepsilon_x \,. \tag{2.228}$$

Equation (2.227) shows that the normalized emittance is conserved under a change in reference momentum [4].

The normalized vertical emittance is defined in the same way as the normalized horizontal emittance and therefore is conserved under a change in the reference momentum. Often, the emittance ε_x described in equation (2.212) is referred to as the *geometric emittance* to distinguish it from the normalized emittance defined by equation (2.228). It is important to note here that during acceleration of particles in a linac and scaling of the reference momentum with average beam energy, the geometric emittance varies in inverse proportion to the beam energy:

$$\varepsilon_x \propto \frac{1}{\beta_0\gamma_0} \,. \tag{2.229}$$

This effect is known as **adiabatic damping**. The result of adiabatic damping is that, for fixed beta functions, the size of a bunch decreases as the energy of the bunch is increased.

Emittance Conservation - Liouville's Theorem

It can be shown that if the transfer matrix is symplectic then the phase space area (a plot of the conjugate momentum vs the corresponding coordinate) of an element of the system (in our case a particle) is conserved. This

[4] For ultra-relativistic particles, $\beta_0' \approx \beta_0 \approx 1$, so the normalised emittance is often written simply as: $\varepsilon_{x,N} = \gamma\varepsilon_x$

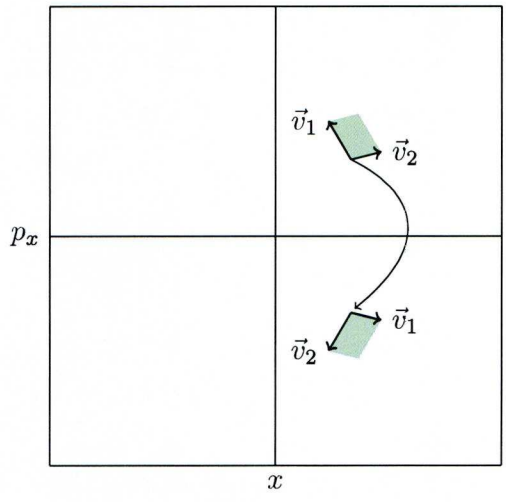

Figure 2.5: Evolution of a phase-space element (a plot of the conjugate momentum vs the corresponding coordinate) defined by vectors $\vec{v}_1$ and $\vec{v}_2$. Under symplectic transport, the area of the phase-space element is conserved.

conservation applies for all systems described by a Hamiltonian even if the dynamics are nonlinear and this is proved by Liouville's Theorem.

Liouville's theorem is a consequence of symplecticity. If we consider a phase-space area defined by vectors $\vec{v}_1$ and $\vec{v}_2$, then for that phase-space element we have:

$$A = |\vec{v}_1 \times \vec{v}_2| = \vec{v}_1^T \cdot S \cdot \vec{v}_2 \,. \tag{2.230}$$

As the system evolves over a period of time, t, the following transformations occur:

$$\vec{v}_1 \mapsto \vec{v}_1' = M(t) \cdot \vec{v}_1 \quad \text{and} \quad \vec{v}_2 \mapsto \vec{v}_2' = M(t) \cdot \vec{v}_2 \,. \tag{2.231}$$

The area of the "time-evolved" phase-space element is:

$$\begin{aligned} A' &= \vec{v}'^{T_1} \cdot S \cdot \vec{v}_2' \\ &= \vec{v}'^{T_1} \cdot M^T(t) \cdot S \cdot M(t) \cdot \vec{v}_2 \,. \end{aligned} \tag{2.232}$$

Since $M(t)$ is symplectic, we have:

$$M^T(t) \cdot S \cdot M(t) = S \,, \tag{2.233}$$

and therefore:

$$A' = \vec{v}_1'^T \cdot S \cdot \vec{v}_2 = A\,, \tag{2.234}$$

the area of the phase-space element is conserved during the motion of the system.

2.2.2 Radiation

Charged particles that undergo acceleration emit radiation. In the case of relativistic particles this phenomenon is called synchrotron radiation. In a storage ring the radiation emission occurs mainly in the bending fields of the dipole magnets. It should be noted that synchrotron radiation is a non-symplectic effect, analogous to a frictional force that steadily damps the motion of a harmonic oscillator.

The particles lose energy through the emission of synchrotron radiation and this loss has to be compensated appropriately in the RF cavities, so that the combination of loss and replenishment of energy leads to some equilibrium value for the emittances. The majority of photons emitted due to synchrotron radiation are located within a cone of angle $1/\gamma$ around the instantaneous direction of motion of the particle. For ultra-relativistic particles, γ is very large, so that the direction of particle motion and the direction of radiation emission are almost aligned. Thus, the direction of motion is not affected by the "recoil" effect. The total momentum of the particles changes with the emission of radiation as:

$$p' = p - dp \approx p\left(1 - \frac{dp}{P_0}\right), \tag{2.235}$$

where dp is the momentum of the radiation, P_0 is the reference momentum and we assume that the total momentum of the particle is close to the reference momentum:

$$p \approx P_0 . \tag{2.236}$$

Substituting this into the expression for the vertical betatron action:

$$2J_y = \gamma_y y^2 + 2\alpha_y y p_y + \beta_y p_y^2 , \tag{2.237}$$

we find the change in the action resulting from the emission of radiation:

$$dJ_y = -(\alpha_y y p_y + \beta_y p_y^2)\frac{dp}{P_0} . \tag{2.238}$$

If we average for all particles in the beam we can find the change in the vertical emittance of the beam:

$$d\varepsilon_y = \langle dJ_y \rangle = -\varepsilon_y \frac{dp}{P_0} , \tag{2.239}$$

where $\langle yp_y \rangle = -\alpha_y \varepsilon_y$, $\langle p_y^2 \rangle = \gamma_y \varepsilon_y$ and $\beta_y \gamma_y - \alpha_y^2 = 1$. Assuming that the non-symplectic effects, such as the radiation in the case at hand, are slow, we can write:

$$\frac{d\varepsilon_y}{dt} = -\frac{\varepsilon_y}{T_0} \oint \frac{dp}{P_0} \approx -\frac{U_0}{E_0 T_0} \varepsilon_y \,, \tag{2.240}$$

where T_0 is the revolution period and U_0 is the energy loss in one turn. For an ultra-relativistic particle with the nominal energy, traveling at around the closed orbit, we can calculate the energy loss per turn by integrating the radiation power around the ring:

$$U_0 = \oint P_\gamma dt = \oint P_\gamma \frac{ds}{c} \,. \tag{2.241}$$

where P_γ is the the power radiated by a particle [65]:

$$P_\gamma = \frac{C_\gamma}{2\pi} c \frac{E^4}{\rho^2} \,, \tag{2.242}$$

with

$$C_\gamma = \frac{4\pi}{3} \frac{r_c}{(mc^2)^3} \approx 8.8846 \times 10^{-5} \, \mathrm{m/GeV^3} \,. \tag{2.243}$$

Then, the damping time is defined as:

$$\tau_y = 2 \frac{E_0}{U_0} T_0 \,, \tag{2.244}$$

and the evolution of the vertical emittance is:

$$\varepsilon_y(t) = \varepsilon_y(0) \exp\left(-2 \frac{t}{\tau_y}\right) . \tag{2.245}$$

Through the process of radiation emission the particles lose longitudinal and transverse momentum. In the RF cavity, where the lost energy of the particles has to be restored, the particles see an accelerating electric field parallel to the closed orbit, therefore the increase in the particle's momentum is parallel to the closed orbit. This leads to a reduction in the amplitude of the betatron oscillation of the particle; however the vertical momentum p_y is not changed.

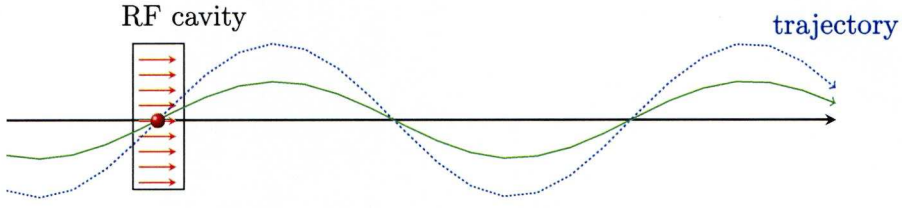

Figure 2.6: Acceleration in an RF cavity. The particles see an accelerating electric field parallel to the closed orbit, therefore the increase in the particle's momentum is parallel to the closed orbit. This leads to a reduction in the amplitude of the betatron oscillation of the particle; however the vertical momentum p_y is not changed.

2.2.2.1 Equilibrium Emittance

The reason that the emittances do not damp to zero, is due to the fact that radiation is not a classical process. Radiation is emitted in discrete units (photons) and this induces noise in the beam. The effect of the noise is to increase the emittance of the beam. Eventually, an equilibrium is reached, determined by a balance between the radiation damping and the quantum excitation.

In the presence of dispersion, the action becomes:

$$2J_x = \gamma\tilde{x}^2 + 2\alpha_x\tilde{x}\tilde{p}_x + \beta_x\tilde{p}_x^2\,, \tag{2.246}$$

where

$$\tilde{x} = x - \eta_x\delta \quad \text{and} \quad \tilde{p}_x = p_x - \eta_{p_x}\delta\,. \tag{2.247}$$

After the emission of radiation carrying momentum dp, we have:

$$\delta \mapsto \delta - \frac{dp}{P_0}\,, \quad \tilde{x} \mapsto \tilde{x} + \eta_x\frac{dp}{P_0}\,, \quad \tilde{p}_x \mapsto \tilde{p}_x\left(1 - \frac{dp}{P_0}\right) + \eta_{p_x}(1-\delta)\frac{dp}{P_0}\,. \tag{2.248}$$

The change in the action then becomes:

$$J_x \mapsto J_x + dJ_x\,. \tag{2.249}$$

The change in the horizontal action is:

$$dJ_x = -w_1 \frac{dp}{P_0} + w_2 \left(\frac{dp}{P_0}\right)^2$$
$$\therefore \quad \frac{dJ_x}{dt} = -w_1 \frac{1}{P_0}\frac{dp}{dt} + w_2 \frac{dp}{P_0^2}\frac{dp}{dt}\,, \tag{2.250}$$

where in the limit $\delta \to 0$:

$$w_1 = \alpha_x x p_x + \beta_x p_x^2 - \eta_x(\gamma_x x + \alpha_x p_x) - \eta_{p_x}(\alpha_x x + \beta_x p_x) \tag{2.251}$$

and

$$w_2 = \frac{1}{2}(\gamma_x \eta_x^2 + 2\alpha_x \eta_x \eta_{p_x} + \beta_x \eta_{p_x}^2) - (\alpha_x \eta_x + \beta_x \eta_{p_x})p_x + \frac{1}{2}\beta_x p_x^2\,. \tag{2.252}$$

If we take the limit $dp \to 0$ in the limit of a small interval time $dt \to 0$, then:

$$\frac{dJ_x}{dt} \approx -w_1 \frac{1}{P_0}\frac{dp}{dt} \approx -w_1 \frac{P_\gamma}{P_0 c}\,. \tag{2.253}$$

Writing the time evolution of the action as equation (2.250) and taking into account the quantization of synchrotron radiation, we get:

$$\frac{dJ_x}{dt} = -w_1 \dot{N} \frac{\langle u \rangle}{P_0 c} + w_2 \dot{N} \frac{\langle u^2 \rangle}{P_0^2 c^2}\,, \tag{2.254}$$

where u is the photon energy, and $\dot{N}$ is the number of photons emitted per unit time. Averaging around the circumference of the ring, the quantum excitation term of equation (2.254) becomes:

$$w_2 \dot{N} \frac{\langle u^2 \rangle}{P_0^2 c^2} \approx \frac{1}{C_0} \oint w_2 \dot{N} \frac{\langle u^2 \rangle}{P_0^2 c^2} ds\,. \tag{2.255}$$

With the help of equation (2.252) for w_2 and the assumption that $x \ll \eta_x$ and $p_x \ll \eta_{p_x}$, the excitation term is written as:

$$w_2 \dot{N} \frac{\langle u^2 \rangle}{P_0^2 c^2} \approx \frac{1}{2E_0^2 C_0} \oint \mathcal{H} \dot{N} \langle u^2 \rangle ds\,, \tag{2.256}$$

where

$$\mathcal{H} = \gamma_x \eta_x^2 + 2\alpha_x \eta_x \eta_{p_x} + \beta_x \eta_{p_x}^2\,. \tag{2.257}$$

Including both damping and excitation terms and averaging over all

particles in the bunch, the horizontal emittance evolves as:

$$\frac{d\varepsilon_x}{dt} = -\frac{2}{\tau_x}\varepsilon_x + \frac{1}{2E_0^2 C_0}\oint \mathcal{H}\dot{N}\langle u^2\rangle ds\,. \tag{2.258}$$

From quantum radiation theory we know that:

$$\dot{N}\langle u^2\rangle = 2C_q\gamma^2 E_0 \frac{P_\gamma}{\rho}\,, \tag{2.259}$$

where the "quantum constant" C_q is:

$$C_q = \frac{55}{32\sqrt{3}}\frac{\hbar}{mc} \approx 3.832 \times 10^{-13}\,\mathrm{m}\,. \tag{2.260}$$

The time evolution of the horizontal emittance then becomes:

$$\frac{d\varepsilon_x}{dt} = -\frac{2}{\tau_x}\varepsilon_x + \frac{2}{j_x}\tau_x C_q\gamma^2\frac{I_5}{I_2}\,, \tag{2.261}$$

where I_2, I_5 are the second and fifth synchrotron radiation integrals respectively, defined by:

$$I_2 = \oint \frac{ds}{\rho^2}\,, \qquad I_5 = \oint \frac{\mathcal{H}}{|\rho|^3}ds\,, \tag{2.262}$$

and j_x is the horizontal damping partition number, given by:

$$j_x = 1 - \frac{I_4}{I_2}\,. \tag{2.263}$$

The fourth synchrotron radiation integral I_4 contains the effects of the variation in path length and field strength with x:

$$I_4 = \oint \frac{\eta_x}{\rho}\left(\frac{1}{\rho^2} + 2k_1\right) ds\,. \tag{2.264}$$

The equilibrium emittance can be calculated from the condition:

$$\left.\frac{d\varepsilon_x}{dt}\right|_{\varepsilon_x=\varepsilon_0} = 0 \quad \therefore \quad \frac{2}{\tau_x}\varepsilon_0 = \frac{2}{j_x\tau_x}C_q\gamma^2\frac{I_5}{I_2}\,. \tag{2.265}$$

Consequently, we get:

$$\varepsilon_0 = C_q\gamma^2\frac{I_5}{j_x I_2}\,. \tag{2.266}$$

The equilibrium emittance is determined by the beam energy, the lattice

functions in the dipoles and the bending radius; it is sometimes called the **natural emittance** of the lattice, since it is the horizontal emittance that will be achieved in the limit of zero bunch charge; as the current is increased, particle interactions can increase the horizontal emittance above the equilibrium value determined by radiation effects.

2.2.2.2 Theoretical Lower Limit of Vertical Emittance

In a planar storage ring, in the absence of alignment, steering and coupling errors, the equilibrium vertical emittance according to the previous analysis should be zero. However, even in such an ideal case, the equilibrium vertical emittance is larger than zero; the quantum excitation sets a limit on the vertical emittance that can be achieved in a storage ring. The photons emitted at the $1/\gamma$ angle exert a recoil effect perpendicular to the direction of particle motion, exciting vertical betatron oscillations.

The fundamental lower limit on the vertical emittance is given by [43]:

$$\varepsilon_y = \frac{13}{55}\frac{C_q}{j_x I_2}\oint \frac{\beta_y}{|\rho^3|}ds\,. \tag{2.267}$$

This fundamental lower limit of the equilibrium emittance is typically of the order of 0.1 pm, assuming the betatron function and the bending radius to be of similar order. This value is very small compared with the actually achieved vertical emittances in real accelerators. That is due to the fact that the observed vertical emittance is affected by the presence of cross-plane betatron coupling and vertical steering errors which lead to a small vertical dispersion and consequently, to a small yet non-zero vertical emittance.

2.3 Lattice Imperfections

Any accelerator system is bound to have deviations from the design values for a number of crucial parameters, like the location of magnets (physical coordinates) and the intensity of the applied fields. Understanding and compensating for machine errors is a significant challenge in modern accelerators, where the structures are very large, involving hundreds or even thousands of magnets. For such machines to work at the design specifications regarding performance, these errors have to be identified and reduced, usually to a very high level of precision.

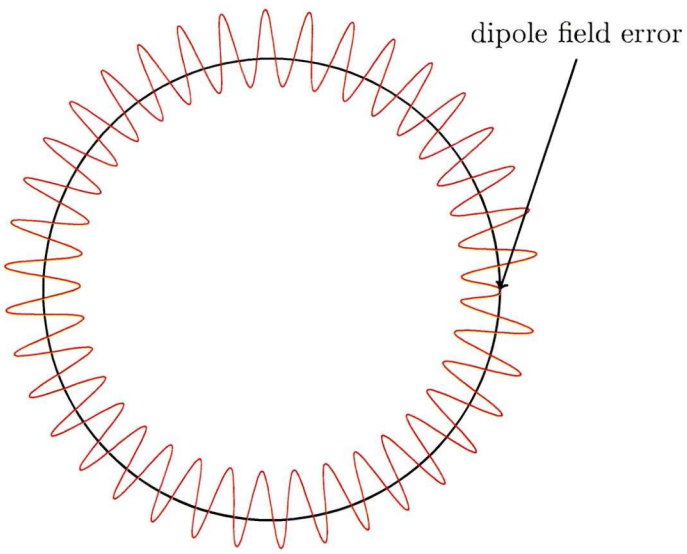

Figure 2.7: Closed orbit distortion. A "kick" occurs in the closed orbit at the location of the dipole field error.

2.3.1 Closed Orbit Distortion (COD)

The design magnet positions and strengths ensure that particles with the reference momentum initially on the reference trajectory will continue to follow that trajectory throughout the accelerator structure. The steering of the beam in the presence of dipole fields leads to a curved reference trajectory. In the event of a dipole field error (i.e. any deviation from the design strength values), particles will be steered away from the reference trajectory at the point of the error. Dipole field errors can happen due to dipole magnets that do not have exactly the right strength or have some rotation about the reference trajectory. Dipole field errors also occur in the case of quadrupole magnets being misaligned horizontally or vertically. With respect to the center of a quadrupole magnet, the field has the following components:

$$B_x = b_2 \frac{y}{r_0}\,, \qquad B_y = b_2 \frac{x}{r_0}\,, \qquad B_z = 0\,. \tag{2.268}$$

If the axis of the quadrupole is displaced vertically by a distance of Δy from the reference trajectory, then we can find the field with respect to the reference trajectory by making the substitution $y \mapsto y - \Delta y$ in equation

(2.268):

$$B_x = b_2\frac{y}{r_0} - b_2\frac{\Delta y}{r_0}, \qquad B_y = b_2\frac{x}{r_0}, \qquad B_z = 0\,. \tag{2.269}$$

A **closed orbit** is defined as the trajectory of a particle that closes on itself after one turn. Clearly, in a storage ring the closed orbit must exist in order to store beam. The closed orbit, in the presence of field errors is not the reference trajectory, but it can still be established and this is usually the first task in beam commissioning a new machine.

An expression for the closed orbit can be derived, taking into account only dipole horizontal field errors, e.g. from a vertical alignment error on a quadrupole magnet. If one such error of integrated strength $B_x\Delta s$ is present, then the change in vertical momentum for a particle crossing the location of the error is:

$$\Delta p_y = \frac{q}{P_0}B_x\Delta s = \Delta\theta_y\,, \tag{2.270}$$

where q is the charge of the particle and P_0 is the reference momentum. Supposing that there is no coupling in the ring, the dipole field error, being horizontal, will have an effect only on the vertical direction. The position and momentum of a particle can be written in terms of the lattice functions and the action-angle variables:

$$y = \sqrt{2\beta_y J_y}\cos\phi_y\,, \tag{2.271}$$

$$p_y = \sqrt{\frac{2J_y}{\beta_y}}(\sin\phi_y + \alpha_y\cos\phi_y)\,. \tag{2.272}$$

If the total phase advance over one turn of the storage ring is μ_y, then the conditions for the closed orbit to exist can be written as:

$$\sqrt{2\beta_y J_y}\cos(\phi_{y0} + \mu_y) = \sqrt{(2\beta_y J_{y0})}\cos\phi_{y0}\,, \tag{2.273}$$

and

$$\sqrt{\frac{2J_y y_0}{\beta_y}}[\sin(\phi_{y0} + \mu_y) + \alpha_y\cos(\phi_{y0} + \mu_y)] + \Delta\theta_y \;=\; \sqrt{\frac{2J_y y_0}{\beta_y}}(\sin\phi_{y0} + \alpha_y\cos\phi_{y0})\,, \tag{2.274}$$

following equations (2.271) and (2.272), where the Twiss parameters are to be evaluated at position $s = 0$. Here J_y and ϕ_{y0} are the action and angle for a particle on the closed orbit.

The solution of equations (2.273) and (2.274) gives:

$$J_{y0} = \frac{\beta_y \Delta\theta^2}{8 \sin^2 \pi\nu_y}, \qquad \phi_{y0} = \pi\nu_y \,, \tag{2.275}$$

where $\nu_y = \mu_y / 2\pi$ is the vertical tune. Immediately apparent from equation (2.275) is that if the tune is an integer number then the action becomes infinite, therefore the closed orbit solution no longer exists. The dependence of the action on the beta function, also indicates that at positions where the latter obtains large values the more sensitive the lattice becomes to errors.

Combining equations (2.272) and (2.275) we get:

$$y_{co}(s) = \frac{\sqrt{\beta_y(0)\beta_y(s)}}{2 \sin \pi\nu_y} \Delta\theta_y \cos\left(\pi\nu_y + \mu_y(s)\right), \tag{2.276}$$

where $\mu_y(s)$ is the phase advance from $s = 0$ to s and the error is located at $s = 0$. In all likelihood more than one dipole field error will be present in the machine. Assuming that the closed orbit distortion is not too large, we can express the combined effect of these errors as the sum of closed orbit distortions caused by each error separately. Adding up all the steering errors in the ring, leads to the expression:

$$y_{co}(s) = \frac{\sqrt{\beta_y(s)}}{2 \sin \pi\nu_y} \oint_0^{C_0} \sqrt{\beta_y(s')} \frac{d\theta}{ds'} \cos\left(\pi\nu_y + \mu_y(s, s')\right) ds' \,, \tag{2.277}$$

where C_0 is the length of the reference trajectory, and $\mu_y(s, s')$ is the phase advance from s' to s along the reference trajectory.

2.3.1.1 Orbit Amplification Factor

It is important to be able to determine, especially in the design phase of a machine, what will be its sensitivity to these errors. This knowledge defines the specifications regarding alignment tolerances and the necessary correction systems.

Real machines usually have a large number of field and alignment errors. Furthermore these errors are also of unknown location and magnitude. In the

absence therefore of a detailed description of the errors present, statistical methods are employed to determine the most probable equilibrium orbit. An expectation value for the orbit distortion can be calculated by the root mean square value of equation (2.277).

For a quadrupole of integrated focusing strength $k_1 L$, vertically misaligned from the reference trajectory by ΔY, the steering is:

$$\frac{d\theta}{ds} = (k_1 L)\Delta Y \,. \tag{2.278}$$

The square of the closed orbit distortion can then be written:

$$\begin{aligned} \frac{y_{co}^2(s)}{\beta_y(s)} &= \frac{1}{4\sin^2 \pi\nu_y} \oint_0^{C_0} \oint_0^{C_0} \sqrt{\beta_y(s')\beta_y(s'')}(k_1 L)_{s'}(k_1 L)_{s''}\Delta Y_{s'}\Delta Y_{s''} \ldots \\ &\quad \ldots \cos\left(\pi\nu_y + \mu_y(s;s')\right)\cos\left(\pi\nu_y + \mu_y(s;s'')\right) ds' ds'' \,. \end{aligned} \tag{2.279}$$

Averaging over many random alignment errors and assuming that the quadrupole alignment errors are uncorrelated, we get:

$$\left\langle \frac{y_{co}^2(s)}{\beta_y(s)} \right\rangle = \frac{\langle \Delta Y \rangle}{8\sin \pi\nu_y} \sum_{\text{quads}} \beta_y (k_1 L)^2 \,. \tag{2.280}$$

The latter equation can also be written as:

$$\sqrt{\langle y_{co}^2 \rangle} \approx A\sqrt{\langle \Delta Y^2 \rangle} \,, \tag{2.281}$$

where A, called the **amplification factor** is equal to:

$$A = \frac{\langle \beta_y \rangle}{8\sin^2 \pi\nu_y} \sum_{\text{quads}} \beta_y (k_1 L)^2 \,. \tag{2.282}$$

2.3.2 Vertical Dispersion and Betatron Coupling

In a storage ring, the major causes of vertical emittance growth are:

- Vertical dispersion;
- Betatron coupling;
- Closed orbit distortion, which effectively leads to the previous phenomena:
  - vertical steering generates vertical dispersion;
  - an off-centered beam in a sextupole effectively "sees" a skew quadrupole field; this leads to betatron coupling and couples horizontal dispersion into the vertical plane.

Vertical dispersion couples longitudinal and vertical motion while betatron coupling leads to coupling between horizontal and vertical motion. The dominant causes of residual vertical dispersion and betatron coupling are the following magnet alignment errors:

- tilts of the dipole magnets around the beam axis;
- tilts of the quadrupole magnets around the beam axis;
- vertical alignment errors of the quadrupole magnets;
- vertical alignment errors of the sextupoles.

To estimate therefore the alignment tolerances of the magnetic components in a storage ring, it is necessary to have a relation between these quantities and the vertical emittance. To this end, the linear imperfections of magnetic components (misalignments, errors in strength) have to be related to both vertical dispersion and betatron coupling. Here, we outline the derivation of such relations [66]. Using the theory described in section 2.1.4.2 we can make estimates in the design phase of any accelerator system.

The emittance may be defined as the betatron action averaged over all particles in the beam:

$$\varepsilon_x = \langle J_x \rangle \quad \text{and} \quad \varepsilon_y = \langle J_y \rangle \,. \tag{2.283}$$

Using the fixed point solutions of equation (2.193), we get:

$$\varepsilon_x = \frac{1}{2}\left(1 + \frac{1}{\sqrt{1+\kappa_-^2/\Delta\omega^2}}\right)\varepsilon_0 \quad \text{and} \quad \varepsilon_y = \frac{1}{2}\left(1 - \frac{1}{\sqrt{1+\kappa_-^2/\Delta\omega^2}}\right)\varepsilon_0 \,. \tag{2.284}$$

It is now sufficient to find an expression for $\kappa/\Delta\omega$ in terms of the lattice functions, magnet parameters and rms alignment. Starting with:

$$\frac{\kappa e^{i\chi}}{\Delta\omega} = \frac{1}{2\pi\Delta\nu}\int_0^C e^{i(\mu_x-\mu_y)} k_s \sqrt{\beta_x\beta_y}\, ds \,, \tag{2.285}$$

taking the modulus squared, and using for sextupoles $k_s = k_2\Delta y$, we get:

$$\left(\frac{\kappa}{\Delta\omega}\right)^2 \approx \frac{\langle \Delta Y_s^2\rangle}{\pi^2\Delta\nu^2} \sum_{\text{sextupoles}} \beta_x\beta_y (k_2 l)^2 \,. \tag{2.286}$$

In order to establish a relationship between the vertical dispersion and the vertical emittance, we can start by writing the equation of motion for the trajectory of a particle with momentum P:

$$\frac{d^2y}{ds^2} = \frac{e}{P}B_x \,. \tag{2.287}$$

For a small energy deviation δ, the relationship between P and the reference momentum P_0 is:

$$P \approx (1+\delta)P_0 \,. \tag{2.288}$$

The horizontal magnetic field to first order is:

$$B_x \approx B_{0x} + y\frac{\partial B_x}{\partial y} + x\partial B_x \partial x \,. \tag{2.289}$$

Considering a particle following an off-momentum closed orbit, so that:

$$y = \eta_y\delta \quad \text{and} \quad x = \eta_x\delta \,, \tag{2.290}$$

we consequently find:

$$\frac{d^2\eta_y}{ds^2} - k_1\eta_y \approx -k_{0s} + k_{1s}\eta_x \,. \tag{2.291}$$

Equation (2.291) is similar to the "equation of motion" for the closed orbit:

$$\frac{d^2 y_{co}}{ds^2} - k_1 y_{co} \approx -k_{0s} + k_{1s} x_{co} \,. \tag{2.292}$$

We can therefore generalise the relationship between the closed orbit distortion and the quadrupole alignment errors, to apply to the dispersion:

$$\left\langle \frac{\eta_y^2(s)}{\beta_y(s)} \right\rangle = \frac{\langle \Delta Y_Q^2 \rangle}{8 \sin^2 \pi \nu_y} \sum_{quads} \beta_y (k_1 L)^2 + \frac{\langle \Delta Y_S^2 \rangle}{8 \sin^2 \pi \nu_y} \sum_{sexts} \eta_x^2 \beta_y (k_2 L)^2 \,. \tag{2.293}$$

It is assumed that the skew dipole fields come from vertical alignment errors on the quadrupoles with mean square $\langle \Delta Y_Q^2 \rangle$, the skew quadrupoles fields come from the vertical alignment errors on the sextupoles, with mean square $\langle \Delta Y_S^2 \rangle$ and that all the alignment errors are uncorrelated.

To relate the vertical emittance to the vertical dispersion, we use equations (2.266) and

$$I_{5y} = \oint \frac{\mathcal{H}_y}{|\rho|^3} ds \tag{2.294}$$

which can be transformed to:

$$I_{5y} = \langle \mathcal{H}_y \rangle \oint \frac{1}{|\rho|^3} ds = \langle \mathcal{H}_y \rangle I_3 \,. \tag{2.295}$$

Hence, the vertical emittance can be written as:

$$\varepsilon \approx C_q \gamma^2 \langle \mathcal{H}_y \rangle \frac{I_3}{j_y I_2} \,, \tag{2.296}$$

where j_y is the vertical damping partition number and if we express the right hand side in terms of the natural rms energy spread:

$$\sigma_\delta^2 = C_q \gamma^2 \frac{I_3}{j_y I_2} \,, \tag{2.297}$$

we obtain:

$$\varepsilon_y \approx \frac{j_z}{j_y} \langle \mathcal{H}_y \rangle \sigma_\delta^2 \,, \tag{2.298}$$

where j_z is the longitudinal damping partition number, given by:

$$j_z = 2 + \frac{I_4}{I_2} \,. \tag{2.299}$$

In a planar ring, where the dispersion is zero (in the absence of errors) in the bending magnets we have $I_{4y} \ll I_2$ and $j_y \approx 1$. Noticing the similarity between equations (2.257) and (2.246) we can write:

$$\eta_y = \sqrt{\beta_y \mathcal{H}_y} \cos \phi_{\eta y} \quad \therefore \quad \left\langle \frac{\eta_y^2}{\beta_y} \right\rangle = \frac{1}{2} \langle \mathcal{H}_y \rangle \,. \tag{2.300}$$

Therefore, we get:

$$\varepsilon_y \approx 2 \frac{j_z}{j_y} \left\langle \frac{\eta_y^2}{\beta_y} \right\rangle \sigma_\delta^2 \,. \tag{2.301}$$

Including the contribution of quadrupole tilts, equation (2.293) becomes:

$$\begin{aligned} \left\langle \frac{\eta_y^2(s)}{\beta_y(s)} \right\rangle &= \frac{\langle \Delta Y_Q^2 \rangle}{8 \sin^2 \pi \nu_y} \sum_{quads} \beta_y (k_1 L)^2 + \frac{\langle \Delta \Theta_Q^2 \rangle}{8 \sin^2 \pi \nu_y} \sum_{quads} \eta_x^2 \beta_y (k_1 L)^2 \\ &+ \frac{\langle \Delta Y_S^2 \rangle}{8 \sin^2 \pi \nu_y} \sum_{sexts} \eta_x^2 \beta_y (k_2 L)^2 \,. \end{aligned} \tag{2.302}$$

Finally, we must add the vertical emittance generated by betatron coupling, according to equation (2.284), where:

$$\left(\frac{k}{\Delta \omega} \right)^2 \approx \frac{\langle \Delta Y_s^2 \rangle}{4 \pi^2 \Delta \nu^2} \sum_{sexts} \beta_x \beta_y (k_2 l)^2 + \frac{\langle \Delta \Theta_Q^2 \rangle}{4 \pi^2 \Delta \nu^2} \sum_{quads} \beta_x \beta_y (k_1 l)^2 \,. \tag{2.303}$$

These formulae will be compared to simulation results for various lattices in section 4.2.

2.3.3 Computation of Equilibrium Distribution

When betatron coupling is present things get more complicated and one turns to numerical methods for computing the equilibrium emittances in practical cases. Two methods have been widely used for this purpose: Chao's method [13] and the envelope method [33]. Chao's method focuses on the evaluation of the beam distribution parameters taking into account the effects of betatron coupling; however it provides little "physics insight". The envelope method, on the other hand (implemented in the code AT, Appendix B) is more enlightening in that respect and a detailed description of it is given here.

2.3.3.1 The Ohmi Envelope Calculation

The full 6×6 sigma matrix has the form:

$$\Sigma = \begin{pmatrix} \langle x^2 \rangle & \langle x p_x \rangle & \langle xy \rangle & \langle x p_y \rangle & \langle xz \rangle & \langle x\delta \rangle \\ \langle p_x x \rangle & \langle p_x^2 \rangle & \langle p_x y \rangle & \langle p_x p_y \rangle & \langle p_x z \rangle & \langle p_x \delta \rangle \\ \langle yx \rangle & \langle y p_x \rangle & \langle y^2 \rangle & \langle y p_y \rangle & \langle yz \rangle & \langle y\delta \rangle \\ \langle p_y x \rangle & \langle p_y p_x \rangle & \langle p_y y \rangle & \langle p_y^2 \rangle & \langle p_y z \rangle & \langle p_y \delta \rangle \\ \langle zx \rangle & \langle z p_x \rangle & \langle zy \rangle & \langle z p_y \rangle & \langle z^2 \rangle & \langle z\delta \rangle \\ \langle \delta x \rangle & \langle \delta p_x \rangle & \langle \delta y \rangle & \langle \delta p_y \rangle & \langle \delta z \rangle & \langle \delta^2 \rangle \end{pmatrix} . \tag{2.304}$$

A more compact form of matrix Σ is:

$$\Sigma_{ij} = \langle x_i x_j \rangle , \quad \text{where} \quad \vec{x}^T = \begin{pmatrix} x & p_x & y & p_y & z & \delta \end{pmatrix} . \tag{2.305}$$

The brackets $\langle\rangle$ indicate the average over all particles in the bunch. In the general case, betatron coupling will be present and therefore the sigma matrix will not be block diagonal.

We have seen that from the eigenvalues of $\Sigma \cdot S$ we can calculate the emittances. We therefore need to know how the sigma matrix transforms. Since it is written as the product of the phase-space coordinates averaged over a bunch, we have:

$$\begin{pmatrix} x \\ p_x \end{pmatrix} \mapsto M \cdot \begin{pmatrix} x \\ p_x \end{pmatrix} \tag{2.306}$$

$$\Sigma \mapsto M \cdot \Sigma \cdot M^T . \tag{2.307}$$

Since S is a constant matrix amd M is symplectic, we can write:

$$\begin{aligned} \Sigma \cdot S &\mapsto M \cdot \Sigma \cdot M^T \cdot S \\ \Sigma \cdot S &\mapsto M \cdot \Sigma \cdot S \cdot M^{-1} . \end{aligned} \tag{2.308}$$

The eigenvalues of $\Sigma \cdot S$ are conserved under a transformation of this type. Therefore, the bunch emittance is conserved under *linear symplectic* transport.

An invariant or "matched" distribution is one that satisfies:

$$\Sigma \mapsto M \cdot \Sigma \cdot M^T = \Sigma . \tag{2.309}$$

In an electron storage ring, we know that radiation effects will damp the emittances to some equilibrium values. It is possible to apply the concept of the matched distribution to find the equilibrium emittance values. However two modifications need to be made to the single-turn transformation of the sigma matrix to account for radiation effects:

- The matrix M will no longer be symplectic; this accounts for radiation damping.
- As well as first-order terms in the transformation, represented by the matrix M, we now also have zeroth-order terms. These terms correspond to quantum excitation.

The condition for a matched distribution is then written as:

$$\Sigma = M \cdot \Sigma \cdot M^T + D , \tag{2.310}$$

where M and D are constant non-symplectic matrices representing the first-order and zeroth-order terms in the single-turn transformation, respectively.

Equation (2.310) is sufficient to determine the sigma matrix uniquely. So, the envelope method for computing the equilibrium emittances in a storage ring can be described as a three-step process:

- Find the first order terms M and zeroth-order terms D in the single turn transformation (2.309).
- Use the matching condition of equation (2.310).

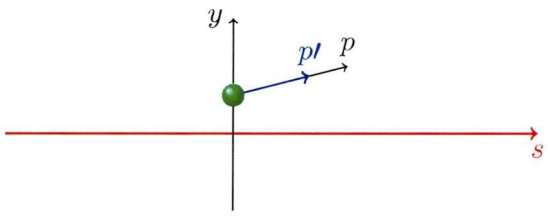

Figure 2.8: Momentum change in a particle emitting a photon

- Find the equilibrium emittances from the eigenvalues of $\Sigma \cdot S$.

It should be noted that since the transfer matrix M is not symplectic, the emittances are no longer conserved and we expect to find a different emittance at each point around the ring. However, if the radiation effects are small, the variations in the emittance will be small.

As an example of the transformation of the matrices M and D we can look at the case of a thin "slice" of a dipole; this case is important because, in most storage rings, radiation effects are only significant in dipoles. "Complete" dipoles can be constructed by concatenating the maps for a number of slices.

Having the map for a thin slice of dipole, one simply has to concatenate the maps for all the elements in the ring in order to construct the map for complete turn starting at any given point.

The transformation of the phase-space variables in the emission of radiation carrying momentum dp is:

$$\begin{array}{ccccc} & x \mapsto x & & y \mapsto y & & s \mapsto s \\ p_x \mapsto \left(1 - \dfrac{dp}{P_0}\right) p_x & & p_y \mapsto \left(1 - \frac{dp}{P_0}\right) p_y & & \delta \mapsto \left(1 - \dfrac{dp}{P_0}\right) , \end{array} \quad (2.311)$$

where P_0 is the reference momentum. For the transformation of matrices M and D, we need to find an expression for dp/P_0 and then write the transformations of equation 2.311 to first order.

In the case of an ultra-relativistic particle, the momentum lost through radiation can be expressed in terms of the synchrotron radiation power, P_γ (energy loss per unit time):

$$\frac{dp}{P_0} \approx \frac{P_\gamma}{E_0} dt \approx \frac{P_\gamma}{E_0} \left(1 + \frac{x}{\rho}\right) \frac{ds}{c} , \quad (2.312)$$

where ρ is the radius of curvature of the reference trajectory.

The radiation power from a particle of charge e and energy E in a magnetic field B is given by [16]:

$$P_\gamma = \frac{C_\gamma}{2\pi} c^3 e^2 B^2 E^2 \,. \tag{2.313}$$

The dipole may have a quadrupole gradient B and the particle some energy deviation E:

$$B = B_0 + B_1 x \tag{2.314}$$

$$E = E_0(1+\delta)\,. \tag{2.315}$$

Making the substitutions and using:

$$B\rho = \frac{P_0}{e} \approx \frac{E_0}{ec}\,, \tag{2.316}$$

we get:

$$\begin{aligned} P_\gamma &= c\frac{C_\gamma}{2\pi}\left(\frac{1}{\rho} + k_1 x\right)^2 (1+\delta)^2 E_0^4 \\ &\approx \left(\frac{1^2}{\rho} + 2k_1\frac{x}{\rho}\right)(1=\delta)^2 E_0^4\,, \end{aligned} \tag{2.317}$$

where k_1 is the normalised quadrupole gradient in the dipole:

$$k_1 = \frac{e}{P_0} B_1\,. \tag{2.318}$$

The normalised momentum loss can therefore be written as:

$$\frac{dp}{P_0} \approx \frac{C_\gamma}{2\pi}\left(\frac{1}{\rho^2} + 2k_1\frac{x}{\rho}\right)\left(1+\frac{x}{\rho}\right)(1+\delta)^2 E_0^3 ds\,, \tag{2.319}$$

and expanding to first order, we get:

$$\frac{dp}{P_0} \approx \frac{C_\gamma}{2\pi}\frac{E_0^3}{\rho^2} + \frac{C_\gamma}{2\pi}\left(\frac{1}{\rho^2} + 2k_1\right)\frac{E_0^3}{\rho} x ds + 2\frac{C_\gamma}{2\pi}\frac{E_0^3}{\rho^2}\delta ds + O(x^2) + O(\delta^2) \tag{2.320}$$

With the expression for dp/P_0 in equation (2.320), the transformations

of phase-space become:

$$x \mapsto x \qquad p_x \mapsto \left(1 - \frac{C_\gamma}{2\pi}\frac{E_0^3}{\rho^2}ds\right) p_x\,, \tag{2.321}$$

$$y \mapsto y \qquad p_y \mapsto \left(1 - \frac{C_\gamma}{2\pi}\frac{E_0^3}{\rho^2}ds\right) p_y\,, \tag{2.322}$$

$$s \mapsto s \qquad \delta \mapsto \left(1 - \frac{C_\gamma}{2\pi}\frac{E_0^3}{\rho^2}ds\right)\delta - \frac{C_\gamma}{2\pi}\left(\frac{1}{\rho^2} + 2k_1\right)\frac{E_0^3}{\rho^2}x ds - \frac{C_\gamma}{2\pi}\frac{E_0^3}{\rho^2}ds\,. \tag{2.323}$$

The first-order terms give us components in the matrix M. The zeroth-order term in the map for the Σ matrix is going to be found by taking into account the quantum nature of radiation:

$$D_{66} = \left\langle \left(\frac{dp}{P_0}\right)^2 \right\rangle \approx \frac{\langle u^2 \rangle}{E_0^2}\,, \tag{2.324}$$

where $\langle u^2 \rangle$ is the mean square photon energy. Using the results:

$$\dot{N}\langle u \rangle = P_\gamma\,, \tag{2.325}$$

and

$$\dot{N}\langle u^2 \rangle = 2C_q\gamma^2 E_0 \frac{P_\gamma}{\rho}\,, \tag{2.326}$$

we find that, to zeroth-order in the phase-space variables:

$$\left\langle \left(\frac{dp}{P_0}\right)^2 \right\rangle \approx 2C_q\gamma^2 \frac{C_\gamma}{2\pi}\frac{E_0^3}{\rho^3}ds\,. \tag{2.327}$$

The latter term is first-order in ds whereas the first contribution was in second-order in ds; therefore in the limit $ds \to 0$ the first contribution vanishes.

The matrices M and D have the following form for a thin slice of dipole:

$$M = \begin{pmatrix} 1 & 0 & 0 & 0 & 0 & 0 \\ 0 & 1 - \frac{C_\gamma}{2\pi}\frac{E_0^3}{\rho^2}ds & 0 & 0 & 0 & 0 \\ 0 & 0 & 1 & 0 & 0 & \\ 0 & 0 & 0 & 1 - \frac{C_\gamma}{2\pi}\frac{E_0^3}{\rho^2}ds & 0 & 0 \\ 0 & 0 & 0 & 0 & 1 & 0 \\ -\frac{C_\gamma}{2\pi}\left(\frac{1}{\rho^2} + 2k_1\right)\frac{E_0^3}{\rho}ds & 0 & 0 & 0 & 0 & 1 - 2\frac{C_\gamma}{2\pi}\frac{E_0^3}{\rho^2}ds \end{pmatrix}, \tag{2.328}$$

and

$$D = \begin{pmatrix} 0 & 0 & 0 & 0 & 0 & 0 \\ 0 & 0 & 0 & 0 & 0 & 0 \\ 0 & 0 & 0 & 0 & 0 & 0 \\ 0 & 0 & 0 & 0 & 0 & 0 \\ 0 & 0 & 0 & 0 & 0 & 0 \\ 0 & 0 & 0 & 0 & 0 & 2C_q\gamma^2\frac{C_\gamma}{2\pi}\frac{E_0^3}{\rho^3}ds \end{pmatrix}. \tag{2.329}$$

For a full transformation for a dipole (or an entire ring) one needs to concatenate the maps. For example, given the sigma matrix at location s_0, we find the sigma matrix at location $s_1 = s_0 + ds$ from:

$$\Sigma(s_1) = M(s_1; s_0) \cdot \Sigma(s_0) \cdot M^T(s_1; s_0) + D(s_1; s_0)\,. \tag{2.330}$$

The sigma matrix at position s_2 is given by:

$$\begin{aligned} \Sigma(s_2) &= M(s_2; s_1) \cdot \Sigma(s_1) \cdot M^T(s_2; s_1) + D(s_2; s_0) \\ &= M(s_2; s_0) \cdot \Sigma(s_0) \cdot M^T(s_2; s_0) + M(s_2; s_1) \cdot D(s_1; s_0) \cdot M^T(s_2; s_1) \\ &\quad + D(s_2; s_1)\,. \end{aligned} \tag{2.331}$$

Hence:

$$\begin{aligned} M(s_2; s_0) &= M(s_2; s_1) \cdot M(s_1; s_0) \\ D(s_2; s_0) &= M(s_2; s_1) \cdot D(s_1; s_0) \cdot M^T(s_2; s_1) + D(s_2; s_1)\,. \end{aligned} \tag{2.332}$$

This process of concatenation can be generalised as:

$$M(s_n; s_0) = M(s_n; s_{n-1}) \cdot M(s_{n-1}; s_{n-2}) \cdot \ldots \cdot M(s_1; s_0)$$
$$D(s_n; s_0) = \sum_{i=1}^{n} M(s_n; s_i) \cdot D(s_i; s_{i-1}) \cdot M^T(s_n; s_i)\,. \tag{2.333}$$

To solve equation (2.310) in order to find the sigma matrix, having obtained the maps M and D for an entire ring, we make use of the eigenvectors U and the diagonal matrix Λ, containing the eigenvalues of, matrix M:

$$M \cdot U = \Lambda \cdot U\,. \tag{2.334}$$

If we define matrices $\tilde{\Sigma}$ and $\tilde{D}$ as:

$$\Sigma = U \cdot \tilde{\Sigma} \cdot U^T\,, \tag{2.335}$$
$$D = U \cdot \tilde{D} \cdot U^T\,, \tag{2.336}$$

then the solution for the sigma matrix elements is given by:

$$\tilde{\Sigma}_{ij} = \frac{\tilde{D}_{ij}}{1 - \Lambda_i \Lambda_j}\,. \tag{2.337}$$

2.4 Betatron Coupling Measurements

The most typical experimental parameterization of betatron coupling is the closest approach or splitting of the normal mode tunes. If the horizontal and vertical tunes can be brought close together (ideally $\nu_x = \nu_y$) by an adjustment of purely horizontal and vertical focusing quads, then the machine is said to be "globally decoupled".

Global decoupling is usually very quick and useful, however it does not guarantee correction of individual (local) coupling errors [5, 19]. On the other hand local coupling can be difficult to diagnose, but, if corrected, can lead to significant improvements on low-emittance tuning.

2.4.1 Phase-Advance Measurements

An alternative method is based on exciting coherent oscillations of the beam at a resonant -betatron or synchrotron- frequency ("shaking") and then measuring the phase of the oscillations at the BPMs around the ring [8, 41, 36]. This technique yields the betatron phases $\phi_{x,y}$ at the BPMs, which can then be related to the beta function via:

$$\frac{d\phi_{x,y}}{ds} = \frac{1}{\beta_{x,y}} \Rightarrow$$
$$\phi(s_i) - \phi(s_0) = \int_{s_0}^{s_i} \frac{1}{\beta(s)} ds \,. \tag{2.338}$$

This technique is fast and is particularly useful where $\beta_{x,y}$ is small or where closed orbit distortions are large and therefore varying quadrupole strengths leads to unacceptable variations in the orbit.

The components of the oscillations in the vertical and horizontal planes can also be resolved, allowing the extraction of local coupling parameters. Using the components of the $\bar{C}$ matrix (see section 2.1.4.1) the coupling can be parametrized. Assuming weak coupling the motion of the horizontal normal mode at a detector is given by:

$$\begin{aligned} x &= A_x \sqrt{\beta_x} \cos n\omega_x \,, \\ y &= -A_x \sqrt{\beta_y} [\bar{C}_{22} \cos n\omega_x + \bar{C}_{12} \sin n\omega_x] \,, \end{aligned} \tag{2.339}$$

where A_x is the overall amplitude and $\beta_{x,y}$ are the beta functions, ω_x is the normal mode frequency and n is the turn number. Equation (2.339) shows that $\bar{C}_{22}$ is the normalized amplitude of the vertical component of the motion that is in-phase with the horizontal motion, while $\bar{C}_{12}$ is the normalized amplitude of the out-of-phase component. For the vertical normal mode excitation, equivalent explanations hold for terms $\bar{C}_{11}, \bar{C}_{12}$ respectively and the equations of motion become

$$\begin{aligned} x &= -A_y \sqrt{\beta_x} [\bar{C}_{11} \cos n\omega_x - \bar{C}_{12} \sin n\omega_y] \,, \\ y &= A_y \sqrt{\beta_y} \cos n\omega_y \,. \end{aligned} \tag{2.340}$$

The $\bar{C}_{ij}$ are a measure of the coupling with $\bar{C}_{ij} \approx 1$ corresponding to full

coupling. The terms $\bar{C}_{11}$, $\bar{C}_{22}$, $\bar{C}_{12}$ are calculated using the measurements and equations (2.339) and (2.340). The term $\bar{C}_{21}$ cannot be measured since the transverse momenta, x', y' are not measurable.

2.4.2 Skew Quadrupole Modulation

A different approach, that overcomes the shortcomings of the skew quadrupole scan method for measuring and characterizing the coupling, has been proposed and applied at the Relativistic Heavy Ion Collider (RHIC) [32, 42]. This technique involves a skew quadrupole strength modulation that replaces the scan. The tune split is again the observable during the modulation. The method benefits from the fact that it is not necessary to move the tunes to the linear difference coupling resonance before the modulation. Modulating the skew quadrupoles is proved to be quite fast and this opens the possibility for continuous correction of the global coupling during acceleration.

The two tunes $Q_{1,2}$, as dictated by perturbation theory, are

$$\begin{aligned} Q_1 &= Q_{x,0} - \frac{\Delta}{2} + \frac{1}{2}\sqrt{\Delta^2 + |C^-|^2} \\ Q_2 &= Q_{y,0} - \frac{\Delta}{2} - \frac{1}{2}\sqrt{\Delta^2 + |C^-|^2} \end{aligned} \tag{2.341}$$

where $Q_{x,0}, Q_{y,0}$ are the tunes for the uncoupled case and

$$\Delta = Q_{x,0} - Q_{y,0} - p\,, \tag{2.342}$$

where p is the integer tune split. C^- is the coupling coefficient and it has the following definition:

$$C^- = |C^-|e^{i\chi} = \frac{1}{2\pi}\oint \sqrt{\beta_x\beta_y}k_s e^{i[\Phi_x - \Phi_y - \Delta(2\pi s/L)]}dl\,, \tag{2.343}$$

with $|C^-|$ being the coupling amplitude, χ the angle of the coupling, β_x and β_y the horizontal and vertical beta functions respectively, Φ_x and Φ_y the betatron phase advances, k_s the skew quadrupole strength, L the ring circumference and s the distance between the skew quadrupole location and the reference point for the coupling calculation.

Following equations (2.341) the tune split $|\Delta Q|$ becomes:

$$|\Delta Q| = |Q_1 - Q_2 - p| = \sqrt{\Delta^2 + |C^-|^2}\,, \tag{2.344}$$

and is a measurable quantity. By modulating one skew quadrupole, its

contribution to the total coupling will also modulate as:

$$C^-_{mod} = C^-_{mod,amp} \sin 2\pi f t\,, \tag{2.345}$$

with C^-_{mod} being the coupling that the skew quadrupole introduces, $C^-_{mod,amp}$ its amplitude and f the frequency of the modulation. The total coupling in the ring is:

$$C^-_{tot} = C^-_{res} + C^-_{mod}\,, \tag{2.346}$$

where $C^-_{res}$is the residual coupling in the ring before the skew quadrupole modulation. Equation (2.346) is justified by the fact that the coupling phenomena present are assumed linear, which is true for weak coupled lattices, and therefore the contributions from different sources are additive.

If the modulation frequency is small enough, then the tunes have enough time to adjust (come to equilibrium) to the coupling change. Substitution of equations (2.345) and (2.346) in equation (2.344) leads to:

$$\begin{aligned} |\Delta Q|^2 &= \Delta^2 + |C^-_{res}|^2 + \frac{1}{2}|C^-_{mod,amp}|^2 \\ &+ 2|C^-_{res}||C^-_{mod_amp}| \cos\Delta\chi \sin 2\pi f t \\ &- \frac{1}{2}|C^-_{mod,amp}|^2 \cos 4\pi f t\,, \end{aligned} \tag{2.347}$$

where $\Delta\chi$ is the angle difference between C^-_{res} and $C^-_{mod,amp}$. The $2f$ term in equation (2.347) is only related to the skew quadrupole modulation amplitude, $|C^-_{mod,amp}|$, and the f term is related to the dot multiplication of the terms C^-_{res} and C^-_{mod}. Therefore, in the frequency domain of $|\Delta Q|^2$, there will be either two distinct peaks located at f and $2f$ if the machine is initially coupled, or only one peak at $2f$ if the machine is initially well decoupled. Thus, the f peak can be considered as a manifestation of the residual coupling.

Chapter 3

Low Emittance Tuning Studies at KEK-ATF

The Accelerator Test Facility (ATF) at KEK is one of the major facilities for research programs related to the International Linear Collider design. It is dedicated to the study of ultra-low emittance beams and the development of robust tuning techniques that will deliver such high-quality beams on a routine basis.

The instrumentation at the ATF damping ring, which is one part of the ATF facility (the others being the linac and the extraction line), consists of [60]:

- Fast, high resolution beam position monitors:

Table 3.1: Key ATF parameters [35].

Beam energy	1.28 GeV (in operation mode)
Circumference	138.56 m
Average current	400 mA
Bunch population	2×10^{10}/ per bunch
Number of bunches	20
Natural emittance	1 nm
Vertical emittance	<5 pm
Typical beam size	70 μm × 7μm (rms horizontal × rms vertical)
RMS energy spread	5.5614×10^{-4} GeV
RF voltage	0.3 MV
RF frequency	714 MHz

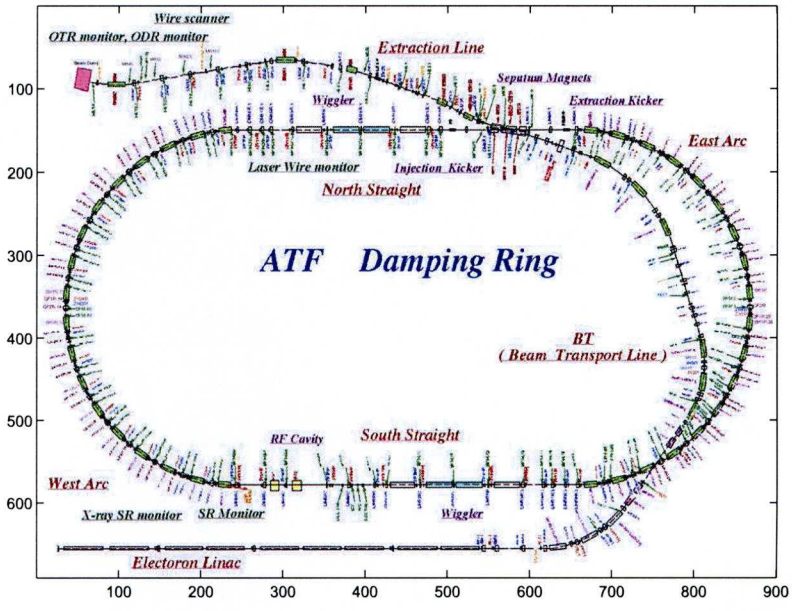

Figure 3.1: ATF ring layout.

  - Button type BPMs, that can be operated in narrow band (average over many turns) or TBT (Turn-By-Turn) mode.

- High resolution beam size monitors:
  - Laser wire monitor.
  - X-ray synchrotron radiation beam size monitor.
  - Synchrotron radiation bunch length monitor.
- Fast and high resolution beam position monitors for the extracted beam:
  - Strip line BPM.
  - Micro wave cavity BPM.

The ATF damping ring contains 50 horizontal orbit correctors and 51 vertical orbit correctors. There are in total 96 BPMs in each plane. Additionally, every sextupole (68 in total) has an independently adjustable skew quadrupole trim winding for compensating the betatron coupling.

ATF has so far achieved one of the lowest values for the vertical emittance, approximately equal to 4.5 pm [28]. However, since the current technology is already pushed to the limit (tighter magnet alignment tolerances, need for high-resolution BPMs, etc.) to reach such low values, the following questions arise:

- Are the currently implemented tuning techniques and instrumentation sufficient to further reduce the vertical emittance to the ILC damping rings specification of 2 pm?
- If not, what are the problems that set limitations?

Furthermore,

- Are these techniques robust and repeatable?

In this chapter we describe a standard procedure for low emittance tuning that has been successfully implemented at various machines (e.g. ALS, SLS, AS [50, 45]), the Orbit Response Matrix (ORM) analysis, discuss results from conducted experiments and finally, attempt to provide an answer to the above questions, based on experimental data and results from computer simulation models.

3.1 Orbit Response Matrix Analysis and Linear Optics from Closed Orbits (LOCO)

3.1.1 The Orbit Response Matrix (ORM)

The ORM is constructed by measuring the closed orbit response to known dipole field perturbations. We consider a set of small dipole perturbations given by $\theta_j, j = 1, ..., N$, where N is the number of correctors (dedicated dipole magnets) around the ring. The measured change in closed orbit caused by each dipole perturbation is $y_i, i = 1, ..., M$, where M is the number of Beam Position Monitors (BPMs). The orbit response matrix R is then defined as:

$$R_{i,j} = \frac{\Delta y_i}{\Delta \theta_j}. \tag{3.1}$$

3.1.2 Analysis Technique

Analysis of the ORM data can help with correcting the optics of an accelerator system (i.e. calibrate quadrupole strengths, rolls, etc.). For example, from the design quadrupole gradients it is possible to calculate the expected orbit response matrix. Reversing the process, from the measured response matrix one can calculate the actual gradients in each quadrupole.

The ORM analysis aims to construct a model response matrix of the storage ring that is as close as possible to the measured response matrix. Mathematically this is achieved by minimizing the quantity:

$$\chi^2 = \frac{1}{N \cdot M} \sum_k \mathbf{W}_k^2 , \tag{3.2}$$

where

$$\mathbf{W}_k = \frac{\mathbf{R}_{mod_{i,j}} - \mathbf{R}_{meas_{i,j}}}{\sigma_i} , \tag{3.3}$$

with

$$k = (i-1)j_{max} + j , \tag{3.4}$$

and σ_i being the rms error of a measurement using the i^{th} BPM. A number of parameters w_m are associated with the modeled response matrix so that:

$$\mathbf{R}_{mod} = \mathbf{R}_{mod}(w_m) . \tag{3.5}$$

These parameters include the kicker angle calibration factor, the BPM's gain factor, the dipole angle and dipole roll, etc. To bring then the measured and response matrices as close together as possible, the aim is to find a set of parameters w_m, such that:

$$\mathbf{W}_k(w_m) = 0 . \tag{3.6}$$

The χ^2 minimisation can be also viewed as:

$$\chi^2 = \sum_{i,j} \frac{(M_{mod_{i,j}} - M_{meas_{i,j}})^2}{\sigma_i^2} \equiv \sum_{i,j} W_{k(i,j)}^2 . \tag{3.7}$$

Minimising $||W^2||$ is equivalent to minimizing χ^2. For a given initial set of values, w_{m_0}, for parameters such as the quadrupole gradients, we obtain an initial vector W_{m_0}. LOCO finds the changes in Δw_n that are the best

solution to the equation $W_{k_0} + \Delta W_k = 0$. If we assume that W_k is a linear function of w_n, $\Delta W_k = \frac{\partial W_k}{\partial w_n} \Delta w_n$, then χ^2 is minimized by solving:

$$-W_{k_0} = \frac{\partial W_k}{\partial w_n} \Delta w_n \,. \tag{3.8}$$

If we have an initial set of parameters w_m we can evaluate $\mathbf{W}_k$. LOCO takes a set of initial values $w_m^{(0)}$ and looks for changes Δw_m so that equation (3.6) is satisfied for:

$$w_m = w_m^{(0)} + \Delta w_m \,. \tag{3.9}$$

3.1.3 The LOCO Algorithm

The linear response of the ORM to certain magnetic field perturbations is the foundation of the algorithm presented here. Linear Optics from Closed Orbits (LOCO) is an implementation of the ORM algorithm [46, 52, 1]. Originally written in FORTRAN it has since been rewritten in MATLAB and linked to the accelerator code AT [59].

Effectively what LOCO does is solve equation (3.8), by inverting the matrix:

$$W \equiv \frac{d\mathbf{W}_k}{dw_m}. \tag{3.10}$$

This inversion is done by Singular Value Decomposition (SVD), a method in which any given matrix A of dimensions $m \times n$ is factorised as

$$A = U \Sigma V^T \,, \tag{3.11}$$

where U and V are unitary matrices of dimensions $m \times m$ and $n \times n$ respectively and Σ is an $m \times n$ matrix containing the singular values of A in descending order. More details about SVD are given in Appendix A. LOCO can be used to calibrate the normal and skew quadrupole gradients in each quadrupole in a storage ring as well as calibrating the gains and cross-plane coupling in the BPMs and strength and rotational alignment (tilts) around the reference trajectory. These are the set of parameters w_m that can be changed so that the model response matrix comes as close as possible to the measured response matrix. It then also is possible to find the changes in quadrupole gradients that best restore the design optics in a storage ring and to find settings for the skew quadrupoles to correct the betatron coupling.

In practice, the response matrix is not a perfectly linear function of the quadrupole gradients, so LOCO performs a correction iteratively until it converges to the best set of parameters w_n.

3.1.3.1 Input Data for LOCO

The primary input data for LOCO is the measured closed orbit response matrix. At the ATF the raw data consist of a set of BPM readings for a set of strength settings of each corrector. These data are pre-processed to give the orbit variation at each BPM with respect to the variation of each corrector.

The horizontal and vertical dispersion can also be provided as input data for a LOCO analysis. Doing so helps in "breaking" the degeneracy between BPM gains and corrector strengths; the effect on the ORM is the same, whether there are BPM gain errors or errors on the corrector strengths. LOCO does not address the effects of closed orbit distortions that lead to contributions to the vertical dispersion and instead assumes that all vertical dispersion is generated by betatron coupling in the skew quadrupoles. For this reason the dispersion readings that are "fed" into LOCO are given individual weight factors which are subsequently used in the fitting routine. Choosing the right weight factor is important in achieving a good fit. For example, if vertical steering does make a significant contribution to the vertical dispersion, then fitting for the latter with an assignment of a large weight factor will distort the values found for the skew quadrupole strengths, compromising therefore the fit to the coupling parts of the response matrix.

3.2 Betatron Coupling Correction at the ATF

The specified vertical emittance for the International Linear Collider damping rings is 2 pm. This specification poses a great challenge in the design of the storage ring since it is almost a factor of two lower than the lowest vertical emittance ever achieved [2]. Therefore, a major goal at the ATF is to demonstrate a reliable tuning technique for operation in this low-emittance regime. Information on the optics of a storage ring can be obtained by analysis of the closed orbit response matrix, as described above. This technique has been applied successfully in a number of machines worldwide.

Two major effects limit the attainment of low vertical emittance values:

- Vertical dispersion.
- Betatron coupling.

There are many effects that cause dispersion to arise in the vertical plane. These are ultimately caused by errors in the lattice leading to vertical steering errors. Betatron coupling is the mechanism whereby motion in one transverse plane is transferred ("coupled") to the other and it is a direct consequence of the fact that due to errors in any real machine the beam dynamics cannot be fully separated into 3 planes. In the case of a damping ring, where the horizontal emittance is orders of magnitude larger than the vertical and where the vertical emittance is crucial for the final luminosity seen at the interaction point, the main concern is about horizontal emittance being coupled into the vertical (though it works vice-versa).

Using ORM analysis, it is possible to determine the changes in the quadrupole gradients that best restore the design optics as well as the settings for skew quadrupoles to correct the betatron coupling and vertical dispersion. LOCO is used to find skew quad values at the sextupoles so that the model ORM matches the measured ORM. These values then are used to set the strengths of the real skew quads; the skew quad values that one gets from the fit are added to the existing settings of the skew quads. In our assessment of the effectiveness of LOCO in betatron coupling correction, we want to project coupling errors (e.g. tilted quads, vertically misaligned sextupoles) onto the skew quadrupoles and check whether the ORM analysis can fit the appropriate parameters to minimize betatron coupling.

3.2.1 Possible Limitations in Coupling Correction using ORM Analysis

Past attempts to minimize the vertical emittance using ORM analysis in the KEK-ATF have met with limited success [68]. The plot in figure 3.2 comes from data taken on an ATF shift on 30 May 2008.

In particular, figure 3.2 shows how the vertical beam size changes as the ORM-calculated coupling correction is applied is percentage steps. There is no significant beam size reduction and the minimum is achieved at 20% of the calculated gradient as opposed to the expected value of 100%. It appears that the application of LOCO at the ATF was able to provide some information about the lattice and the diagnostics. However, when applying a be-

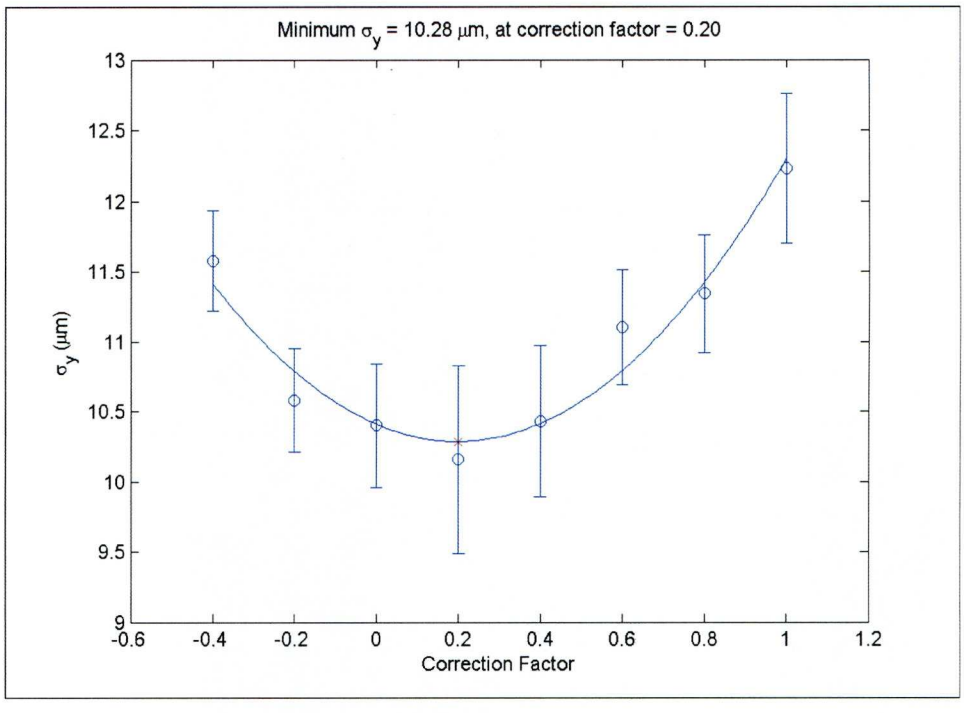

Figure 3.2: Effect of applied correction to the vertical beam size at the ATF-KEK. The points indicate the application of the coupling correction in percentage steps(termed as "Correction Factor" in the x-axis). The error bars indicate the standard deviation of the number of measurements (5) taken by the XSR monitor.

tatron coupling correction with skew quadrupole strengths determined from the LOCO analysis, then the vertical emittance actually increased. This failure can be the result of different factors; for example, the significance of the dispersion weight factor applied in fitting the model to the measured data [50]. If the dispersion weight factor is too low, then the vertical dispersion remains large after the correction and dominates the generated vertical emittance; if it is too high, then the fitted skew quadrupole strengths are incorrect because of the effects of vertical steering. Futhermore, the vertical emittance level at which the ATF usually operates is very small to begin with. It is very likely that the "correct" skew quadrupole settings (strengths) have been found and any changes thereafter, lead to a reduction in betatron coupling at the expense of increasing the vertical dispersion, generated by vertical steering, and vice-versa. In this case it would be essential to reduce the vertical steering by performing a beam-based alignment [14].

It is worth noting that at the time the data shown in figure 3.2 were taken, it was not fully realised that the resolution of the beam size monitor was limited to around 10 μm, because of mechanical vibration of the monitor from a nearby cooling water channel [73]. This problem was subsequently corrected. The laser wire gives a better estimate of the emittances, but measurements take much longer than with the XSR monitor.

3.2.1.1 No BPM Coupling Case Scenario

Results such as these described in section 3.2.1 prompted an investigation on the applicability of ORM analysis to the ATF for low emittance tuning. Here we present the results of simulations aiming to address this issue.

For our simulations we first introduce random errors on the skew quadrupoles, which for the ATF case are superposed as extra windings on the focusing sextupoles, and then simulate the ORM data. The simulations for the latter are performed using the Accelerator Toolbox (AT) code. In principle, LOCO can be fed with data calculated by any tracking code, but since LOCO is implemented in MATLAB it is convenient to use the MATLAB-based code AT.

The parameters that are varied when fitting the model to the simulated response matrix of the ring with the skew quadrupole errors are the following:

- BPM gains and couplings;
- corrector magnet kicks and couplings;
- quadrupole strengths;
- one family (focusing) skew quadrupole strengths.

Typical values for BPM gains are in the order of 1% to 3% but larger values have been observed [49].

We should note that in the ATF, every sextupole has an independently adjustable skew quadrupole trim winding for compensating the betatron coupling. Therefore, in principle, the skew quadrupole (SQ) components on the focusing (SF) and defocusing (SD) sextupoles can be independently fitted as parameters in the LOCO analysis; however, since the horizontal and vertical phase advances between the adjacent SF and SD sextupoles are

nearly equal, such a fit will result in a degeneracy from the coupling point of view. This is illustrated in figure 3.3.

When attempting a fit using both families of skew quads, we therefore end up with a good correlation between the sum of the adjacent skew quadrupole gradients that were fitted and the skew quadrupole gradients that were applied, similar to the correlation achieved in the case of fitting just one family of skew quadrupoles. Therefore only the skew quadrupoles in one family of sextupoles (focusing sextupoles) were used as parameters in the fit.

Figure 3.4 shows the "measured" response matrix (matrix computed for a set of applied random skew quadrupole strengths) and the difference between the "measured" response matrix and the modeled response matrix, after the model is fitted to the "measured" response matrix using LOCO. We see that the scales on the two plots are different as well as that the cross-plane sectors of the response matrix are much smaller than the in-plane sectors. The horizontal BPMs are numbered 1-96, vertical BPMs 97-192; horizontal corrector magnets are numbered 1-47, vertical corrector magnets 48-97.

The cross-plane sectors of the response matrix are shown in figures 3.5 and 3.6. The fact that it is possible to find a good fit to the "measured" data in the cross plane sector of the ORM suggests that LOCO can be successful in performing a betatron coupling correction.

The quality of the fit performed by LOCO to the "measured" response matrix can be indicated by the distribution of residuals. The units of the residuals are BPM standard deviations. To construct the distribution, the difference between the "measured" orbit response matrix and the fitted orbit response matrix is taken, and every element in the difference matrix is then divided by the resolution of the BPMs. For our simulations the BPM resolution was set to a common value of $1\,\mu m$, based on the resolution believed to be achieved by the ATF BPMs. The distribution, shown in figure 3.7, is a histogram over all elements in the difference response matrix, normalised by the total number of points.

Figure 3.8 shows the fitted quadrupole strengths. The fit appears to be extremely accurate, indicating that LOCO has been able to correctly calibrate the optics.

The fitted BPM couplings are shown in figure 3.9. The coupling is defined

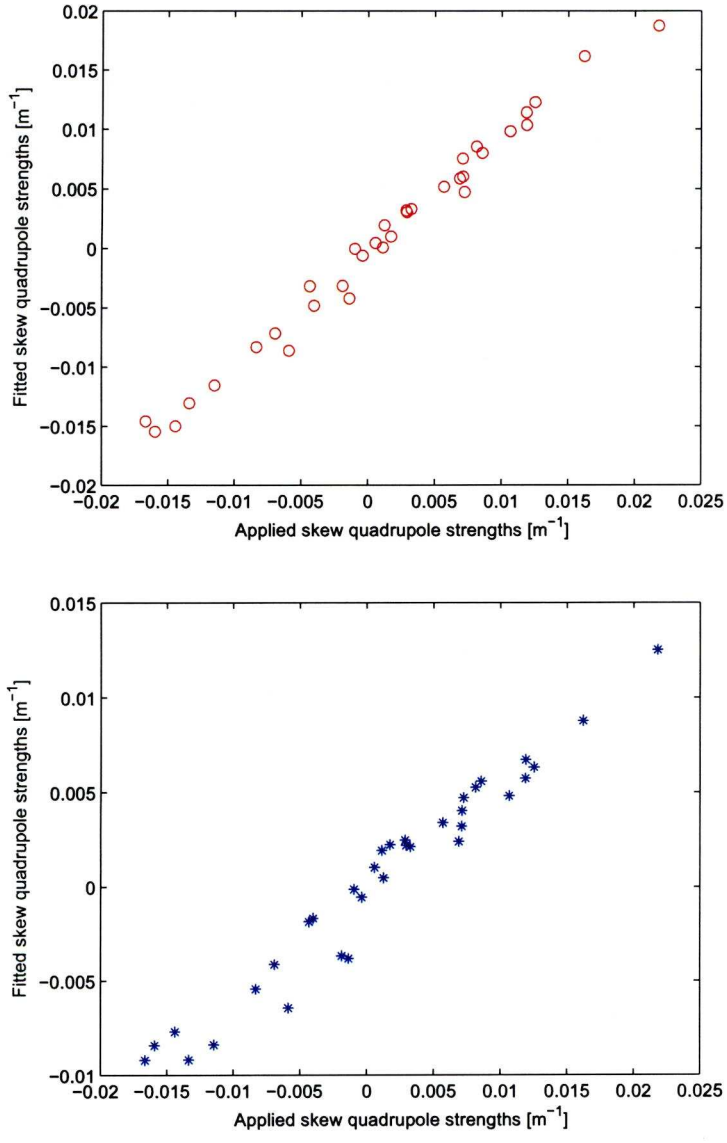

Figure 3.3: Correlation between applied and fitted skew quadrupole (SQ) strengths, in simulation of ORM analysis in the ATF. Upper plot: All SQs used in the fit, red circles represent the sum of the strengths for each pair of sextupoles. Bottom plot: Correlation between one family of SQs. The similar quality of the correlations indicates a degeneracy between the two different fits.

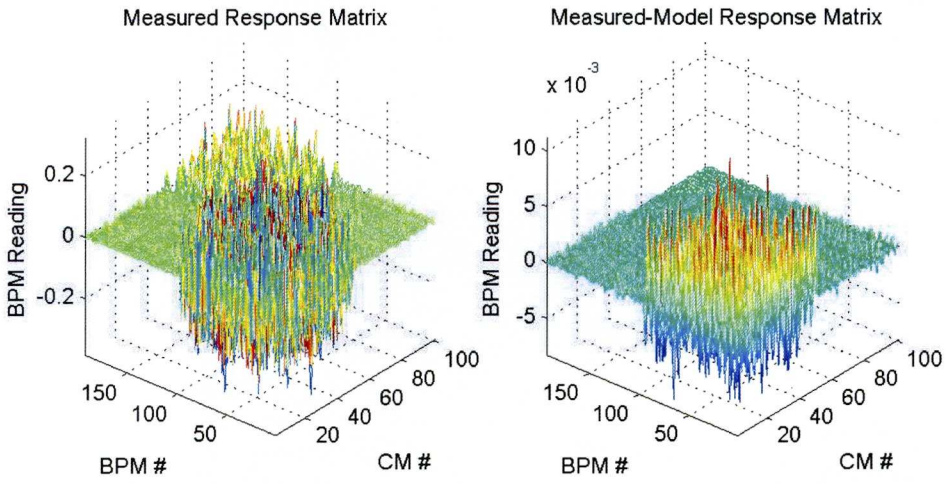

Figure 3.4: Measured response matrix (left) and difference between the measured response matrix and the modeled response matrix after LOCO fitting (right). Note the different scales on the two plots and that the cross-plane sectors of the response matrix are very much smaller than the in-plane sectors. The color change from blue to red is an indication of the increasing magnitude of BPM readings.

as the *measured* beam motion in one plane resulting from a *real* unit beam motion in the other plane. For a given BPM, if the coupling measured arises from a rotation of that BPM around the beam axis, then a coupling of 0.01 would correspond to a rotation of 10 mrad. The fitted values are very small, as we can observe from the appropriate scale on the graph, indicating that LOCO has been reasonably accurate in estimating the BPM coupling, since there is no BPM coupling introduced in the simulation parameters.

Similarly the fitted BPM gains shown in figure 3.10 are very close to one, resulting in a gain matrix [equation (3.12)] approximately equal to the identity matrix; that is as expected, since no BPM gain errors have been introduced in the simulation.

The corrector magnet kicks have also been fitted with high accuracy to the applied value of 35 mrad, as shown in figure 3.11.

The "measured" and fitted horizontal and vertical dispersion are shown in figure 3.12. The fit is very accurate and this is a result of choosing the "correct" weight factor for the dispersion in the fitting routine of LOCO.

The aim at this point is to try to identify the skew quadrupole strengths that were applied by using LOCO to fit the simulated ORM data.

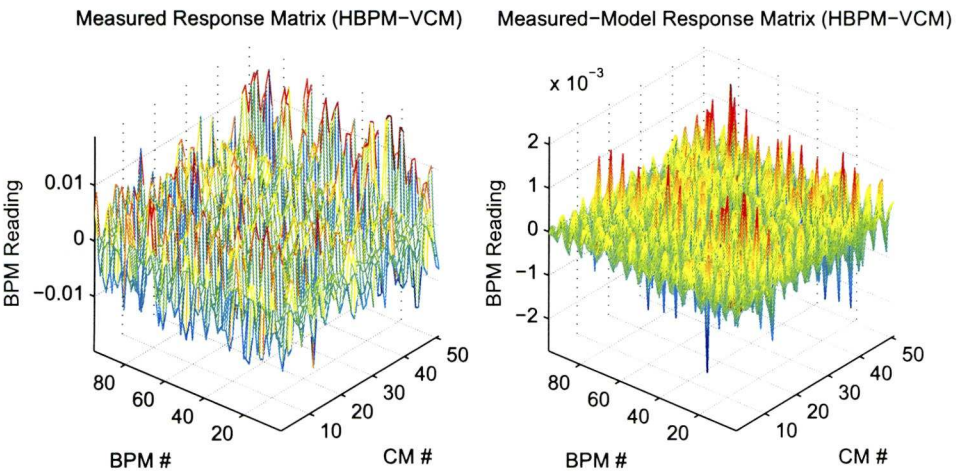

Figure 3.5: Sector of the response matrix corresponding to horizontal BPMs and vertical corrector magnets (cross-plane response).

Figure 3.13 shows that a good fit to the applied skew quadrupole strengths can be achieved, if the conditions of the fit are optimised. In this case Fit Conditions 1 and 2 refer to different cut-off thresholds, 2×10^{-5} and 2×10^{-4} respectively, for the singular values used in the singular value decomposition stage of the fitting process. The singular values are shown in figure 3.14.

The dispersion weight factor used in the LOCO simulation is also a very important parameter that has to be chosen "correctly" in order to get the best possible values for the skew quadrupole strengths; figure 3.15 shows how the correlation between applied and fitted skew quadrupole strengths is affected by a "bad" weight factor choice (weight factor value = 10 as opposed to the optimal value of 0.01). This choice also affects the dispersion fit as shown in figure 3.16.

Figure 3.17 shows the distribution of the vertical emittance, after correction has been applied, for different sets of random skew quadrupole errors. Since there are no other errors included at this stage, this indicates the best possible emittance that could be achieved using this technique; the average is just under 2 pm starting from an average initial emittance of around 30 pm.

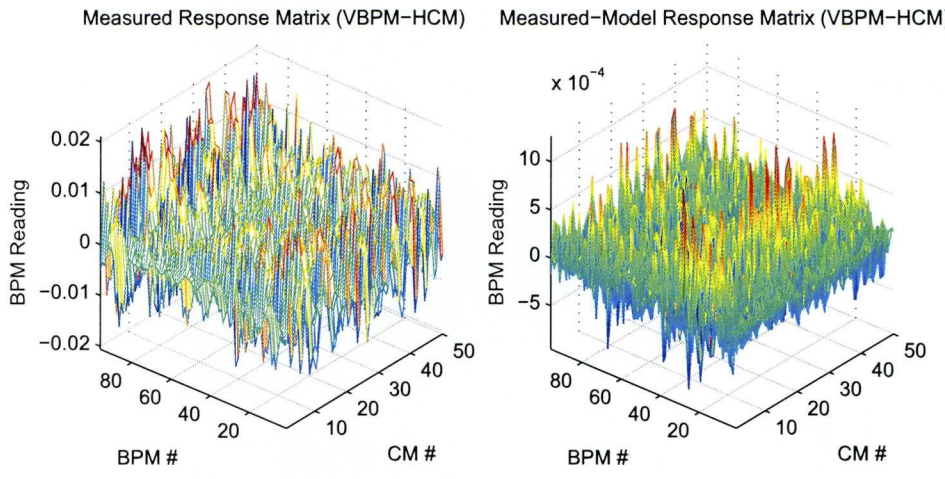

Figure 3.6: Sector of the response matrix corresponding to vertical BPMs and horizontal corrector magnets (cross-plane response).

3.2.1.2 Degeneracies

Degeneracies in the fit can be identified by applying one kind of error in simulation, and fitting for another. Of particular concerns are degeneracies between orbit corrector magnets and BPM parameters, and skew quadrupole strengths. Corrector magnet or BPM tilts will give the appearance of coupling in the measured ORM and dispersion, without actually generating coupling in the machine. Should these errors be degenerate with the strengths of the skew quadrupoles, the attempted correction using skew quadrupole strengths determined from ORM analysis could *increase* the coupling in the machine.

To investigate the possibility of such degeneracies, LOCO was used to fit skew quadrupole strengths to data generated from a model of the ATF lattice where the only errors present were corrector magnet rotations around the beam axis (tilts). The vertical emittance was then calculated after a correction based on the fitted skew quadrupole strengths. Figure 3.18 shows the distribution of the final vertical emittance for a number of sets of corrector tilts of 50 mrad rms as the only errors present in the lattice. The average final vertical emittance is below 0.1 pm. This is much smaller than the limit of just below 2 pm, that comes from the accuracy with which real skew quadrupole errors can be determined. Since the actual corrector tilts in ATF are believed to be much smaller than 50 mrad [29], we can conclude

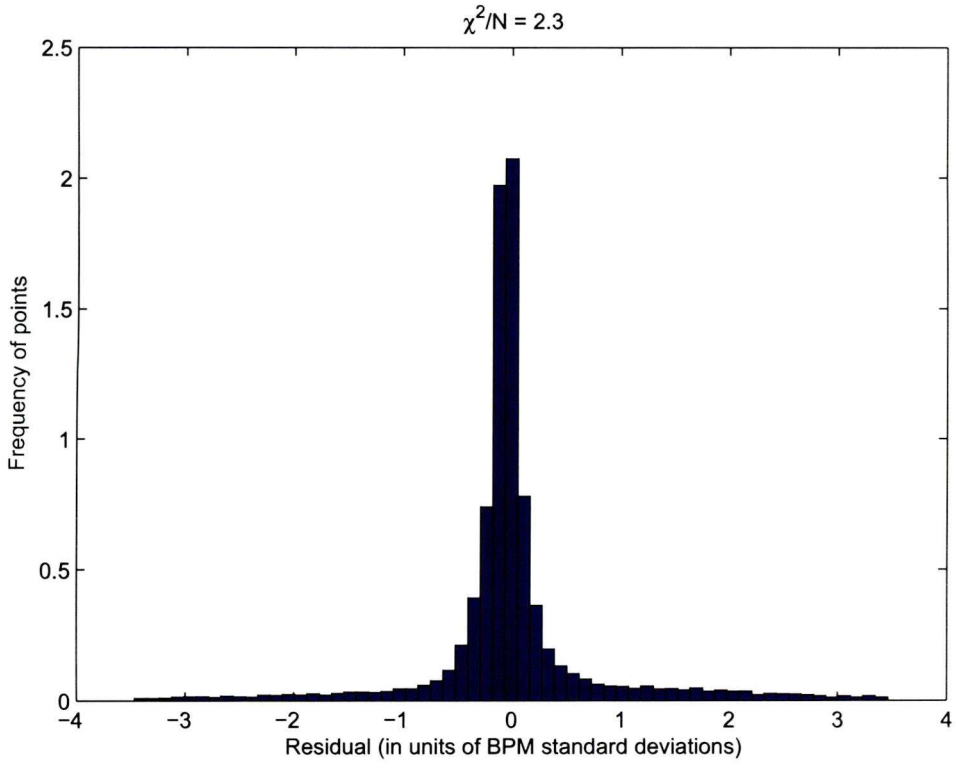

Figure 3.7: Distribution for the residuals of the LOCO fit to the response matrix, in units of BPM resolution. To construct the distribution, we take the difference between the "measured" ORM and the ORM fitted by LOCO, divide each value by the resolution of the associated BPM and plot a histogram over all elemets in the ORM, normalised by the total number of points.

that there is no significant degeneracy between the corrector magnet tilts and the skew quadrupole strengths.

Next, we applied BPM coupling errors, and again fitted for skew quadrupole errors. The BPM coupling errors were modeled by off diagonal terms in the gain matrix:

$$\begin{pmatrix} x_m \\ y_m \end{pmatrix} = \begin{pmatrix} g_{xx} & g_{xy} \\ g_{yx} & g_{yy} \end{pmatrix} \begin{pmatrix} x \\ y \end{pmatrix}, \tag{3.12}$$

where x_m, y_m and x, y are the measured and real positions of the beam, respectively. Independent values for g_{xy} and g_{yx} were used for each BPM, with rms 0.02. The distribution of vertical emittances after a "correction"

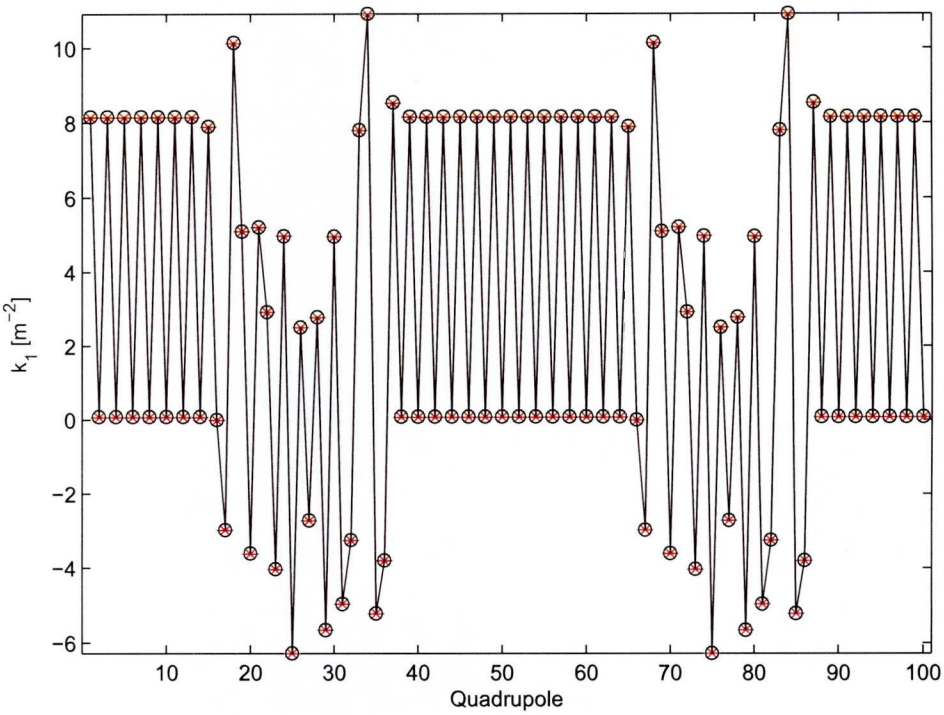

Figure 3.8: Nominal and fitted quadrupole gradients for the ATF in the case of no BPM coupling. Red points are the nominal values, black circles are the fitted values.

based on skew quadrupole strengths is shown in Fig. 3.19. The average final vertical emittance is 5.6 pm. This is significantly larger than the target value of 2 pm, and may imply a limitation in the technique. Values of order 0.02 for the coupling components of the BPM gain matrix are believed to be realistic for the BPMs in ATF.

To further investigate this degeneracy, we created a lattice where both BPM coupling and random skew quadrupole errors are present and simulated the appropriate ORM data. We then used LOCO to fit this dataset using skew quadrupoles. The results of the fit are shown in figure 3.20.

This fit is consistent with the proposed degeneracy. All fit conditions have remained the same as in the case where only skew quadrupole errors are present (figure 3.13) but now the fit is quite poor and suggests that LOCO cannot distinguish between the two sources of error.

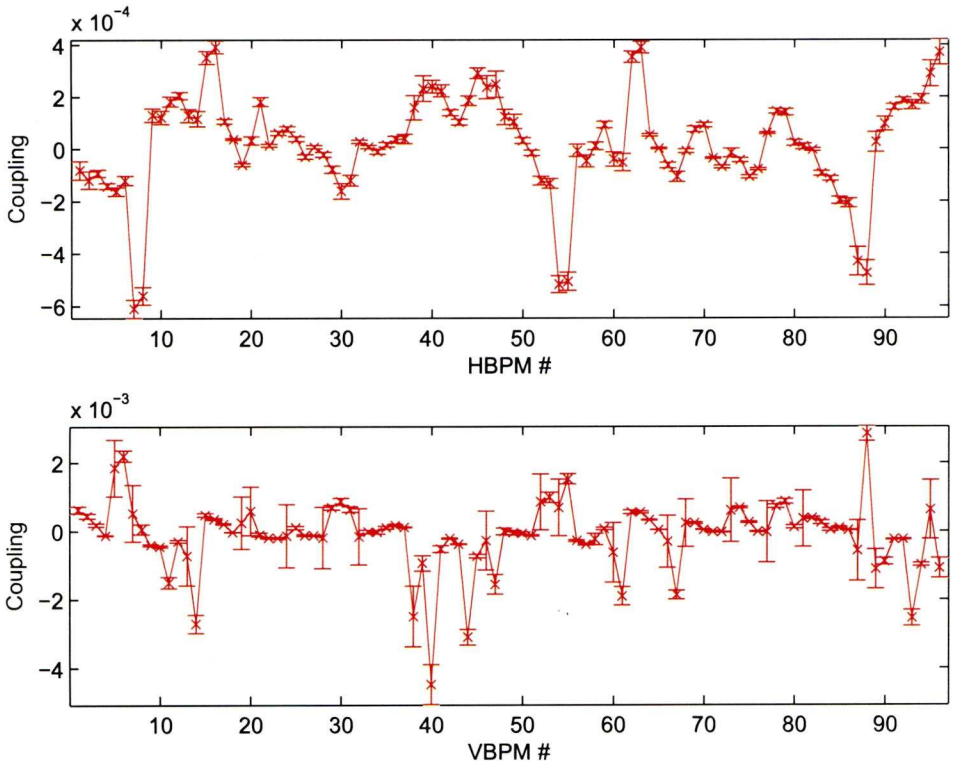

Figure 3.9: BPM couplings fitted by LOCO for the ATF in the case of no BPM coupling. The error bars indicate the standard deviation of the BPM couplings.

3.2.2 Reducing Correctors

The ORM analysis, even though it appears that it will not be effective for correction at the desired level for the ILC damping rings, remains a very useful analysis technique and provides significant information for the optics of a given accelerator system.

Collection of a full set of ORM data, using all the orbit correctors in the ATF, takes between two and four hours. However, even with a large set of fit parameters (normal and skew quadrupole gradients, BPM gains and couplings, corrector magnets strengths and tilts) the fit is highly over-constrained. This suggests that it may be possible to reduce the number of constraints (e.g. the number of correctors) without adverse effects on the results. The benefit would be a reduction in the time taken for data collection and data processing.

To determine the most effective orbit correctors to use for correcting cou-

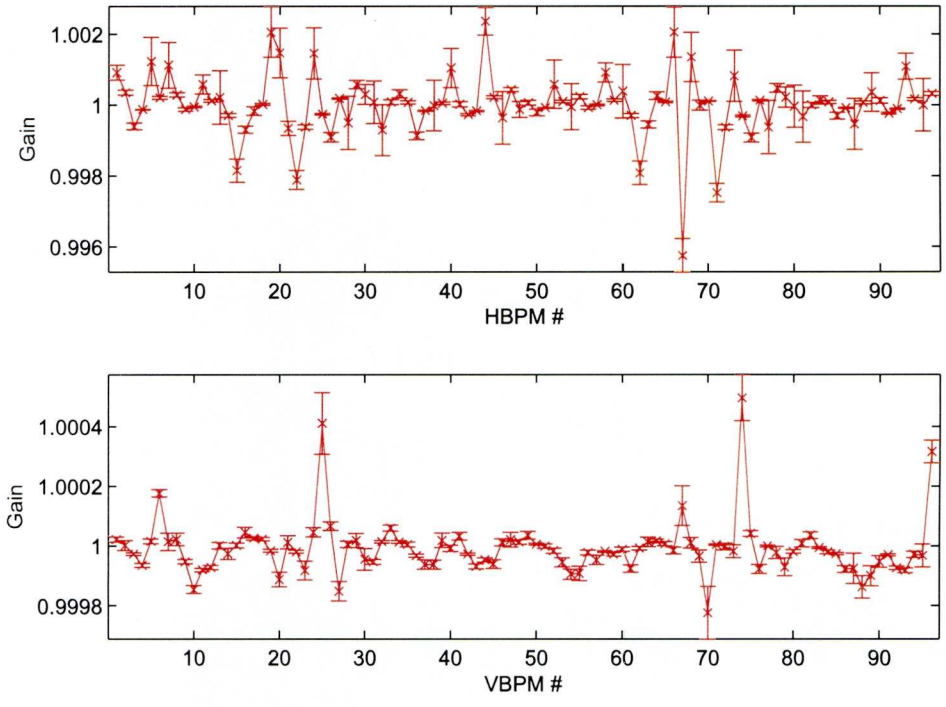

Figure 3.10: BPM gains fitted by LOCO for the ATF in the case of no BPM coupling. The error bars indicate the standard deviation of the BPM gains.

pling errors, we simulate ORM data for a model of the ATF in which only one skew quadrupole error has been applied at a time. Using only the skew quadrupoles on one family of sextupoles, we construct 34 orbit response matrices. From these matrices, we take the components corresponding to the horizontal response to a vertical kick, constructing a 3-D array of dimension $96 \times 51 \times 34$ (96 horizontal BPMs, 51 vertical correctors and 34 skew quadrupoles). This array can be reshaped into a set of 51 matrices B_k,each with dimensions 34×96: each of the matrices B_k gives (for a particular orbit corrector) the responses of the BPMs to changes in strength of the skew quadrupoles. Finally, we construct the matrix C where each column corresponds to an orbit corrector k, and the elements within a column are the elements of B_k:

$$\begin{pmatrix} \frac{\partial X_i}{\partial S_j} \\ \vdots \end{pmatrix} = C \cdot \begin{pmatrix} Y_k \\ \vdots \end{pmatrix}, \tag{3.13}$$

where X_i is the reading on (horizontal) BPMs i, S_j is the strength of skew quadrupole j, and Y_k is the strength of (vertical) orbit corrector k. Now we

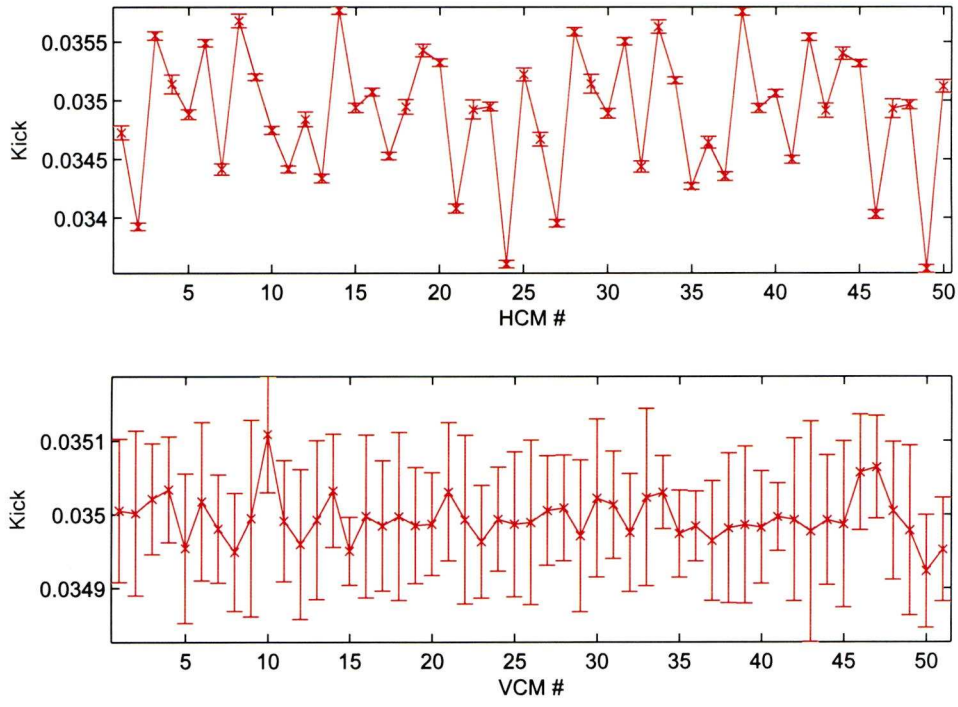

Figure 3.11: Fitted corrector kicks using LOCO for the ATF in the case of no BPM coupling. The error bars indicate the standard deviation of the BPM corrector kicks.

perform a singular value decomposition of C which gives a factorization:

$$C = U \cdot W \cdot V^{\mathrm{T}}. \tag{3.14}$$

where W is a diagonal matrix of the singular values of C, and V and U are unitary matrices. The rows of V^{T} corresponding to the smallest singular values indicate those correctors to which the various $\partial X_i/\partial S_j$ are least sensitive; in other words, those correctors that are least effective in telling us the skew quadrupole strengths based on analysis of the ORM. If we can identify a set of correctors residing almost entirely in the lowest rows of V^{T}, then we should be able to exclude those correctors from the ORM data, without affecting our ability to fit the skew quadrupole errors. In figure 3.21 we can see the elements in the rows of V^T corresponding to the smallest singular values of C. We find that these rows are populated almost entirely by orbit correctors in the two long straight sections of the ATF lattice. This is perhaps expected given the fact that the skew quadrupoles are located entirely

in the arcs.

Using only correctors in the arcs would reduce the time taken to collect ORM data by a factor of two. To test whether this would impact the quality of the fit, we simulated a correction procedure using ORM data including different sets of correctors:

- correctors located in the straight sections only;
- correctors located in the arc sections only;
- half of the correctors, evenly spaced around the ring;
- all available correctors.

The distributions of final vertical emittances for each set are shown in Fig. 3.22. The results suggest that using ORM data collected from half of the total number of available correctors, leads to a correction outcome similar to the correction achieved using ORM data collected from all available correctors. The practical benefit of this is the reduction in the time needed for measurements and the possibility of performing repeated correction attempts within a normal eight-hour shift.

3.2.3 Assessment of Coupling Correction Effectiveness using Experimental Data

Using data collected from a shift at ATF we attempt to evaluate our LOCO routine for betatron coupling correction. The routine uses the optimal fit conditions that have been identified in simulations (e.g. singular value cut-off threshold and weight factors on vertical and horizontal dispersion).

The measurement process involved three steps:

- Collect the ORM data for LOCO and perform the analysis assuming that all coupling comes from the skew quadrupoles;
- Adjust the strengths of the skew quadrupole magnets according to the values coming from the analysis in step 1;
- Collect another set of ORM data and again apply a LOCO analysis, to determine a new set of "measured" skew quad strengths.

The ability of LOCO to correct the coupling is directly indicated by a comparison between the change in the skew quadrupole strengths found by LOCO between the two iterations (two different ORM sets) and the known changes applied to the currents in the trim windings. The data were taken from the machine in its initial condition and after the first applied correction.

Figure 3.23 shows the aforementioned comparison. The appropriate data were collected at ATF on April 10 2008. We observe that the fitted changes in skew quadrupole strengths are reasonably well correlated with the known changes in the currents of the trim windings. The correlation is not as successful as the one achieved in simulation (figure 3.3), but given the fact that in the real machine the possibility of multiple sources of error is more than likely, we can be confident that the LOCO analysis provides meaningful results.

3.2.4 Analysis of January 2010 Data

Here we present the analysis of data received during more recent shifts (January 19-20 2010). We were able to take ORM and beta-function measurements. A LOCO analysis, varying the same parameters as before (section 3.2.1), was subsequently performed.

Figure 3.24 (upper plot) shows the measured orbit response matrix, and the difference between the measured and the modeled response matrix. The large spikes on the difference plot indicate that some BPMs were not working properly during the measurements and should be excluded from the data set (13 out of 96 BPMs). Having done that, the new fit is also shown on figure 3.24 (bottom plot).

We should note the different scales between the two plots of figure 3.24 and also that the cross-plane sectors of the response matrix are considerably smaller than the in-plane sectors. The horizontal BPMs are numbered 1 to 96 and the vertical BPMs 97 to 192; horizontal correctors are numbered 1 to 50, vertical correctors 51 to 101.

In figure 3.25 the cross plane sectors of the response matrices are presented. The residuals of the coupling components after the fit are significant and this is an indication that the effectiveness of a coupling correction based on the LOCO algorithm may be limited.

The quality of the fit to the response matrix can be indicated by a distribution of residuals in units of the "resolution" of the associated BPM.

The fit according to figure 3.26 appears to be reasonable, compared to the simulations where the introduced errors were limited (figure 3.7). Furthermore, the calculated projected vertical emittance from the fitted model is around 16 pm. This result however indicates that reaching the 2 pm goal for the vertical emittance using ORM analysis is practically going to be quite difficult. These results are illustrated in figure 3.27.

3.2.4.1 Beta function Measurements and Comparison

The beta beat is defined as the quantity:

$$\frac{\beta_{meas} - \beta_{nom}}{\beta_{nom}}, \tag{3.15}$$

where $\beta_{meas}, \beta_{nom}$ stand for the measured and nominal beta functions, respectively, in the ring.

Figures 3.28, 3.29 and 3.30 illustrate the beta beat in different sections of the beam. The "measured" data refers to beta function measurements taken during the aforementioned shifts and the "fit" data come from the beta functions calculated with the fitted model produced by LOCO.

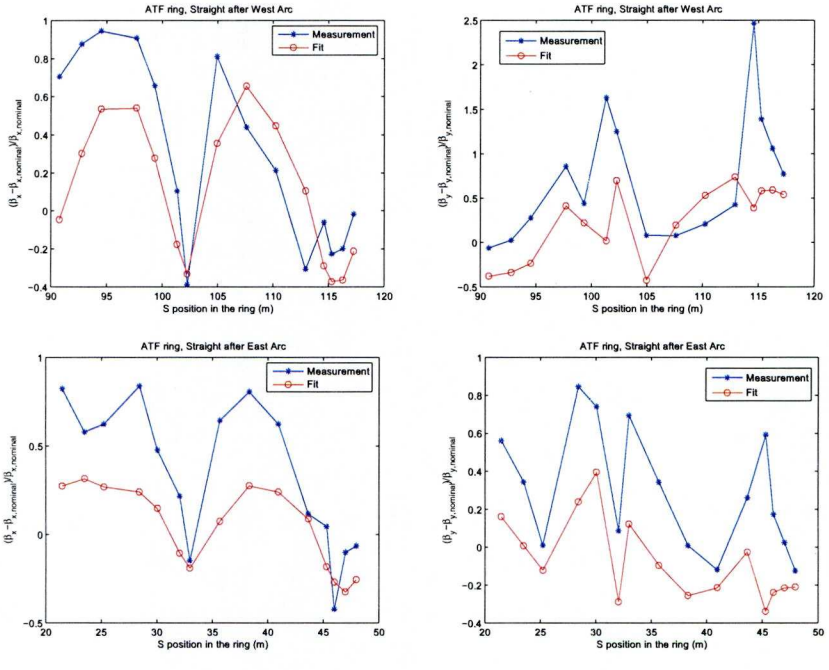

Figure 3.30: Beta beats (β_x, β_y) in the straight sections of the ATF.

It is evident that there is very good agreement between the measurements and the fitted model in some sections of the ring, while there are considerable discrepancies elsewhere. However, in all cases the trend of the two curves is approximately the same, which suggests that the ORM analysis gives sensible results. It is not clear whether the results from the ORM analysis are sufficiently accurate and reliable for the technique to form the basis of a procedure for tuning the ATF damping ring to a vertical emittance of 2 pm. It should be noted that the fitting process appears to be quite robust even in the case of erroneous measurements. This is shown in figure 3.31, where the beta functions of both the original fit and the improved (excluded BPM measurements) fit are depicted. The exclusion of the "bad" BPMs seems to have only a marginal effect on the fit.

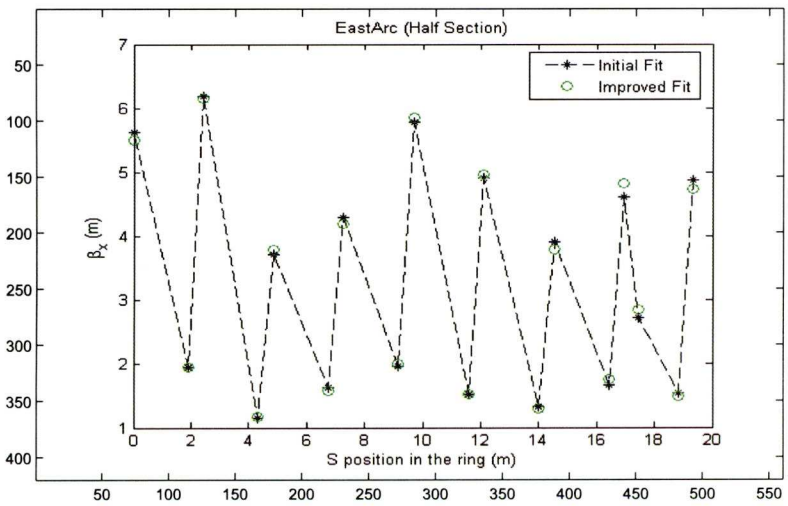

Figure 3.31: Comparison of the original and improved (excluded erroneous BPM measurements) fit for the beta functions in the east arc. The fitting process appears to be quite robust, even in the case of "bad" BPM measurements.

3.3 Conclusions

We evaluated the use of the LOCO algorithm for betatron coupling correction, in the context of the challenging goal regarding the specifications for the ILC Damping Ring vertical emittance. This included investigation of

possible situations where a correction based on ORM analysis is likely to be of limited success.

For the simple case of a lattice with only skew quadrupole errors, the simulations suggest that we can achieve a vertical emittance of just below 2 pm in the ATF damping ring. We also established that there is no significant degeneracy between skew quadrupole strengths and corrector magnet tilts. However, there appears to be a degeneracy between the skew quadrupole strengths and the BPM couplings, that may put a lower limit on the vertical emittance that can be achieved using this technique, of around 6 pm.

The impact of BPM coupling errors is therefore significant for the performance of LOCO and it is likely to limit the technique's practical usefulness in view of the ultra-low vertical emittance levels required. Equally important is the fact that the current implementation of the LOCO algorithm will not be able to handle a lattice the size of the ILC damping ring. Consequently, it would be worthwhile investigating alternative modeling and tuning techniques.

Simulations also suggest that the ORM data can be collected using about half the total number of orbit correctors, without compromising the final outcome of the correction. This would have significant practical benefit, in reducing the amount of time needed for ORM data collection by half.

Further measurements and attempts with LOCO at the ATF support the conclusion that orbit response matrix analysis will not be able to "tune" the machine down to the low levels of vertical emittance specified for the ILC Damping Rings.

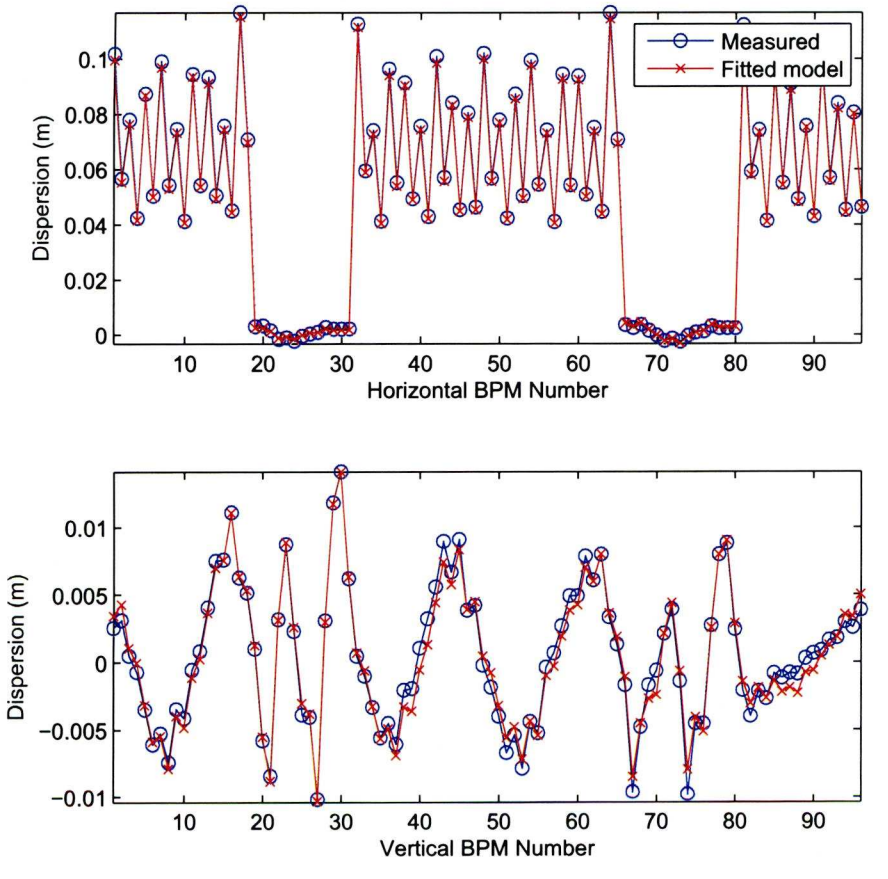

Figure 3.12: Horizontal and vertical dispersion fit using LOCO for the ATF in the case of no BPM coupling. The "measured" values are shown as crosses in red; the fitted values are shown as circles in blue. Choosing the "correct" weight factor for the dispersion can lead to a very accurate fit.

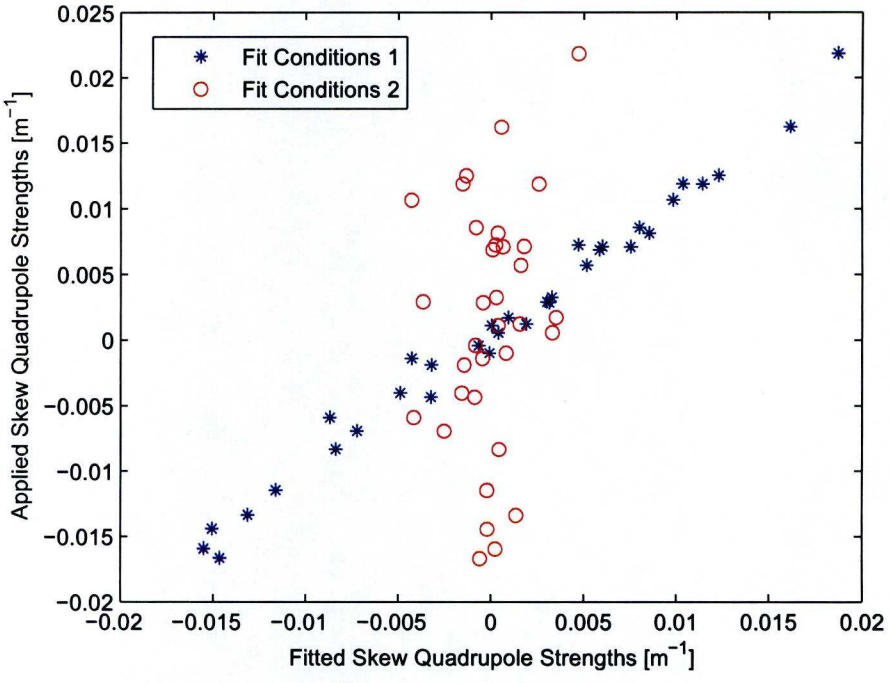

Figure 3.13: Effect of singular value cut-off thresholds in the fit of the skew quadrupole strengths. Choosing the appropriate threshold can make the difference between a poor (red circles) and a good fit (blue asterisks).

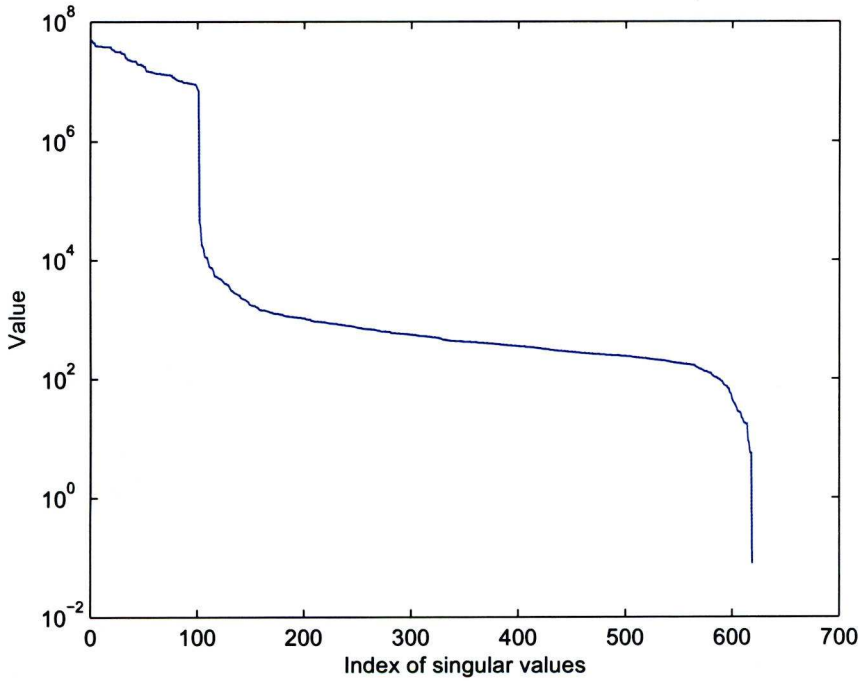

Figure 3.14: Singular values of the "measured" response matrix used in LOCO.

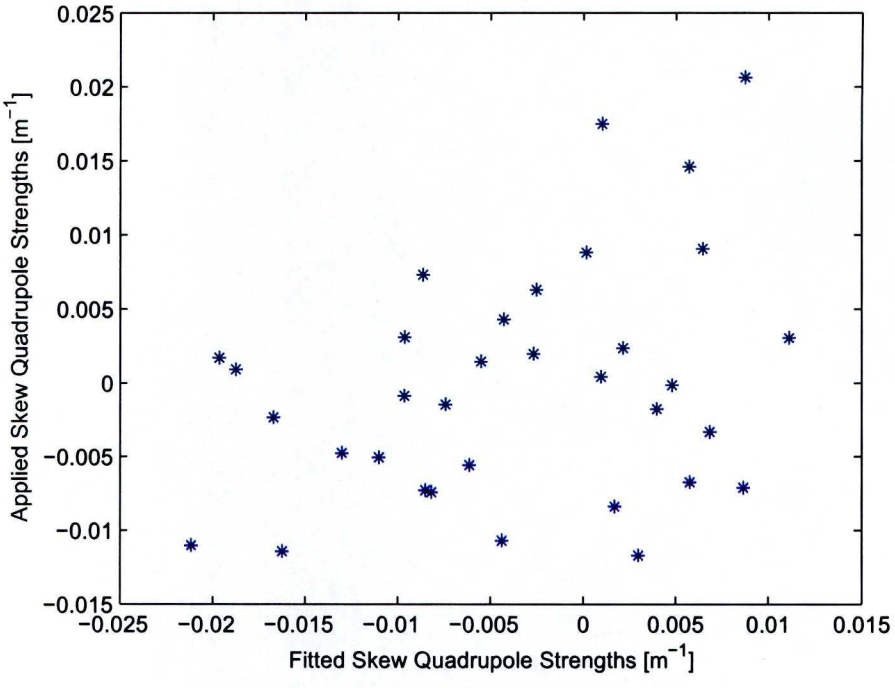

Figure 3.15: Dispersion weight factor parameter choice severely affecting the correlation between applied and fitted skew quadrupole strengths: A value of 10 as opposed to the optimal value of 0.01 was chosen in this case.

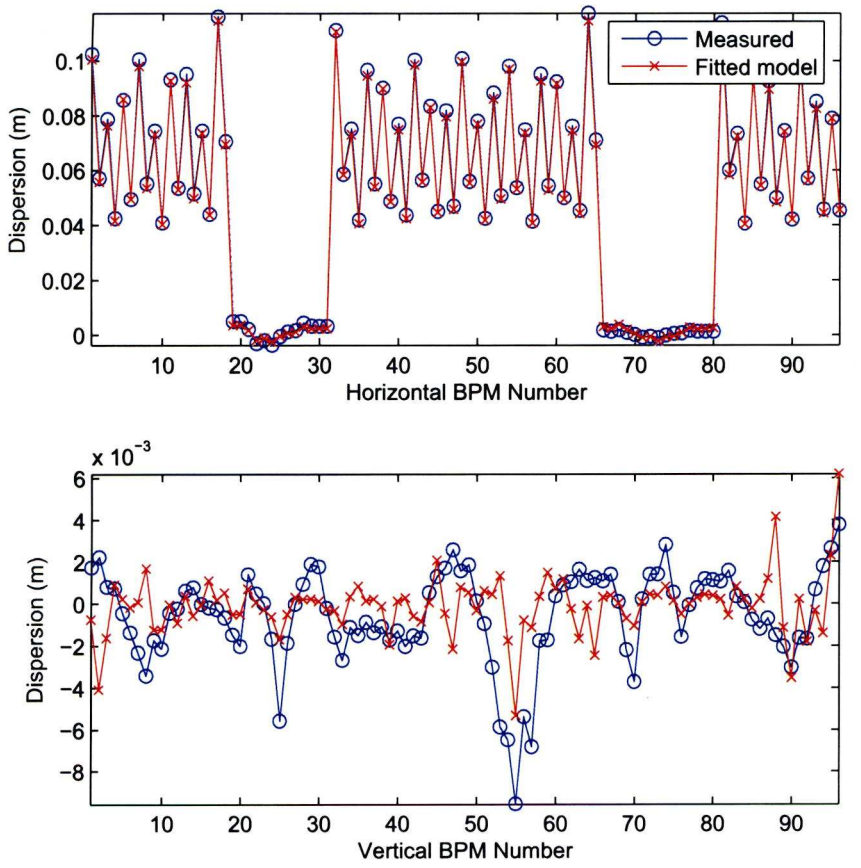

Figure 3.16: Poor fit of dispersion, especially in the vertical plane as a result of a "bad" vertical dispersion weight factor.

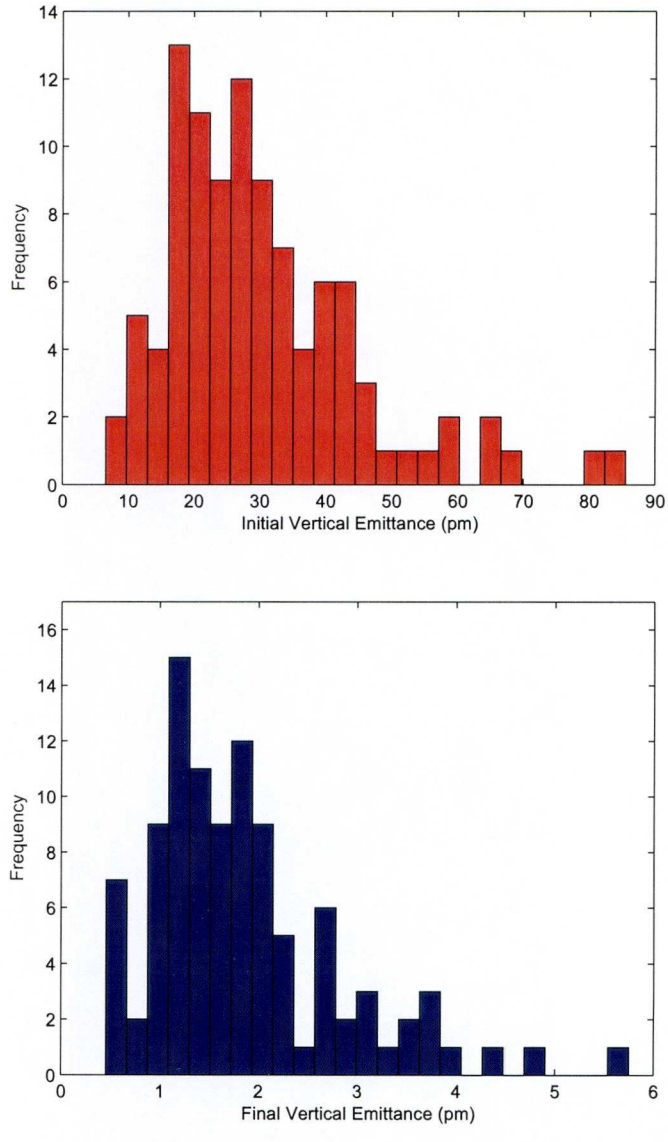

Figure 3.17: Distribution of vertical emittance, initially (upper plot) and after correction using the LOCO fitted skew quadrupole values (bottom plot). This indicates that the best possible emittance (no other errors besides skew quadrupole errors present) that could be achieved using this technique is just under 2 pm starting from an average initial emittance of around 30 pm.

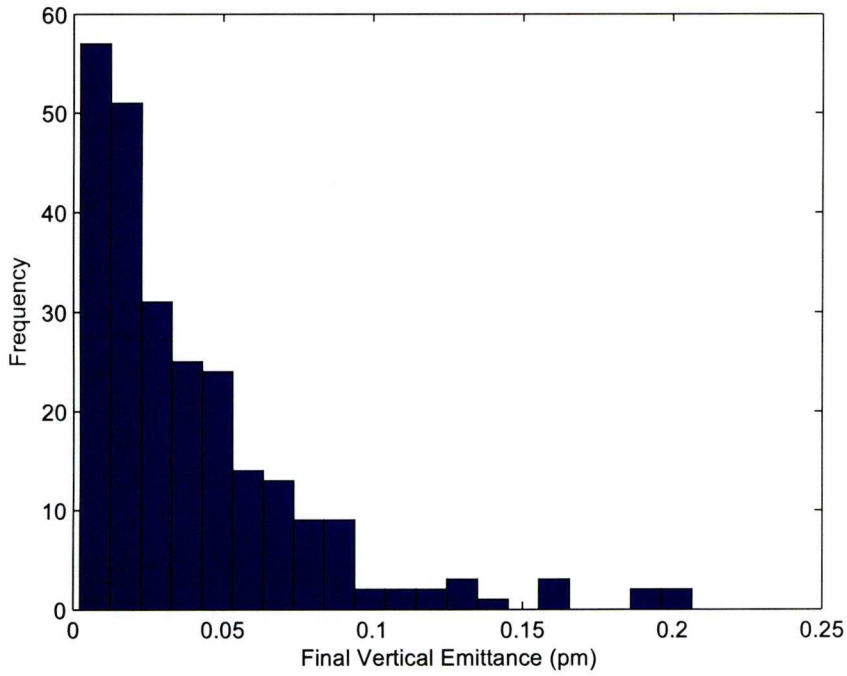

Figure 3.18: Distribution of "corrected" vertical emittance (250 seeds). The only errors present were corrector magnet rotations around the beam axis (tilts).

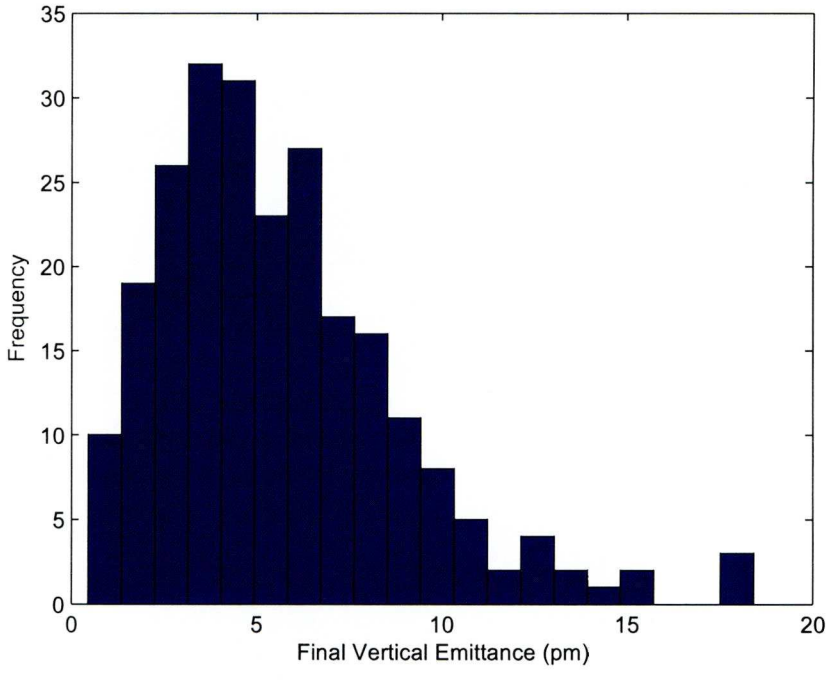

Figure 3.19: Distribution of "corrected" vertical emittance (250 seeds). The only errors present were BPM couplings of order 2%.

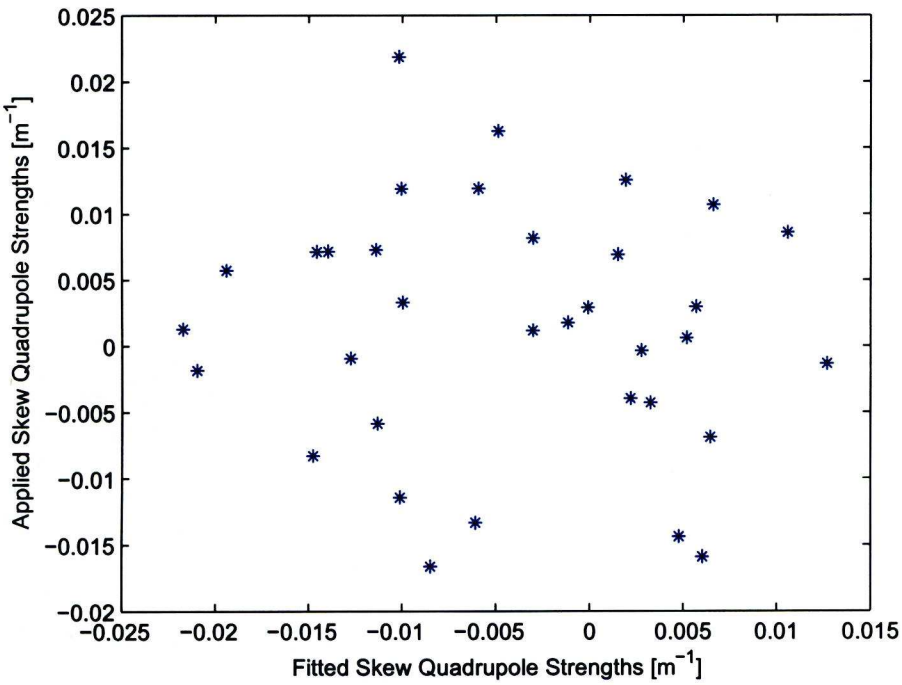

Figure 3.20: Degradation of the correlation between applied and fitted skew quadrupole strengths in the presence of both BPM coupling errors and skew quadrupole errors.

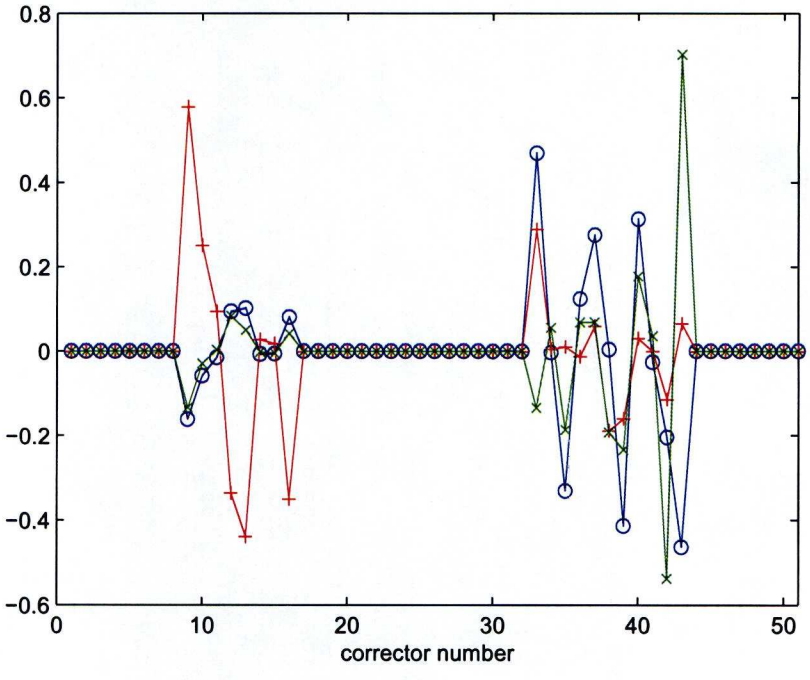

Figure 3.21: Elements in the rows of V^{T} corresponding to the smallest singular values of C.

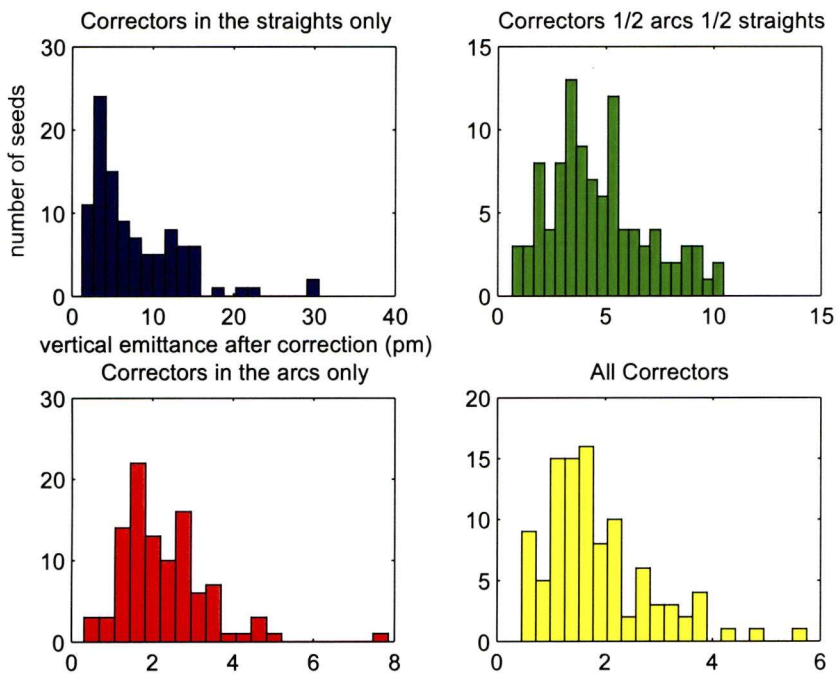

Figure 3.22: Distribution of final vertical emittance after correction based on ORM data using different sets of orbit correctors. The results suggest that using ORM data collected from half of the total number of available correctors, leads to a correction outcome similar to the correction achieved using ORM data collected from all available correctors.

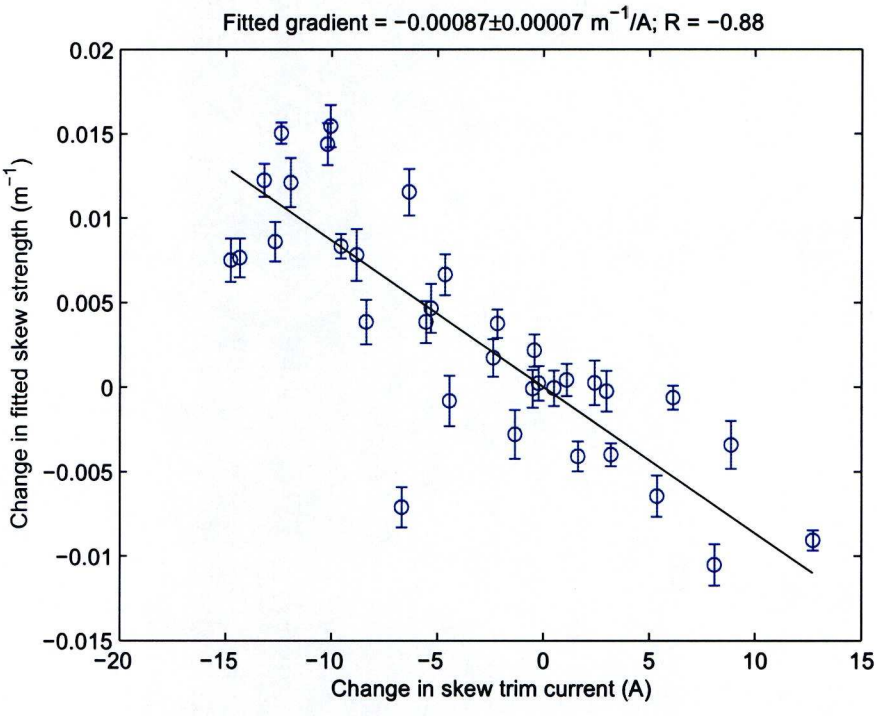

Figure 3.23: Change in fitted skew quadrupole strengths as determined by the LOCO analysis of the ORM data versus known changes in current in the skew quadrupole trim windings on the sextupoles.

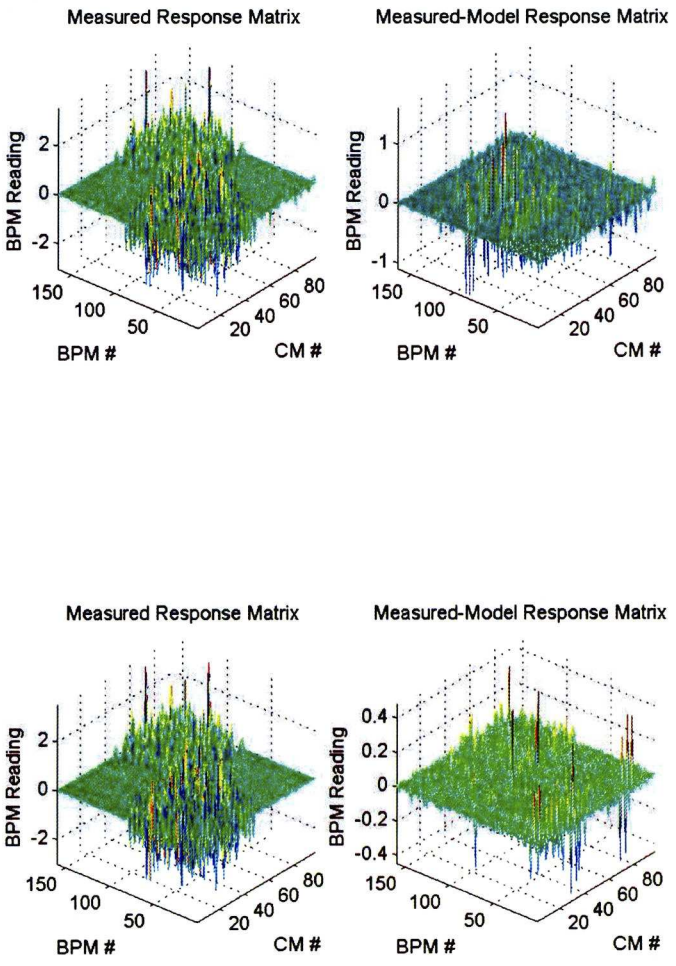

Figure 3.24: ORM Fit, before (top) and after removal of malfunctioning BPMs (bottom). Note the different scales between the two plots in the bottom.

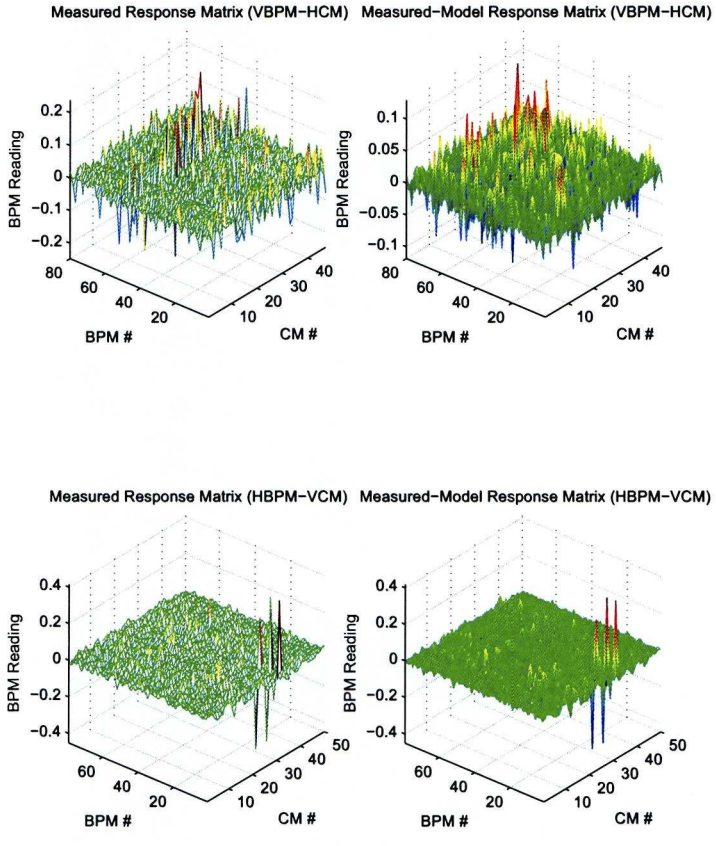

Figure 3.25: Cross-plane responses; vertical BPMs to horizontal correctors(top), horizontal BPMs to vertical correctors (bottom). The residuals of the coupling components after the fit are significant; this is an indication that the effectiveness of a coupling correction based on the LOCO algorithm may be limited.

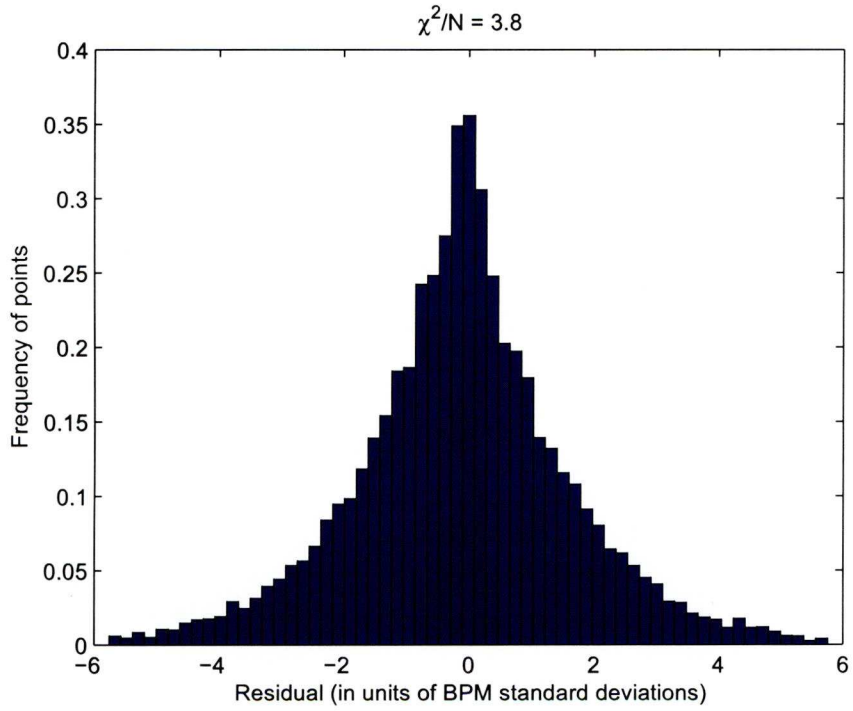

Figure 3.26: Data from shift at ATF on January 2010): Distribution of the residuals of the fit to the response matrix in units of BPM resolution.

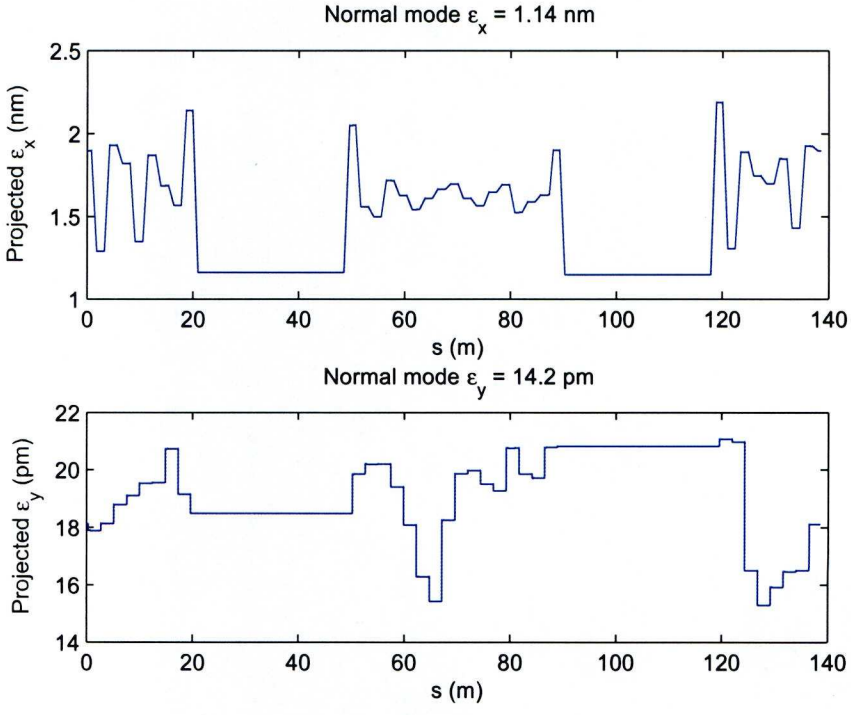

Figure 3.27: Calculated projected emittance in a model of the ATF fitted to measured ORM data.

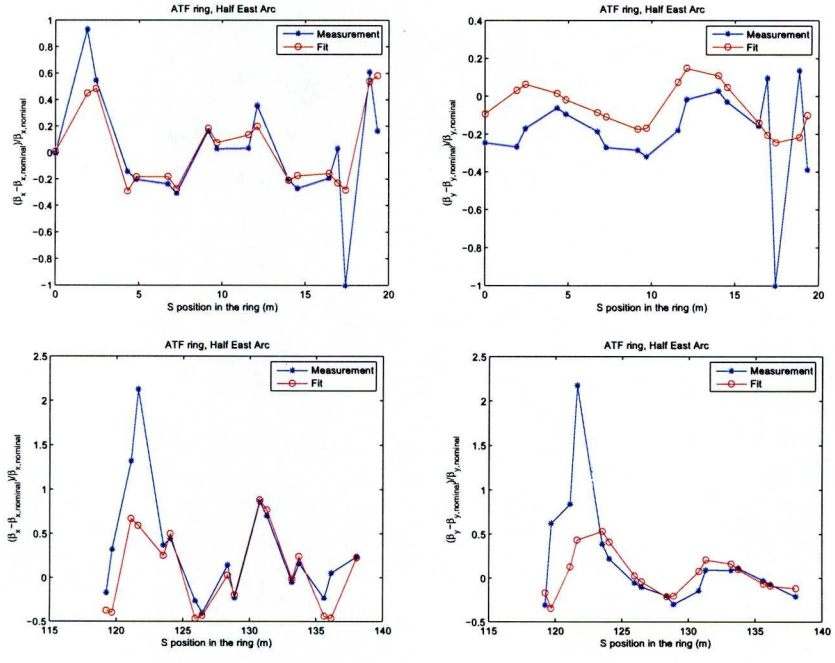

Figure 3.28: Beta beats (β_x, β_y) in the east arc of the ATF.

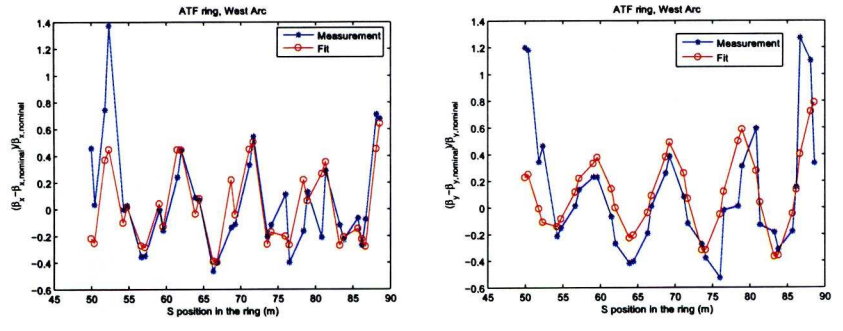

Figure 3.29: Beta beats (β_x, β_y) in the west arc of the ATF.

Chapter 4

LET Studies for the ILC Damping Rings

The specifications for the ILC damping rings define operation with a vertical emittance of 2 pm. This is an especially challenging goal, given the fact that the lowest vertical emittance demonstrated is approximately 3.2 pm [2]. Low-emittance tuning techniques have to be checked for reliability and ease of implementation. For any correction procedure to be successful an effective diagnostics and correction system is paramount. However, BPMs add impedance to the ring, and diagnostics and correctors add complexity and cost. It is therefore desirable to understand how the final achievable emittance depends on the numbers, locations and performance of the BPMs and correctors, and to determine the minimum number of these components required.

In this chapter, we present the results of simulations for some of the different configurations of the damping rings, aimed at different lattice characteristics that are important for achieving the desired performance as well as for operational stability. In particular, we investigate the sensitivity of different lattice configurations to magnet misalignments and the effectiveness of some widely used correction schemes for low-emittance tuning. The simulations are idealized, i.e. not all types of possible errors were included. This approach may not be realistic, however it provides a necessary and crucial step in understanding the dynamics of each configuration and the relative effect of different types of errors when studied separately. Performing more realistic simulations (i.e. by including all possible errors that are

Figure 4.1: Evolution of the ILC Damping Rings design.

usually encountered in real operating accelerators) is of course possible, but doing so would not help in identifying the effect of individual types of errors, such as magnet misalignments, and their contribution to the overall machine performance. The major goal of this effort is to make informed suggestions about the design and operational conditions needed for the ILC damping rings which will allow the production of the specified high quality beams.

The ILC damping ring design has been through a number of revisions and refinements (figure 4.1). We give a brief description of the lattice evolution and show results from simulations regarding the most important lattice designs.

4.1 Evolution of the Lattice Design

The ILC damping ring design and specifications have gradually evolved from the first configuration studies [67, 71, 72, 24] to the 6.4 km baseline lattice [25]:

The OCS6 design (figure 4.4) was based on Theoretical Minimum Emittance (TME) arc cells, while all the DCO lattice designs are based on a racetrack layout with FODO-style arc cells. The transition from a TME lattice to a FODO lattice was motivated by reducing construction costs and complexity. The TME lattice requires extra quadrupoles so that both the horizontal beta function and horizontal dispersion function have a minimum in the middle of the bending magnet of each cell. Given that the equilibrium emittance in the damping rings is expected to be dominated by the wiggler section, there is no real need for a TME lattice. In the DCO2 lattice the injection and extraction lines were placed in opposite sides of the ring and there were 2 separate wiggler sections. In the DCO3 lattice the wiggler sections were unified and injection and extraction lines were placed on one side of the ring. These changes were driven by global configuration issues. Finally in the DCO4 lattice the positron injection and electron extraction beam lines for both positron and electron rings are in the same tunnel when two rings are on top of each other. Positron injection and electron extrac-

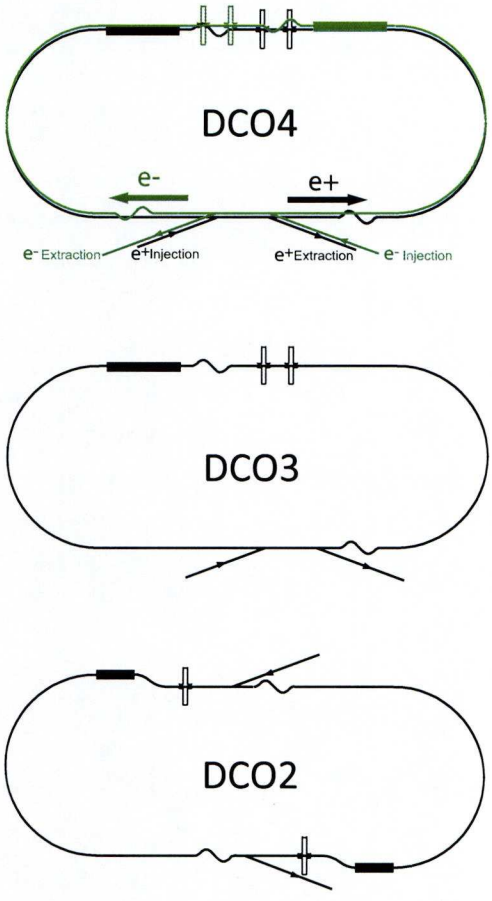

Figure 4.2: ILC Damping Rings Lattice Designs

tion beam lines have to be in the same tunnel as well as electron injection and positron extraction beam lines when the arc bending magnets of the positron and electron damping rings are put on top of each other. These modifications also simplify the cryogenic systems required for the wigglers and the RF modules of the rings.

Figure 4.2 shows these changes in the different versions of the damping ring design.

The present baseline lattice for the ILC damping rings has a circumference of 6476 m and a racetrack layout, shown in figure 4.3. The circumference of the damping ring is driven by the available performance of the extraction kicker; for a given number of bunches there has to be enough "gap" between them so that the kicker can extract them. The most important operational parameters are shown in table 4.1.

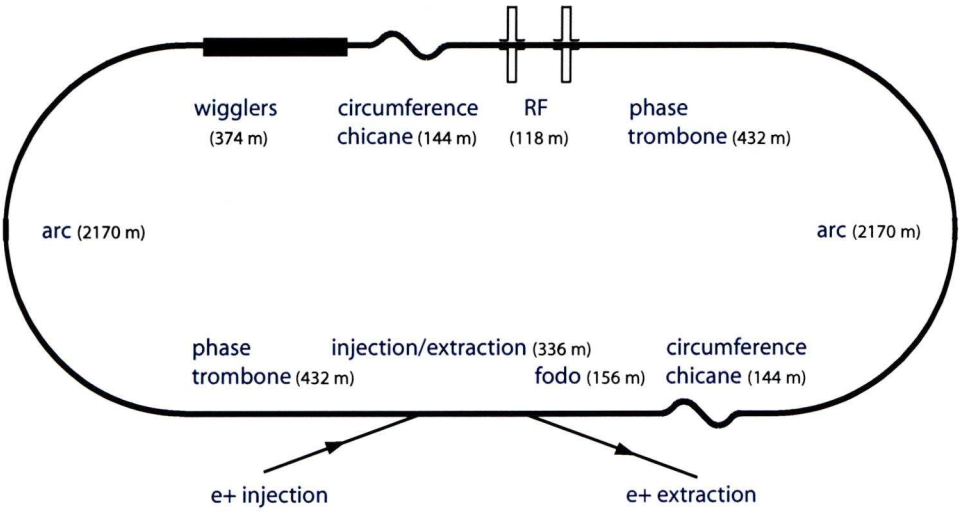

Figure 4.3: DCO4 layout

Circumference	6476 m
Beam energy	5 GeV
Average current	400 mA
Max bunch population	2×10^{10}
Transverse damping time	25 ms
Natural Emittance	0.8 nm
Vertical emittance	2 pm
RMS bunch length	9 mm
RMS energy spread	0.13%
RF voltage	24 MV
RF frequency	650 MHz

Table 4.1: Basic ILC Damping Ring parameters

Two arcs, each consisting of 96 FODO cells, are joined by two long straights containing the damping wiggler, RF cavities and injection/extraction systems. To provide operational flexibility, the momentum compaction factor is tunable between 1.3×10^{-4} and 2.8×10^{-4}; the reason for this is to be able to lower the RF voltage and therefore increase the single bunch instability threshold. Adjustment of the momentum compaction factor is achieved by changing the phase advance in the arc cells. To achieve the specified damping time of 20 ms with a beam energy of 5 GeV, a damping wiggler of length 200 m is needed. Under ideal conditions the equilibrium emittance is dominated by the lattice functions in the wiggler; however orbit distortion

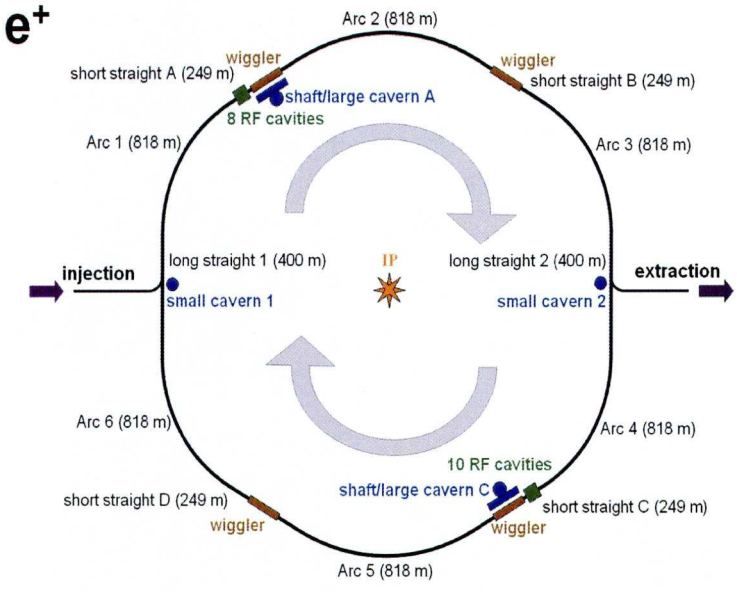

Figure 4.4: Schematic layout of the OCS6 positron damping ring

and dispersion in the arcs can make a significant contribution to the vertical emittance if not corrected carefully.

4.2 Sensitivity to Linear Imperfections

The luminosity of a linear collider will depend on the vertical emittance of the beam extracted from the damping rings. In an electron storage ring, the dominant sources of vertical emittance are the vertical dispersion and the betatron coupling. An important part of the design of the damping rings is the specification of the systems capable of measuring and correcting the dispersion and the coupling at the necessary level. To understand the issues and optimize the design we performed simulation studies exploring different design scenarios. As a first step, we looked at the sensitivity of the vertical emittance to vertical alignment errors on the quadrupoles and sextupoles: these errors are expected to make a significant contribution to the vertical emittance in the operating rings. These investigations provide a solid foundation for more complete studies where additional effects are

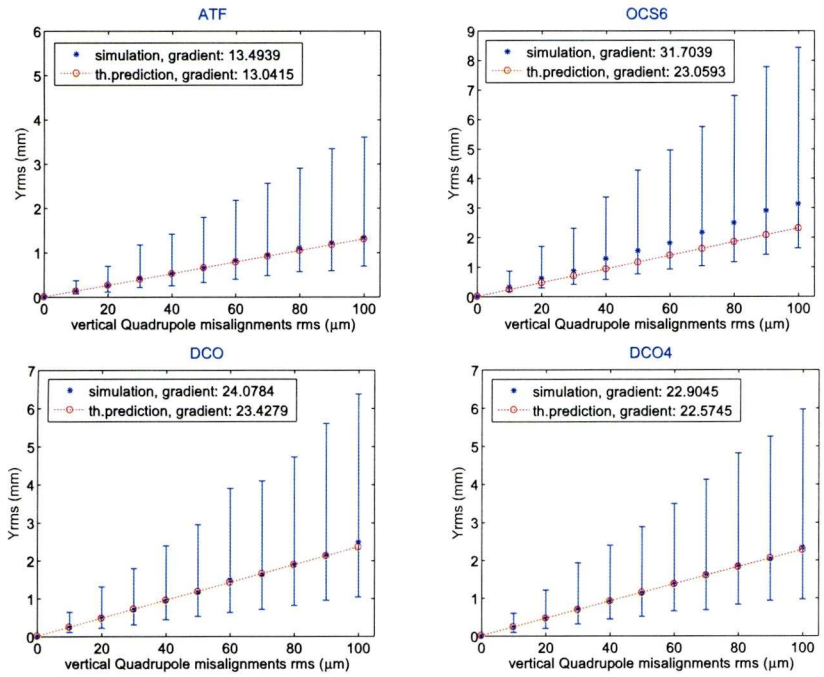

Figure 4.5: Sensitivity of vertical rms beam position to quadrupole misalignments. Red circles indicate the theoretical prediction based on equation (2.282) while blue asterisks represent the simulation results. All ILC damping ring designs appear to be more sensitive than the ATF lattice.

included, such as BPM noise and rotation.

Here we present the results of simulations for the three "milestone" designs for the ILC Damping Rings, which are based on ATF and the initial recommendations of the configuration studies for the ILC damping rings [67]. We first apply the type and range of errors in the specific lattice and then calculate the relevant beam parameters. This is done for 100 seeds and the blue vertical lines represent the total range of possible values for these beam parameters. We compare where appropriate, the simulation results with theoretical equations from the literature and chapter 2.

Figure 4.5 shows the dependence of the closed orbit distortion (COD) on vertical quadrupole misalignments for different lattice designs. It also includes results from the same simulations for the ATF damping ring which can serve as a reference; the latter is the major "testbed" for low emittance tuning studies. The orbit amplification factor [equation (2.282)] is used for the theoretical prediction of the closed orbit distortion.

There is very good agreement between the simulation and the theoreti-

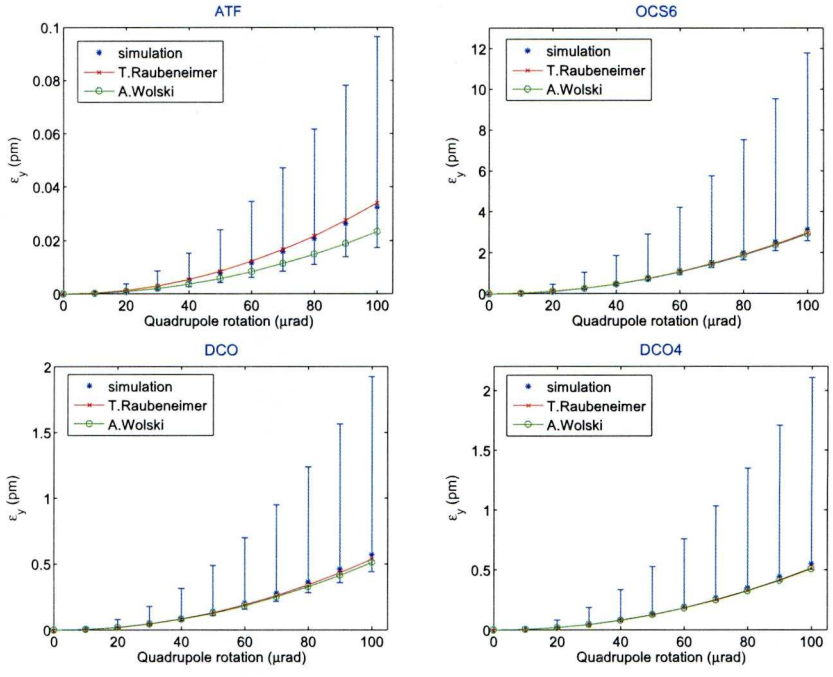

Figure 4.6: Sensitivity of vertical rms emittance to quadrupole rotations (tilts). Green circles and red asterisks indicate theoretical prediction based on theoretical equations (4.1) and (2.284),(2.301), while blue asterisks represent the simulation results.

cal predictions. All the ILC damping ring designs appear to have a similar level of sensitivity with regard to vertical quadrupole misalignments, with the DCO4 lattice achieving marginally the lowest closed orbit distortion of just over 2 mm for an rms value of 100 μm of vertical quadrupole misalignment. However, all three designs are almost twice as sensitive as the ATF lattice; and that means that the alignment tolerance specifications for the ILC damping rings will have to be relatively demanding.

The effect of quadrupole rotations (tilts) with respect to the reference trajectory on the vertical emittance of the beam is shown in figure 4.6.

Raubenheimer [43] gives a formula for the dependence of the vertical emittance with respect to quadrupole rotations:

$$\begin{aligned} \frac{\varepsilon_y}{\langle\theta^2_{quad}\rangle} &\approx \frac{j_x[1-\cos 2\pi\nu_x \cos 2\pi\nu_y]}{j_y[\cos 2\pi\nu_x - \cos 2\pi\nu_y]^2}\varepsilon_x \sum_{quads} \beta_x\beta_y(k_1L)^2 \\ &+ \frac{j_z\sigma_\delta^2}{\sin^2 \pi\nu_y} \sum_{quads} \beta_y\eta_x^2(k_1L)^2\,, \end{aligned} \tag{4.1}$$

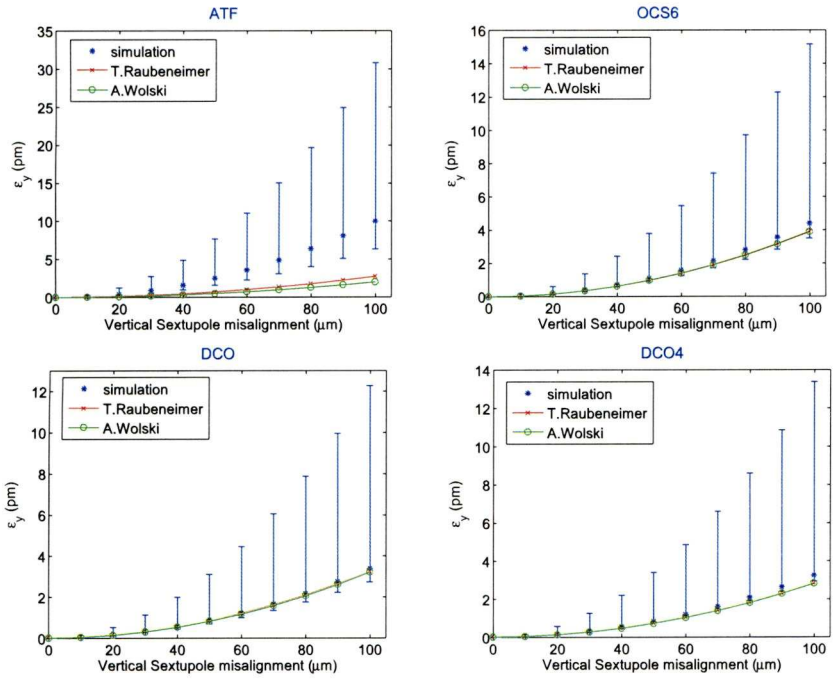

Figure 4.7: Sensitivity of vertical rms emittance to sextupole vertical misalignments. Analogous line notation to figure 4.6.

where $\langle\theta^2_{quad}\rangle$ is the mean square quadrupole rotation, j_x, j_y and j_z are the horizontal, vertical and longitudinal damping partition numbers respectively, ν_x, ν_y are the betatron tunes, β_x, β_y are the beta functions, η_x is the horizontal dispersion, σ_δ is the rms energy spread and $k_1 L$ is the integrated quadrupole strength. The first term in equation (4.1) gives the contribution to the vertical emittance from betatron coupling and the second term gives the contribution from vertical dispersion. An alternative theoretical equation for the vertical emittance, used in the sensitivity graphs, is the addition of the contributions of vertical dispersion and betatron coupling and is the combination of equations (2.284) and (2.301) given by Wolski [66].

The simulation results are in good agreement with the theoretical predictions. Both the DCO and DCO4 designs appear to be less sensitive to quadrupole rotations than the OCS6 lattice regarding vertical emittance growth.

Similarly, the dependence of the vertical emittance on sextupole misalignments is shown in figure 4.7.

The theoretical equation that correlates the sextupole vertical alignment

errors and the generated vertical emittance is very similar to equation (4.1):

$$\frac{\varepsilon_y}{\langle y_{sext}^2 \rangle} \approx \frac{j_x[1-\cos 2\pi\nu_x \cos 2\pi\nu_y]}{4j_y[\cos 2\pi\nu_x - \cos 2\pi\nu_y]^2}\varepsilon_x \sum_{sexts} \beta_x\beta_y(k_2L)^2 + \frac{j_z\sigma_\delta^2}{4\sin^2\pi\nu_y}\sum_{sexts}\beta_y\eta_x^2(k_2L)^2\,, \tag{4.2}$$

where this time $\langle y_{sext}^2 \rangle$ is the mean square sextupole alignment error.

The sensitivity of the different damping ring designs and the ATF to quadrupole vertical misalignments is shown in figure 4.8. The theoretical equation used for the prediction of the vertical emittance in the presence of quadrupole vertical misalignments is:

$$\varepsilon_y = \varepsilon_{dispersion} + \varepsilon_{coupling}\,, \tag{4.3}$$

according to the aforementioned equations of chapter 2. We again see that the ILC damping ring designs are much more sensitive to alignment errors than the ATF.

4.3 Orbit and Dispersion Correction

The next step in these series of investigations is to study the effectiveness of a simple combined correction of the orbit and the dispersion in minimizing the vertical emittance [3, 4]. The different operation parameters have been set to accommodate necessary compromises (dynamic aperture, stability). It is therefore important to know how the correction procedure "behaves" under different machine parameters and configurations.

Furthermore, we focus our studies on the more recent designs; the OCS6 lattice having been superseded since its initial proposal, we concentrate our combined correction simulations on the DCO and DCO4 lattice designs.

4.3.1 Correction Procedure

Under ideal conditions the equilibrium horizontal emittance is dominated by the lattice functions in the wiggler and the vertical emittance damps to the limit set by the opening angle of the radiation, equation (2.267); however, orbit distortion and dispersion in the arcs can make a significant contribution to the vertical emittance if not corrected properly. Therefore it is useful to

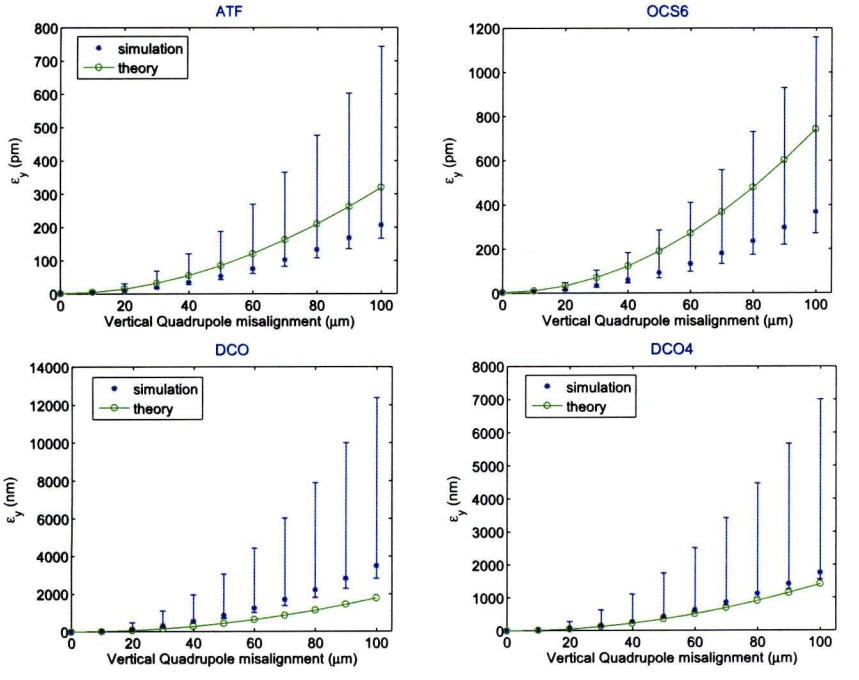

Figure 4.8: Sensitivity of vertical rms emittance to quadrupole vertical misalignments. Red circles indicate the theoretical prediction based on equation (2.282) while blue asterisks represent the simulation results. The ILC damping ring designs are much more sensitive to alignment errors than the ATF lattice.

investigate operating scenarios with different BPM arrangements in the arcs. The DCO (and subsequent) lattices are designed to provide flexibility in the working point [26]. In particular, good dynamic properties are achieved with phase advance in the arc cells set to (approximately) 72°, 90° or 100°. However, the larger the phase advance, the less stable a lattice becomes; the sensitivity of the lattice to magnet alignment errors increases and correction of the vertical emittance becomes harder to achieve. Therefore, we opted, for the early version of the ILC damping ring lattice (DCO), to study the cases of 72° and 90° which provided a better foundation for the attempted correction process.

The beam position is measured with a set of N BPMs, which are distributed over the ring depending on the scenario (table 4.2). The beam is steered using a set of M dipole magnets (correctors). The BPM readings are represented by a vector $\vec{u}$ of dimension N and the corrector strengths (kicks) by a vector $\vec{\theta}$ of dimension M. Measured dispersion at the BPMs is represented by vector $\vec{D}$ (dimension N). The orbit response matrix (ORM) A describes the change in beam position at each BPM resulting from a change in strength of each corrector. Similarly, the dispersion response matrix (DRM) B describes the change in dispersion at each BPM resulting from a change in strength of each corrector. Both A and B are matrices of dimension $N \times M$.

For both orbit and dispersion to be corrected simultaneously, a set of corrector kicks $\vec{\theta}$ must be found that solves the following system of linear equations:

$$\begin{pmatrix} (1-\alpha)\vec{u} \\ \alpha\vec{D}_u \end{pmatrix} + \begin{pmatrix} (1-\alpha)A \\ \alpha B \end{pmatrix} \vec{\theta} = 0 \tag{4.4}$$

In general, there are $2N$ equations in M unknowns. If, as is the case here, $2N > M$ then it is not possible, in general, to find exact solutions for the kicks $\vec{\theta}$ (the system is over-constrained). However, using singular value decomposition (SVD), we can find a solution that minimizes the residual orbit and dispersion. A more detailed description of the SVD method and its "mechanics" is given in Appendix A. The factor α appearing in Eq. (4.4) determines whether more weight is given to correcting the orbit ($\alpha = 0$) or to correcting the dispersion ($\alpha = 1$) in finding the solution. The optimum value of α for minimizing the vertical emittance depends on the lattice and the arrangement of BPMs and correctors: the goal is to investigate this

Scenario	Arc phase advance	Arc BPM locations
I	72°	every quad
II	90°	every quad
III	72°	every D-quad
IV	90°	every D-quad
V	72°	2/3 D-quads
VI	90°	2/3 D-quads

Table 4.2: Scenarios studied in orbit and dispersion correction simulations for the DCO lattice.

dependence and assess the performance of the correction algorithm under the different configurations.

4.3.2 Simulation Results for the DCO Lattice: No BPM Gain Errors

Here we present the results of simulations of orbit and dispersion correction in six different scenarios, shown in table 4.2, using the DCO lattice design. In each case the phase advance across a single arc cell is either 72° or 90°. BPMs are located at every quadrupole in the straights; in the arcs BPMs are located either at every quadrupole, or only at every defocusing quadrupole, or only at two out of every three defocusing quadrupoles. In these series of simulations for the DCO lattice, all BPMs are considered to have no gain errors. Note that the number of correctors that we use is always equal to the number of BPMs. For each scenario we apply random vertical misalignments to all quadrupoles (50 μm rms) and to all sextupoles (100 μm rms). These values are chosen in accordance with realistic rms errors for quadrupoles and sextupoles [27, 29]. We then apply a combined orbit and dispersion correction, with the goal of minimising the vertical emittance.

For each scenario in our simulations, we first obtain the ORM and DRM. For a given set of random misalignments we then find the closed orbit and the dispersion at each BPM. The solution for the corrector strengths in equation (4.4) can then be found, for a given weight factor, by singular value decomposition.

One of the first issues we can investigate is how the orbit and the dispersion behave as we apply the correction. These observations can serve as

a basic test as to whether our correction scheme is in fact acting according to the formulation hypotheses. Figure 4.9 shows the results for scenario

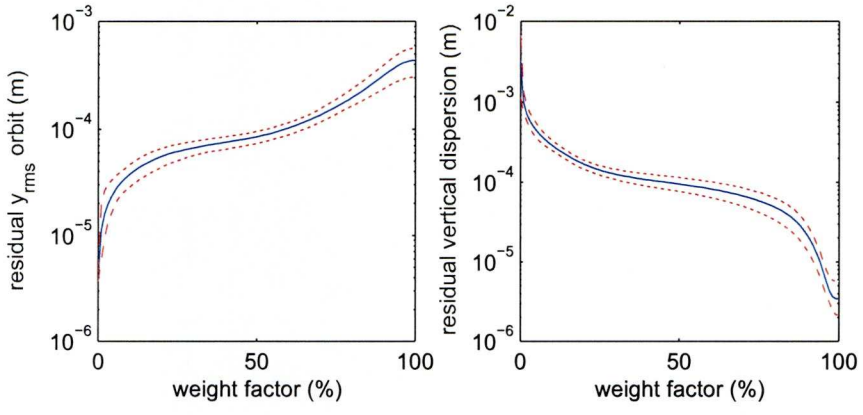

Figure 4.9: Orbit and dispersion correction in scenario I as a function of the weight factor α. Red lines indicate the standard deviation over 100 seeds of random alignment errors.

I averaged over 100 seeds of random errors. As expected the orbit is almost perfectly corrected for $\alpha = 0$, and the dispersion is almost perfectly corrected for $\alpha = 1$.

Given the orbit and dispersion, it is possible to make an analytical estimate of the vertical emittance using equation (4.5):

$$\begin{aligned} \varepsilon_y \;=\; & \frac{j_x}{4j_y}\frac{1-\cos(2\pi\nu_x)\cos(2\pi\nu_y)}{[\cos(2\pi\nu_y)-\cos(2\pi\nu_x)]^2}\varepsilon_x \times \\ & \sum_{sexts} \beta_y\beta_x(k_2L)^2\left[\langle y_{sext}^2\rangle + \langle y_{orbit}^2\rangle\right] \\ & +j_z\sigma_\delta^2\left\langle\frac{\eta_y^2}{\beta_y}\right\rangle , \end{aligned} \tag{4.5}$$

where j_x, j_y and j_z are the horizontal, vertical and longitudinal damping partition numbers; ν_x and ν_y are the betatron tunes; ε_x is the horizontal emittance; β_x and β_y are the horizontal and vertical beta functions; k_2L is the integrated normalised sextupole strength; σ_δ is the rms energy spread; η_y is the vertical dispersion; y_{sext} is the vertical displacement of a sextupole magnet with respect to the design reference trajectory; and y_{orbit} is the vertical closed orbit distortion with respect to the design reference trajectory. This equation provides an estimate of the vertical emittance based on equa-

tion (4.2). The two terms on the right side represent the betatron coupling and the vertical dispersion components of the vertical emittance. In the presence of both sextupole and quadrupole vertical alignment errors, the offset of the beam at the sextupoles, generating the betatron coupling, can be assumed to be a linear combination of the vertical alignment error of the sextupoles and the vertical closed orbit distortion caused by the vertically misaligned quadrupoles.

The estimate of the vertical emittance using this formula may be compared to that obtained from the simulation code. The result, for scenario I, is shown in figure 4.10. It is evident that while the theoretical vertical emit-

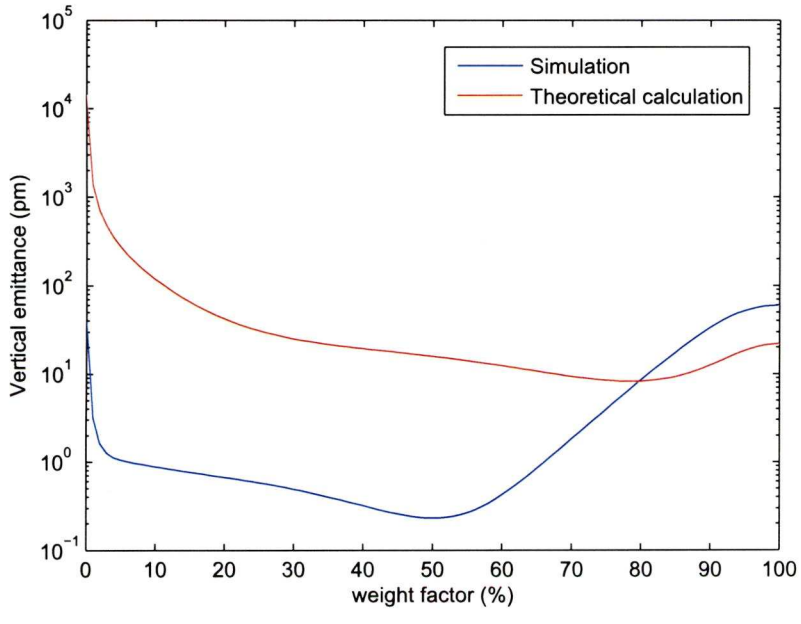

Figure 4.10: Emittance following orbit and dispersion correction, as a function of weight factor in scenario I. The red line shows the theoretical expected emittance from the corrected orbit and dispersion; the blue line shows the actual calculated emittance.

tance shows broadly similar behaviour to the simulated emittance there are also considerable discrepancies, particularly at low values of α. It appears that the theoretical relationship can not be used for a quantitive prediction of the vertical emittance. This is probably due to the fact that the assumptions made in the derivation of equation (4.5) are not completely valid in the present model. In the simulations, the vertical dispersion and the be-

tatron coupling have a common origin: the beam offset in the sextupoles. Therefore, an orbit and dispersion correction effectively corrects both the dispersion and the betatron coupling, leading to a very low vertical emittance. However, the theoretical formula treats the dispersion and betatron coupling seperately.

Now we compare the final vertical emittance as a function of the weight factor for the different scenarios given in Table 1. For each scenario, we vary the weight factor in steps of 0.01, between 0 and 1. For each weight factor, we apply the correction to each of 100 seeds of random misalignments. The final vertical emittance averaged over 100 seeds is shown in figure 4.11. We see that in several scenarios the final vertical emittance is less than 1 pm; this is not realistic, and occurs because of the limited set of errors we have applied. In practice additional types of errors such as quadrupole rotations, BPM gain errors and dipole field strength errors are to be expected for any operating accelerator system and therefore the achieved final vertical emittance after correction would be much larger. On the other hand, in scenarios V and VI the vertical emittance does not come down below 10 pm, signifying that the combined correction algorithm is ineffective with the proposed BPM configuration in the lattice. We therefore focus our attention on scenarios I to IV. As well as a distribution in the final emittance there is a distribution in the weight factor that gives the minimum vertical emittance. For tuning the machine in practice, i.e. without explicit knowledge of the magnet misalignments, it is important to know the optimum weight factor, i.e. the weight factor that is (in a statistical sense) most likely to lead to minimum emittance. One way to define the optimum weight factor is as follows. For a given scenario and set of random errors, we can determine the weight factor that leads to the minimum emittance. We can repeat for a number of sets of random errors, recording the "best" weight factor for each set. The weight factors thus recorded have some distribution–see figure 4.12 for the cases of scenarios I through IV. The optimum weight factor can be chosen as the point at which the distribution peaks. The width of the distribution is also important: a lattice that has a very wide distribution for the optimum weight factor may be harder to tune than a lattice with a very narrow distribution, since the statistical optimum weight factor is less likely to be close to the "best" weight factor in any given case. On the other hand, if the final vertical emittance has a very broad minimum, then tuning

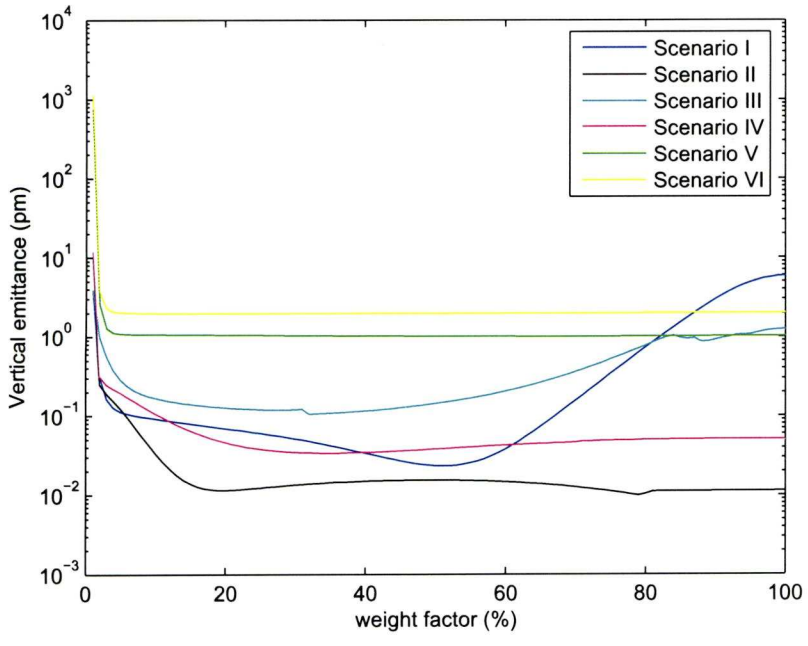

Figure 4.11: Corrected vertical emittance for the DCO lattice, averaged over 100 seeds of random errors, as a function of weight factor.

the lattice may not be very sensitive to the weight factor.

Finally, we can apply the correction to each of a number of sets of random errors, using a single optimized weight factor for each scenario. The average final vertical emittances obtained in this way are shown in figure 4.13. Note that, as already mentioned, the absolute values obtained are not very meaningful, because of the idealised nature of the simulations. However, the relative value obtained (and the spread in each case) gives some indication of how the different scenarios behave in comparison with each other.

4.3.3 Simulation Results for the DCO4 Lattice: Effects of BPM Gain Errors

For the DCO4 lattice we performed simulation studies using the same technique described in section 4.3.1. The investigated scenarios now include the case of the 100° phase advance instead of the reduced BPMs (present in 2 out of every 3 defocusing quadrupoles). These scenarios are shown in table 4.3.

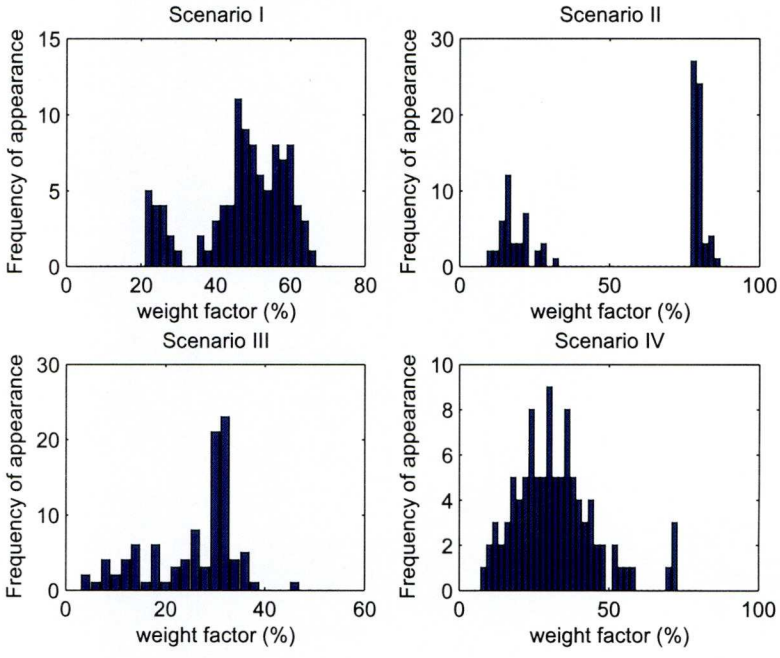

Figure 4.12: Distribution of weight factors leading to the lowest emittance for each of 100 seeds of random errors.

For the case of BPMs with no gain errors, figure 4.14 shows how the correction algorithm behaves with respect to the applied weight factor.

For the same configuration scenarios, namely the 72° and 90° phase advance and their reduced BPMs variants, the two lattices DCO and DCO4, appear to have very similar behaviour (comparison with figure 4.11). This is reasonable given the fact that the two lattices are quite similar, as indicated also by the sensitivity graphs presented earlier. The average final vertical emittance for a single optimized weight factor used in the correction algorithm for each scenario is shown in figure 4.15. The 90° phase advance lattice appears to achieve the lowest corrected vertical emittance.

We also investigated the effect of BPM coupling on this combined correction algorithm. The BPM coupling is implemented as described in BPM gain modeling [equation (3.12)]. The behaviour of the correction algorithm for the DCO4 lattice is illustrated in figure 4.16 for the different phase advance settings.

In the presence of BPM coupling of up to 2% there is still a small range of values for the weight factor that will lead to a minimization of the vertical

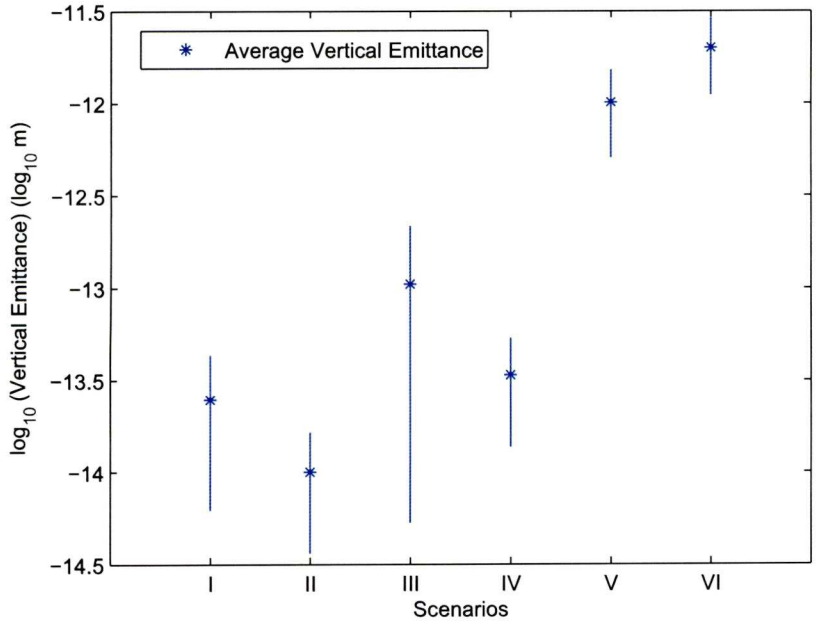

Figure 4.13: Final vertical emittance for the DCO lattice, for each lattice configuration (Table 4.2).

emittance similar to that of the ideal case (perfect BPMs).

It is interesting to investigate how the correction process behaves for very low weight factors, since at that region of weight factor values, the final vertical emittance changes significantly, compared to larger values. Figure 4.17 shows the results of the combined correction simulation run for very low weight factors in the presence of 2% BPM gain errors. Almost immediately after "leaving" the complete orbit correction area (weight factor=0) the correction achieves very low vertical emittance values that very rapidly reach a minimum; however, the algorithm starts to loose its correcting ability as soon as the weight factor shifts the correction towards vertical dispersion correction. This degradation is severe enough to the point that correction is no longer possible (the correction algorithm does not converge) and that is indicated by the end points of the red and blue lines in the equivalent case shown in the first plot of figure 4.16. Effectively, as the algorithm shifts the weight towards full dispersion correction, the coupling in the BPMs leads to increasingly erroneous "correction" based on the dispersion and consequently the correction process fails.

Scenario	Arc phase advance	Arc BPM locations
I	72°	every quad
II	90°	every quad
III	100°	every quad
IV	72°	every D-quad
V	90°	every D-quad
VI	100°	every D-quad

Table 4.3: Scenarios studied in orbit and dispersion correction simulations for the DCO4 lattice.

For low dispersion weights ($\alpha = 0$, pure orbit correction) the behaviour of the correction is little affected in the sense that it is still possible to achieve a very good correction; this is not surprising, since the simulation includes no horizontal orbit distortion, so the BPM coupling makes no real difference. However, as soon as one starts to increase the weight factor more than 5% then the effectiveness of the combined orbit-dispersion correction is significantly impaired. This is due to the fact that, the horizontal dispersion is large (of order of 0.5 m) compared with the vertical dispersion (a few mm), which would generate a few pm vertical emittance. Even a small amount of BPM coupling can have significant impact on the measurement of the vertical dispersion.

A frequency analysis, as shown in figures 4.18, 4.19 and 4.20, of the optimum weight factor for the different scenarios complements our findings regarding the effects of BPM coupling in the correction process. The optimum weight factor is defined as the weight factor that achieves the lowest vertical emittance after the correction process has been implemented.

It is evident that for all the different phase advance settings for the DCO4 lattice, the distribution of optimum weight factors changes radically with the introduction of BPM coupling. As a result one needs to be more accurate in determining the exact value for the optimum weight factor, since there no longer exists such a wide range of possible values as in the case of ideal BPMs.

Furthermore, taking into account the values on the y-axes of the plots, we can see that there is a decrease in the sum of the seeds for the cases where BPM coupling is introduced in the simulations. Table 4.4 shows the

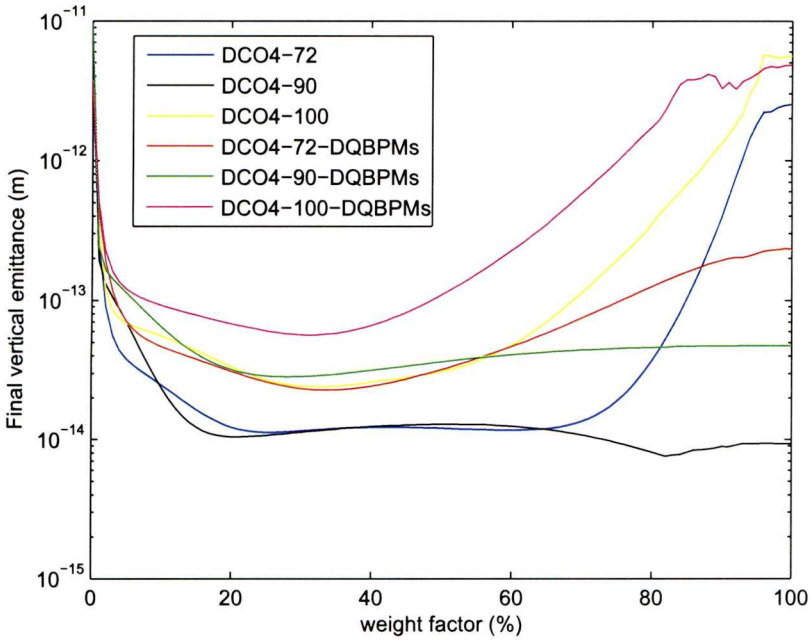

Figure 4.14: Corrected vertical emittance, averaged over 100 seeds of random errors, as a function of weight factor.

successful correction percentages.

Effectively, from nearly 100% of successful seeds (i.e. successfully implemented correction), that percentage drops with the increase in BPM coupling. That signifies that BPM coupling can in certain cases (depending on the particular magnitude of the magnet alignment errors) render the combined correction process ineffective.

Figure 4.21 shows how the ratio

$$\frac{\eta_{y,Real}}{\eta_{y,Measured}}$$

changes in the case of 1% BPM coupling for the DCO4 lattice 72°. For a weight factor of up to approximately 50% (correction equally directed towards vertical dispersion and closed orbit distortion) the ratio is smaller than unity, indicating that in the presence of BPM coupling the real dispersion is less than the measured one. Shifting the weight of the correction to larger values (targeting more the dispersion correction) the real dispersion becomes larger than the measured one, indicating that the "untreated"

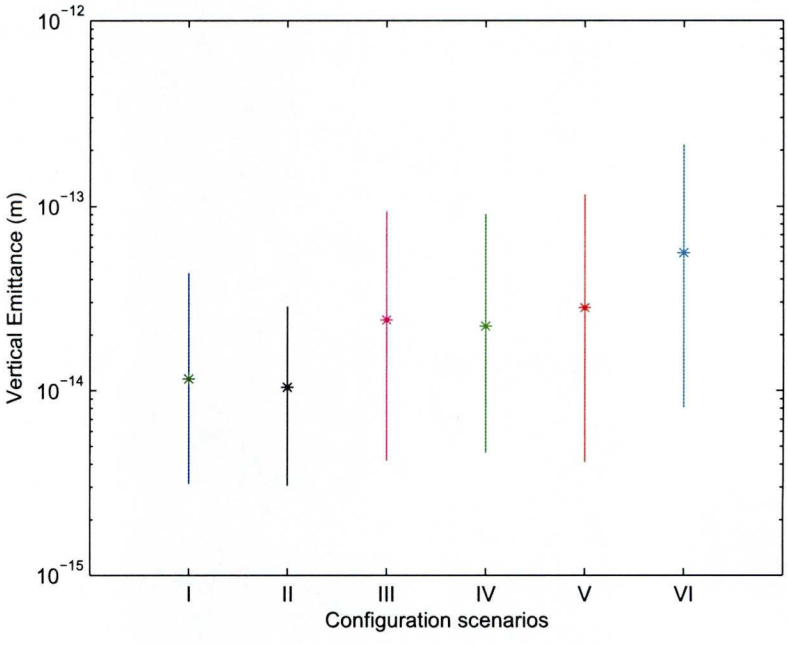

Figure 4.15: Final vertical emittances for each lattice configuration (Table 4.3).

closed orbit distortion leads to residual vertical disperion through the off-centered beam at the sextupoles. Interestingly though (since one would expect this behaviour to continue) shifting the weight to even larger values (targeting almost exclusively the dispersion correction), leads to a drop of the ratio below unity. The reasons for this are currently unclear. The important information from these results lies in the fact that in the presence of even very low levels of BPM coupling there exists a significant difference between measured and real dispersion and this can hinder low emittance tuning attempts.

4.4 Conclusions

A combined orbit and dispersion correction will be an important first step in tuning the ILC damping rings for the goal of 2 pm vertical emittance. Quadrupole and sextupole vertical alignment errors are expected to be one of the main sources of vertical emittance blow-up, since it is these errors that lead to vertical closed orbit distortion and vertical dispersion. In the

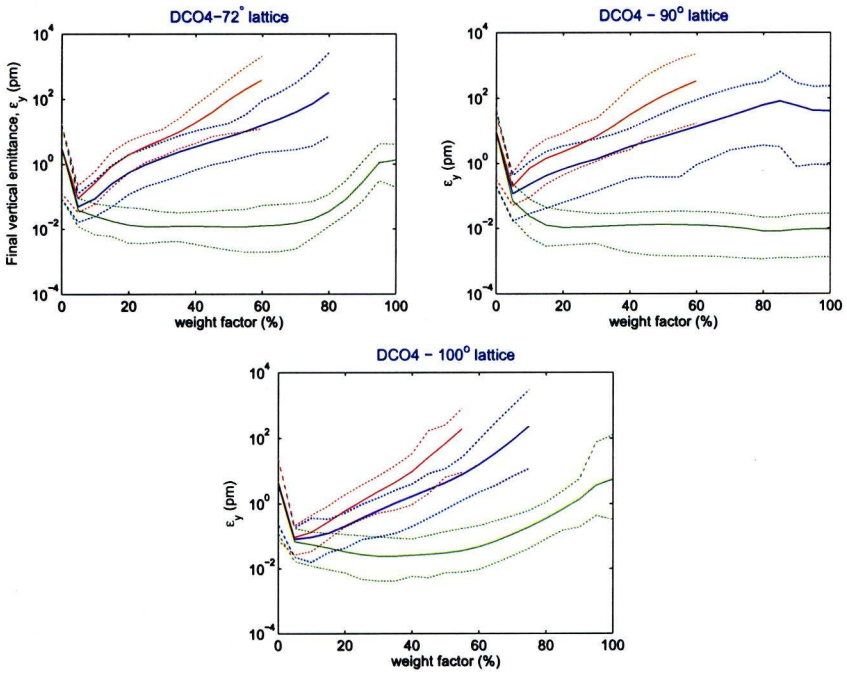

Figure 4.16: Final vertical emittance as a function of weight factor in the presence of BPM coupling for the DCO4 72°, 90° and 100° lattices. Green lines: No BPM coupling; Blue lines: 1% BPM coupling; Red lines 2% BPM coupling. Dotted lines indicate the range of final vertical emittances over different seeds.

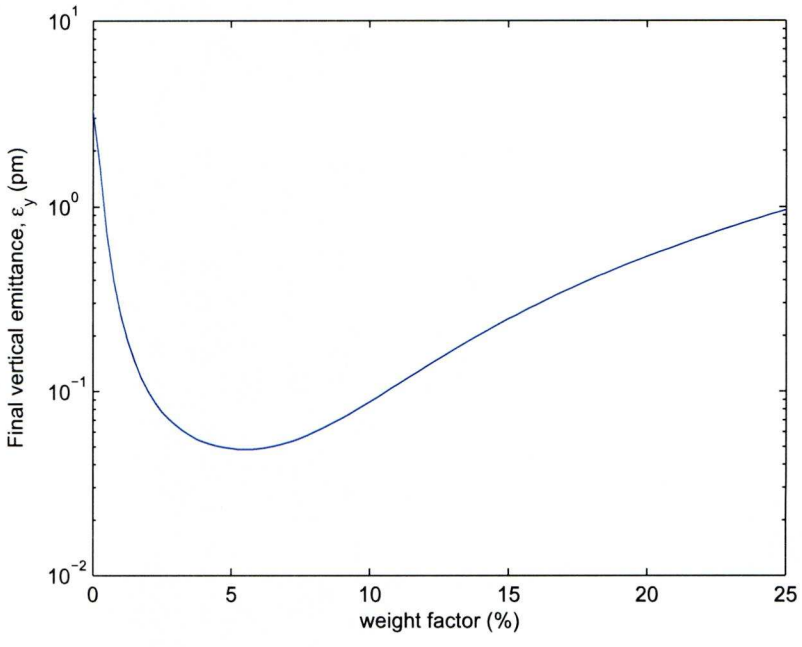

Figure 4.17: Final vertical emittance to weight factor for very low weight factor values- DCO4 72° lattice.

presence of only these errors, it is possible to optimize the correction process so that in simulations, a vertical emittance significantly below 1 pm can be achieved, even where the number of BPMs and correctors are reduced by half in the arcs. Such a reduction can be quite significant, since it reduces the overall cost of the accelerator and most importantly, it reduces the impedance contributed by the BPMs to the damping ring.

The comparison between simulations regarding the sensitivity to alignment errors for the ATF and the ILC damping rings, show that the ILC damping ring is significantly more sensitive and therefore, the alignment tolerances will have to be more strict in order to achieve the specified vertical emittance.

In a real machine, other kinds of errors will inevitably be present and they are likely to play a significant role. In particular we have identified that BPM coupling errors can have a large impact on the behaviour of the combined orbit-dispersion correction. BPM performance is often dependent on a number of parameters, like temperature and bunch charge [15, 12]. Where only quadrupole and sextupole vertical alignment errors are present,

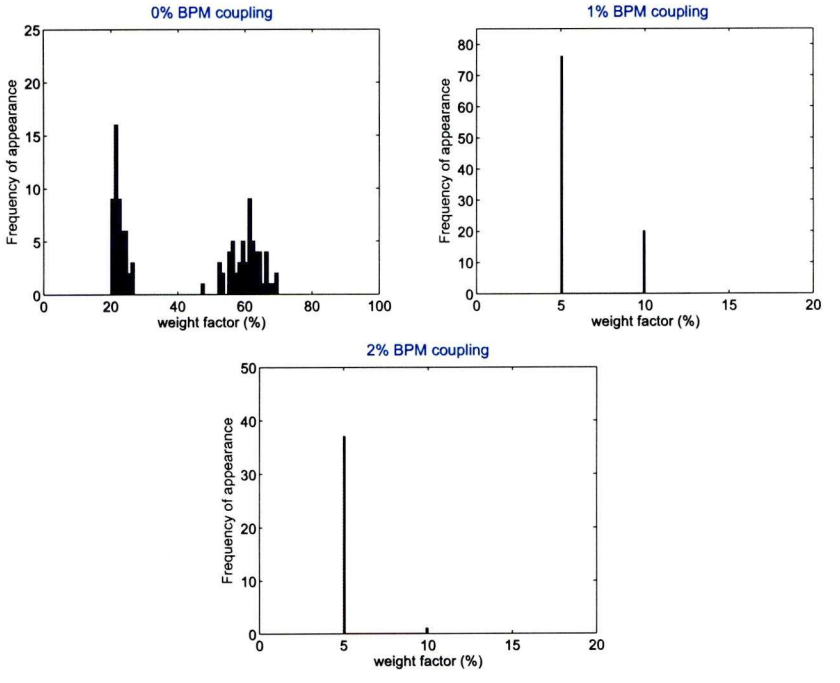

Figure 4.18: Frequency plots indicating the optimum weight factor for the DCO4 lattice 72° for different values of BPM gain errors.

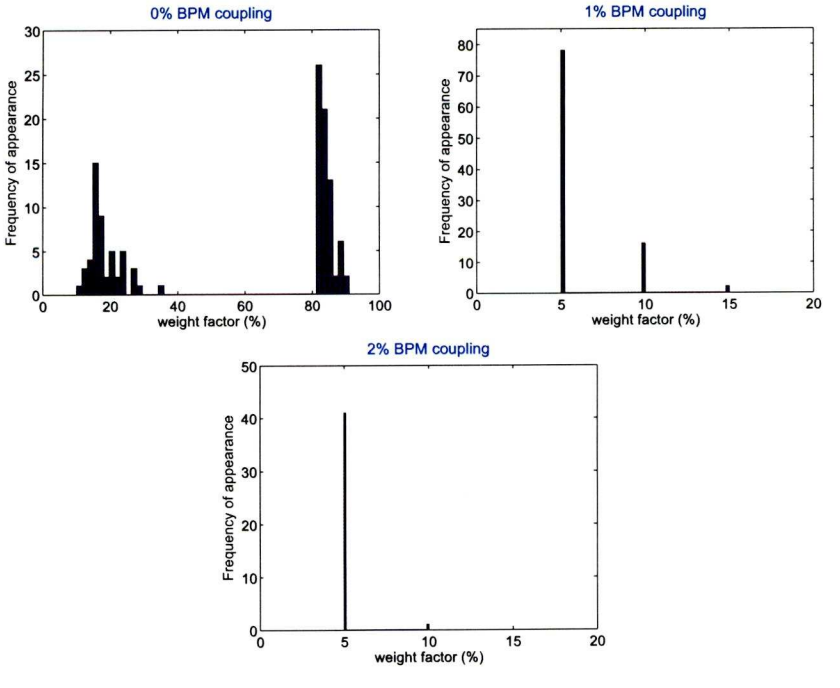

Figure 4.19: Frequency plots indicating the optimum weight factor for the DCO4 lattice 90° for different values of BPM gain errors.

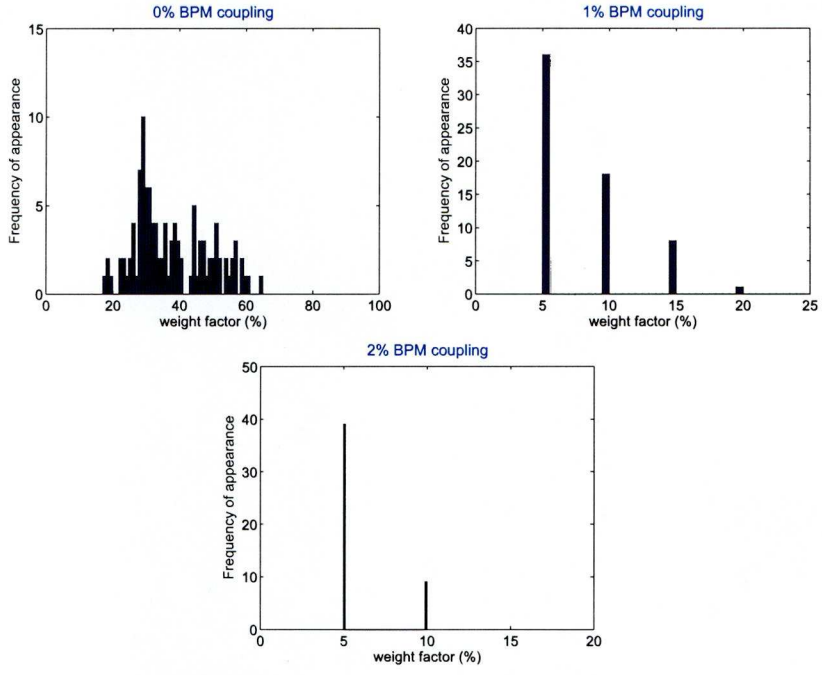

Figure 4.20: Frequency plots indicating the optimum weight factor for the DCO4 lattice 100° for different values of BPM gain errors.

BPM Gain Error (%)	Successfully corrected seeds (%)
DCO4 - 72° lattice	
0	100
1	80
2	52
DCO4 - 90° lattice	
0	100
1	80
2	46
DCO4 - 100° lattice	
0	92
1	53
2	40

Table 4.4: Percentages of successfully implemented combined correction for the different values of phase advance. From nearly 100% of successful seeds (i.e. successfully implemented correction), that percentage drops with the increase in BPM coupling.

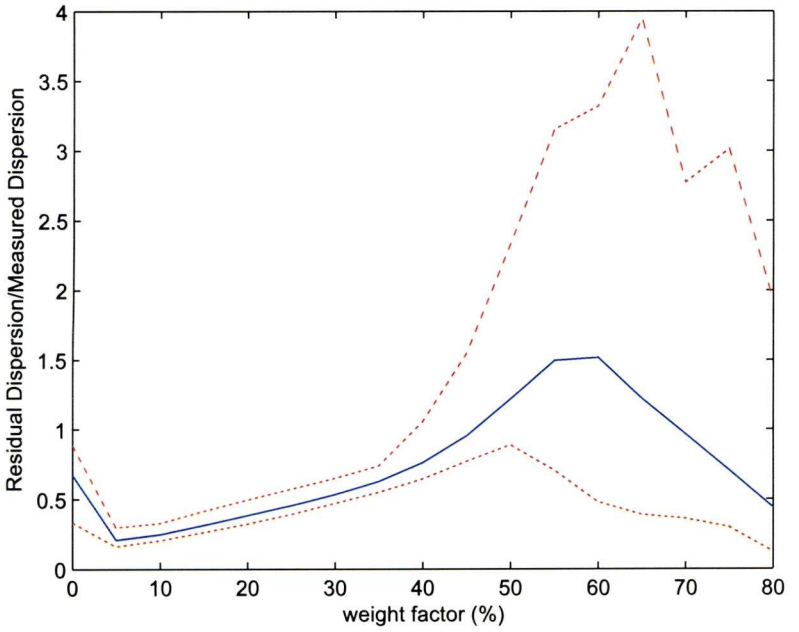

Figure 4.21: Real to Measured Dispersion ratio for the case of the DCO4 lattice 72° with 1% BPM coupling. The dotted lines indicate the minimum and maximum ratio at each weight factor.

a tuning technique using only orbit and dispersion correction can be highly effective and reliable. However, there are clear indications that where other kinds of errors are present, the effectiveness or reliability of the orbit and dispersion correction can be significantly impaired. For example, with BPM coupling errors, the correction can fail to converge in a significant proportion of cases. The reliability and ease of application (including large rings) of any correction algorithm to be employed is a paramount feature for operational conditions and therefore alternative/novel correction techniques should be explored and developed.

Experience at the ATF has shown the difficulty of achieving vertical emittances of a few pm using existing techniques. In reality, the ILC damping rings are likely to be even more difficult, because of the greater sensitivity to alignment errors, and the larger scale (number of components) of the rings. This motivates the development of new tuning techniques; in particular, to address limitations from BPM coupling errors.

Chapter 5

BPM Gain and Turn-by-Turn Data Analysis

Tuning any machine to achieve its design values for key operational parameters can be, and usually is, a very demanding task; it is often time consuming and there are a number of parameters that, as has been demonstrated in previous chapters of this work, can significantly inhibit or render ineffective the use of traditional low-emittance tuning techniques.

In view of the very demanding specifications for the vertical emittance of the ILC, the investigation and development of tuning techniques that will be robust, reliable and quick to implement, is paramount. In this chapter we present two novel techniques [69] and assess their effectiveness based on results from simulations and experiments. For the second technique, based on calibration of the BPMs using excitation of normal mode motion of the beam, we present experimental data indicating the practicality of the approach. Application of the calibration data for low emittance tuning has yet to be fully tested experimentally, though it works well in simulation. An important aspect of these techniques is that they address local coupling, based on local measurements. They are therefore as easily applied to a large ring (such as the ILC damping ring) as to a small ring.

5.1 Using Turn-By-Turn (TBT) Data

The development of BPMs capable of high resolution turn-by-turn bunch position measurements can offer a new approach for the tuning of storage

rings. Data coming from a set of such BPMs can be analyzed to give useful information for the optics of the machine and therefore improve the performance with the necessary adjustments. There are significant advantages to this approach of optics measurement compared to more traditional tuning methods; the data collection is very fast, leading to quick correction implementation, and analysis can be local, so that correction can be applied to storage rings irrespective of their size.

In the following sections we describe a technique for using turn-by-turn BPM data in order to determine the lattice functions that describe the local coupling in a storage ring; reducing the betatron coupling is a major target in any low emittance tuning attempt. We discuss the principles of the technique, present the simulation results for some example situations and consider possible limitations arising, for example from BPM gain and coupling errors.

5.1.1 Optics Tuning

A very important procedure routinely performed in any accelerator system is tuning of the optics, so that operational parameters are brought into line with the design specifications. There exist well-established techniques [32, 10, 6, 7] generally used to characterize the optics. Adjusting the magnet strengths to bring the measured values of the lattice functions close to the design values can help to improve machine performance.

A common procedure for measuring the beta functions at the location of a particular quadrupole is to observe the variation in betatron tunes with respect to changes in the strength of the quadrupole fields. For example, if the change in quadrupole strength is known then the horizontal beta function β_x at the location of the quadrupole can be determined from the equation:

$$\Delta\nu_x = \frac{1}{4\pi}\beta_x \Delta k_1 L \tag{5.1}$$

where $\Delta\nu_x$ is the change in horizontal tune resulting from the change in the integrated normalized strength of the quadrupole. However, there are several disadvantages to this technique, such as time inefficiency and possible beam loss [47].

An alternative technique is to measure, at a set of BPMs, the coherent betatron oscillations resulting from either a "kick" to a stored bunch, or from

resonant excitation of the beam. In the absence of coupling and processes that damp the amplitude of the coherent oscillations (such as decoherence and synchrotron radiation), the horizontal coordinate at a given BPM on a turn t can be written as:

$$x(t) = \sqrt{2\beta_x J_x} \cos(2\pi\nu_x t + \phi_{x0}), \tag{5.2}$$

where β_x is the beta function at the location of the BPM and ν_x and J_x are the horizontal betatron tune and action respectively. ϕ_{x0} is the initial betatron phase of the bunch at the BPM (turn $t = 0$). In the event that the betatron action is not known, it is still possible, from measurement of the oscillation amplitude at each BPM, to determine the *relative* beta functions.

Information on the optics is also provided by the phase of the betatron oscillation at each BPM. This is very useful information, since one can determine the phase advance between any two BPMs with very good accuracy by measuring the coordinates at the BPMs over many turns. The use of phase advance data has been applied successfully for optics measurement and correction is storage rings [42, 11, 34, 31]. The current state of development and availability of high-bandwidth BPMs with good resolution offers the possibility for a different approach in analyzing turn-by-turn data and extracting the maximum information embedded in them.

The proposed technique changes the aim from global to local coupled lattice function determination, with the use of turn-by-turn data. Appropriate data from 3 (or more) BPMs is combined with a model of the lattice between them, in order to determine the lattice functions at the BPMs. In principle it is possible to fit BPM gains and magnet strengths to the data, as well as the lattice functions. However, simulations suggest that the BPM data may have a rather poor sensitivity to errors on individual magnets. The obvious drawback is that this makes the determination of the individual errors by the collected data difficult; this insensitivity can be considered also an advantage, in the sense that magnet strengths should generally be known accurately enough to justify the use of a model in fitting the data.

5.1.2 Description of the Technique

For our purposes, it is convenient to use for the lattice functions in a coupled beamline the definition:

$$\beta_{ij}^{k} = N \cdot T^{k} \cdot N^{T} \tag{5.3}$$

where (in n degrees of freedom) N is a $2n \times 2n$ matrix that normalizes the single-turn transfer matrix at a given point in the lattice, i and j are indices taking values from 1 to $2n$ (corresponding to components of the cartesian phase space vector), $k = I, II...$ (corresponding to the normal mode), and T^{k} have components $T_{ij}^{k} = 1$ for $i = j = 2k$ and $i = j = 2k-1$, and $T_{ij}^{k} = 0$ otherwise (definitions described in chapter 2). Following these definitions, the beam distribution at any point in the lattice is given by:

$$\langle x_i x_j \rangle = \sum_{k=I,II...} \beta_{ij}^{k} \varepsilon_k \tag{5.4}$$

where ε_k are the emittances, invariant under symplectic transport;

$$\text{eigenvalues}(\Sigma) = \pm i\varepsilon_k \tag{5.5}$$

The normalizing transformation N_A at a point A in the lattice relates the cartesian variables to the action-angle variables. Considering two degrees of freedom we can write:

$$\begin{pmatrix} x \\ p_x \\ y \\ p_y \end{pmatrix} = N_A \cdot \begin{pmatrix} \sqrt{2J_I}\cos\phi_I \\ -\sqrt{2J_I}\sin\phi_I \\ \sqrt{2J_{II}}\cos\phi_{II} \\ -\sqrt{2J_{II}}\sin\phi_{II} \end{pmatrix} \tag{5.6}$$

where J_I and J_{II} are the invariant actions associated with the amplitudes of the oscillations in each normal betatron mode and ϕ_I and ϕ_{II} are the corresponding phase-angles.

Since the matrix N_A represents a transformation between two sets of canonical variables, it must be symplectic; we know that a symplectic matrix in two degrees of freedom can be specified by 10 parameters [18, 17]. However, it is possible to choose the reference phase angles with respect to the cartesian coordinates by specifying values for $N_{A,12}$ and $N_{A,34}$. For given reference values for the phase angles, the normalizing matrix N can

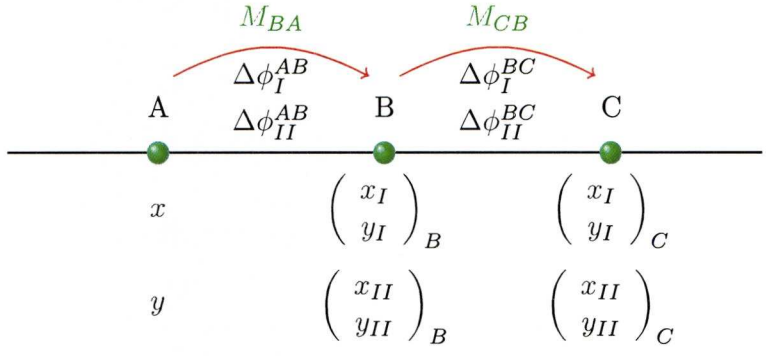

Figure 5.1: Schematic representation of the local BPM arrangement

be specified with 8 parameters.

Knowing the strengths and positions of magnets between point A and another point elsewhere in the ring, we can determine the transfer matrix between these points. Then the same 8 parameters can be used to specify the normalising matrices at the new point.

The measurement of phase and amplitude data using BPMs at three different locations A, B and C provide 14 constraints.

Each mode (called mode I and mode II) is associated with two phase advances, one from A to B and one from B to C. Assuming that mode I excitation leads predominantly to horizontal motion, we can identify further constraints from measurements of the amplitude of an oscillation in mode I, relative to the "x" amplitude at BPM A; specifically, we measure the "y" amplitude at BPM A and both the "x" and "y" amplitudes at BPMs B and C. Similarly, assuming that mode II leads predominantly to vertical motion, we can identify the remaining constraints from measurements of an oscillation in mode II, relative to the "y" amplitude at BPM A; accordingly, we measure the "x" amplitude at BPM A and both the "x" and "y" amplitudes at BPMs B and C.

If one knows the transfer matrices between the BPMs and the BPM gains are not included as parameters, then there are 8 parameters available (the parameters that determine the normalizing matrix N) to fit 14 constraints. Therefore the system of equations is over-constrained. In principle, the surplus of constraints can be used to determine BPM gain errors or magnet focusing errors.

In a linear approximation, the BPM gains can be represented as a 2×2

matrix [eq.(3.12)] relating the measured beam coordinates to the actual beam coordinates. Each BPM then can potentially add four variables to the fit; however, if we do not know the exact amplitudes of the induced oscillations in the two normal modes, then we can exclude from the set of variables two of the components of the gain matrix of one BPM. The gains would then be fitted relative to these components. With three BPMs we are led to a total of ten additional variables; including all of these new parameters would result in an under-constrained fitting problem.

5.1.3 Methods for Solving the Fitting Problem

We apply two different methods for performing the fitting problem described in the previous section.

The first method ("method 1") involves the fitting of the 8 variables that parameterize the normalizing transformation at point A, and subsequently determine the normalizing transformations at points B and C by applying the transfer matrices that are computed using the "ideal" model.

In the second method ("method 2") the attempt is to fit all 24 variables that parameterize the normalizing matrices at all 3 BPMs, and apply the transfer matrices computed from the "ideal" model as additional constraints.

The fit is performed with the help of a convenient parameterization of the group of symplectic matrices. A convenient such parameterization is of the form:

$$N = \exp(S \cdot Q) \tag{5.7}$$

where S is a $2n \times 2n$ block-diagonal antisymmetric matrix [eq.(2.88)]. If additionally Q is any symmetric $2n \times 2n$ matrix, then N will be symplectic, though not necessarily with $N_{12} = N_{34} = 0$. The conditions on N_{12} and N_{34} cannot be simply expressed in terms of constraints on Q, but they can be added as additional constraints on the fit.

5.1.4 Simulation Set Up and Results

The simulation is set up to track particles for 600 turns in a model of the ATF damping ring lattice. The initial conditions of the particles are chosen to correspond to each of the two "transverse" normal modes, in succession. In practice, collection of such data would involve recording turn-by-turn data at the BPMs, while resonantly exciting the beam at a frequency corre-

sponding to one or the other of the betatron tunes. In the results presented here, strength errors of the order of 0.5% rms variation were applied to all the normal quadrupoles. Random strengths with rms $0.04\,\mathrm{m}^{-1}$ integrated normalised gradient were also applied to the skew quadrupoles in order to generate some betatron coupling. Generating betatron coupling in this way, would roughly correspond to vertical offset with rms 1 mm in the sextupoles. The errors were applied only for generating the orbit data: when performing the fit using the second method described in 5.1.3, a model of the lattice with the errors removed is used.

In figures 5.2 and 5.3 the correlation between the actual and fitted values of some of the lattice functions at one BPM (BPM B in particular, figure 5.1) is shown for the two fitting methods described above respectively. The lattice functions shown are:

- β^{I}_{11}, corresponding to β_x in the uncoupled case;
- β^{I}_{12}, corresponding to $-\alpha_x$;
- β^{I}_{13}, representing the beam tilt $\langle xy \rangle$ dependence on $\varepsilon_{\mathrm{II}}$.

A good correlation exists between the actual and fitted values, particularly for β^{II}_{33} and β^{II}_{34}. The correlation for β^{I}_{13} and β^{II}_{13}, which are the lattice functions describing local coupling, is less satisfactory than in the other cases; this may very well reflect the fact that these lattice functions are significantly smaller than the others. This effectively means that the error in the fit becomes of a similar order of magnitude to the quantity being measured and therefore the relative error is much larger. The "bow-tie" shape observed in the cases of β^{I}_{13} and β^{II}_{13} is due to the fact that we artificially establish the sign of the simulated values in accordance with the sign of the values coming from the model.

Figures 5.4 and 5.5 show the results of the same simulation with the addition of 2% rms BPM gain errors using the different fitting procedures, respectively. In this case, while the correlations for the "in-plane" lattice functions are still good, the correlations between actual and fitted values for β^{I}_{13} and β^{II}_{13} have deteriorated considerably. This again, may be a direct consequence of the magnitude of these functions compared to the rest.

We also observe that, comparing between the two different approaches in performing the fit, the second method appears to give slightly better results in all the different cases examined.

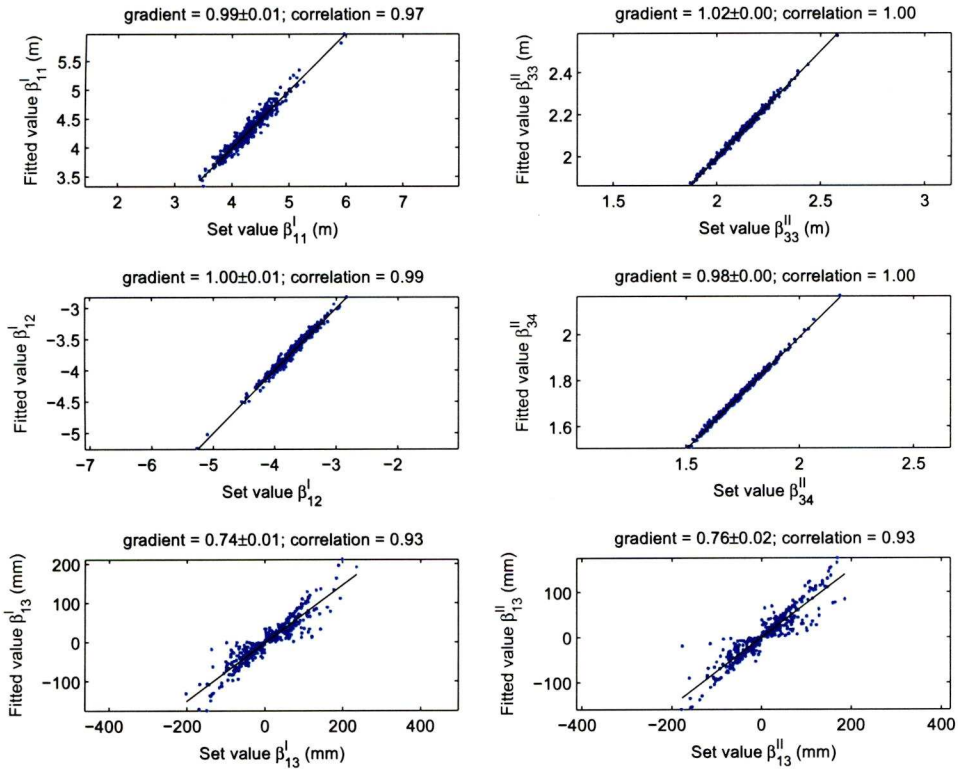

Figure 5.2: Selected lattice functions at the central BPM (BPM B) from a set of three providing data for a fit. The fitted values from the turn-by-turn data shown on the vertical axis are plotted versus the set of values resulting from the applied normal and skew quadrupole strength errors. No BPM gain errors applied. The fit is obtained using method 1.

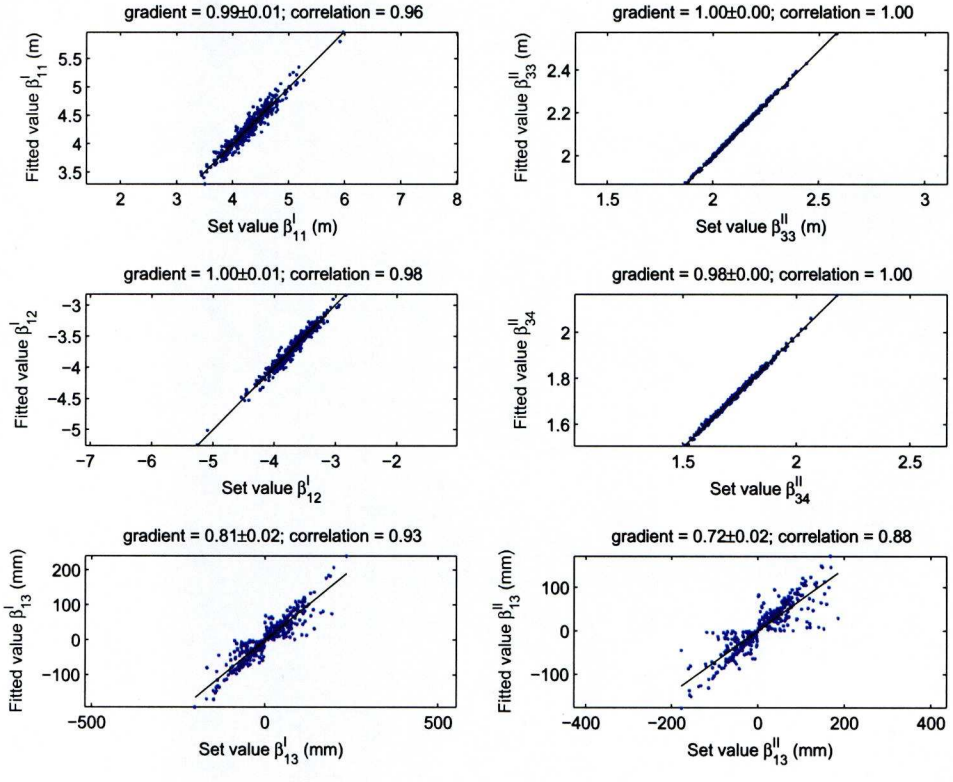

Figure 5.3: As figure 5.2; but the fit is obtained using method 2.

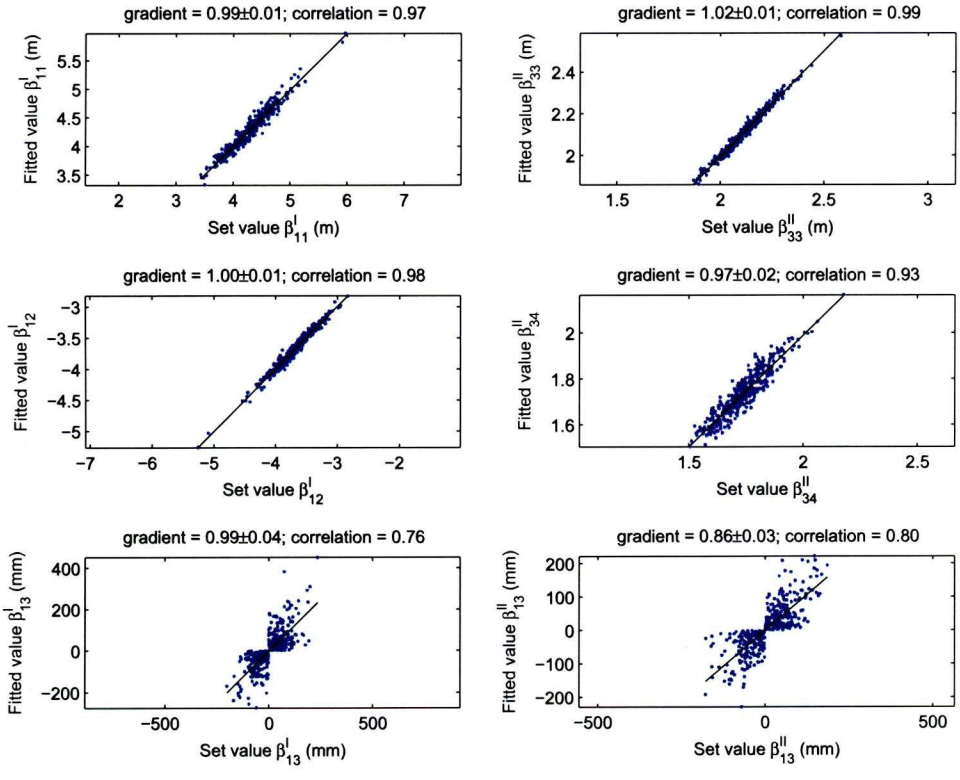

Figure 5.4: As figure 5.2, but with 2% BPM gain errors applied.

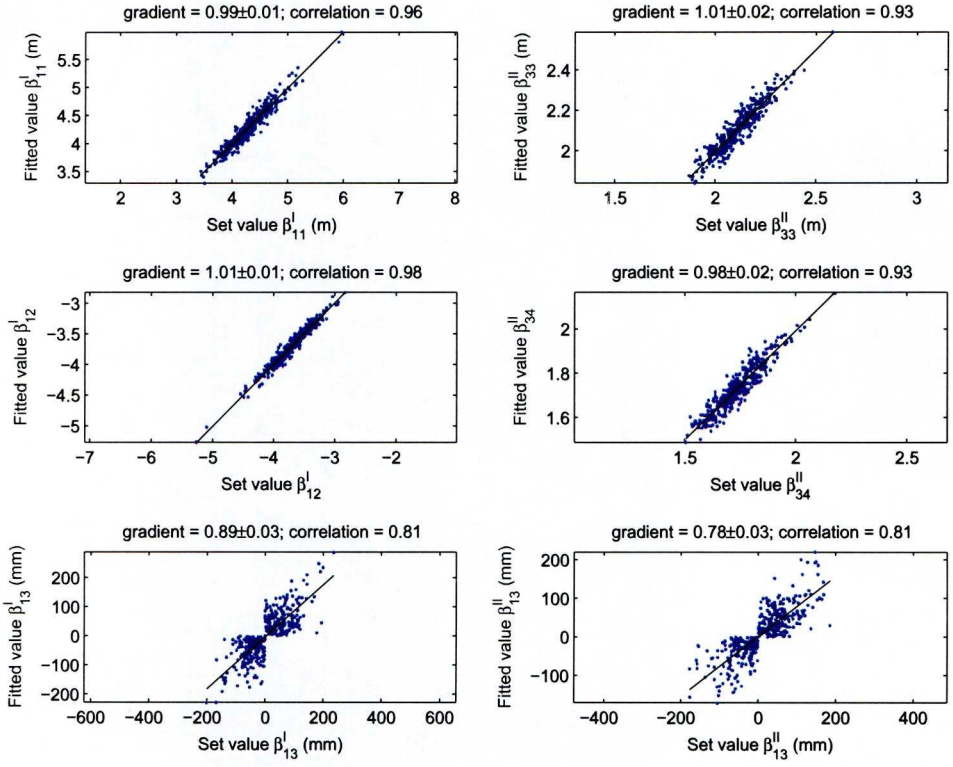

Figure 5.5: As figure 5.3, but with 2% BPM gain errors applied.

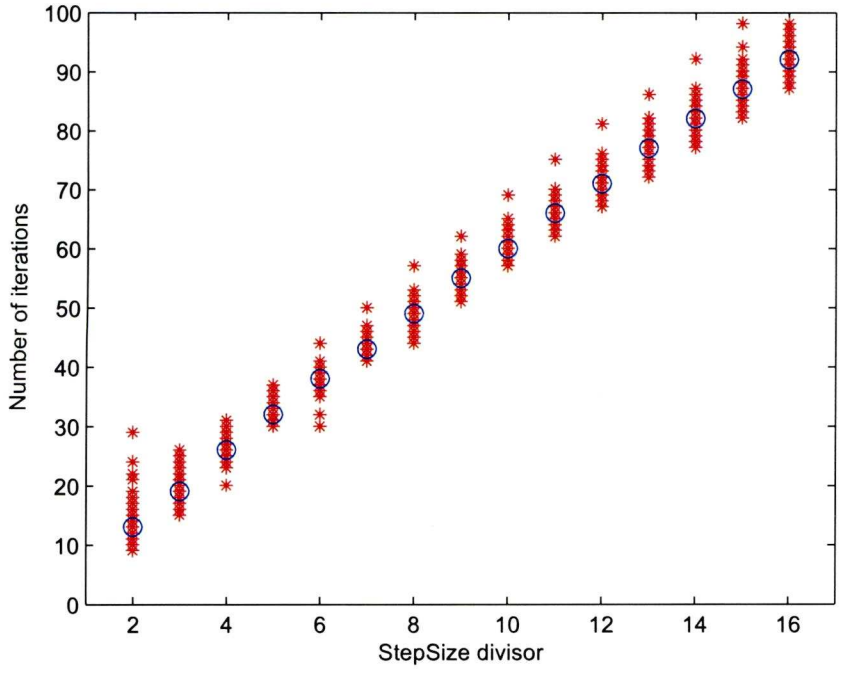

Figure 5.6: Average number (blue) of iterations -out of 400 seeds (red)- until the residual threshold has been met for different step-sizes.

The fit is based on an iterative procedure (Newton-Raphson), where small changes are made to some initial values of the parameters of N and then "verified" with equation (5.6) until a certain level of agreement is reached. To check the robustness of the fitting method we vary the step-size of the changes in the parameters. Figure 5.6 shows the number of iterations needed for different step-sizes in method 2.

Figure 5.7 shows the correlation achieved for the beta functions fit in relation to different step-sizes. The solution does not appear to be affected by the step-size.

It is also important to determine how the accuracy of the fitting procedure depends on the magnitude of the BPM gain errors. Figures 5.8 and 5.9 show this dependence for the two different fitting techniques, respectively.

Both methods appear to behave the same way; the in-plane functions achieve a consistently high correlation, almost irrespective of the BPM gain errors, while the cross-plane function fitting gets progressively worse.

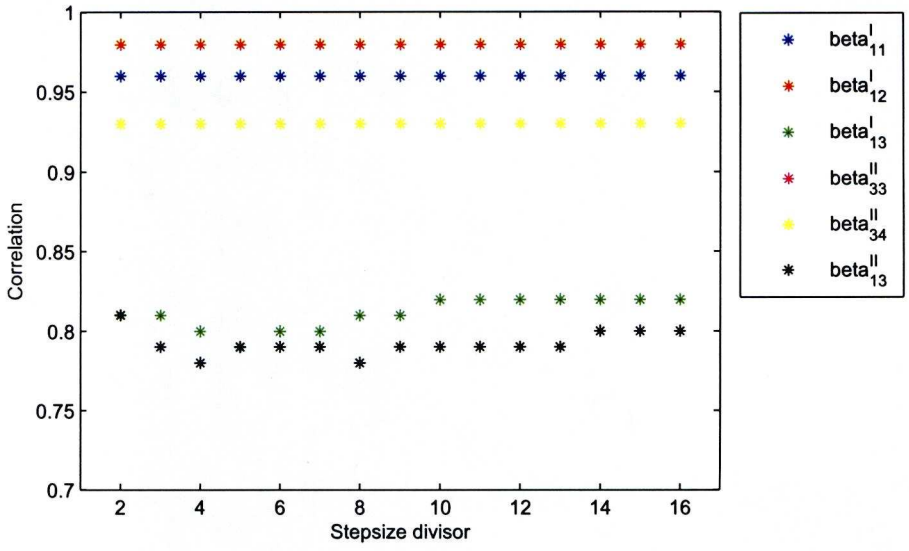

Figure 5.7: Correlation between fitted and measured beta function values for various step-sizes.

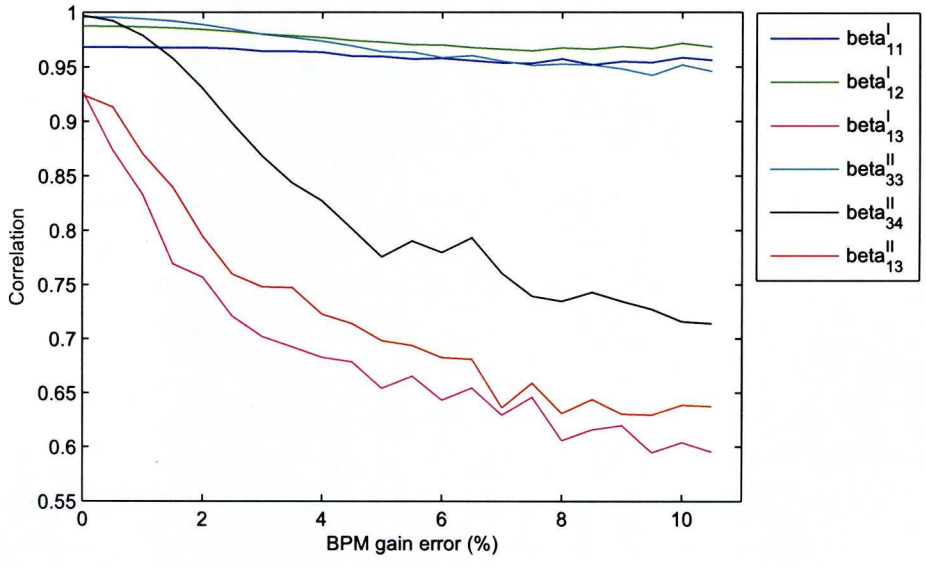

Figure 5.8: Correlation between fitted and measured beta function values for increasing BPM gain errors, using method 1.

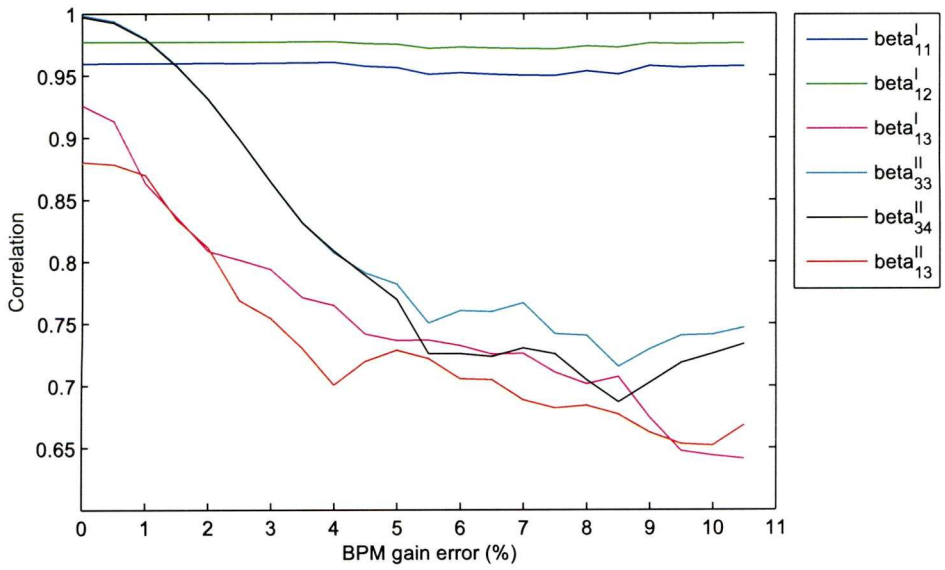

Figure 5.9: Correlation between fitted and measured beta function values for increasing BPM gain errors, using method 2.

5.2 Normal Mode Calibration of BPMs

The quality of BPM data is very important in tuning any accelerator system, especially at the ultra low emittance level required for the ILC damping rings. Throughout this work, all of the performed simulations regarding the ATF as well as the ILC damping ring lattices, have shown that correction attempts are significantly affected by the errors introduced by BPM coupling errors. It is therefore necessary to be able to address the problem of BPM calibration. Here we present a technique for calibrating the BPMs using excitation of the normal mode oscillations of the beam. We show data collected at the Cornell Electron Storage Ring-Test Accelerator (CesrTA) regarding the use of normal mode excitation in BPM calibration and assess the results. We also present the results of simulations showing the use of BPM calibration data for low-emittance tuning in ATF and the DCO4 ILC damping ring lattice. The results appear very promising and it is hoped that the technique will soon be fully tested experimentally.

5.2.1 Description of the Technique

There are three "natural" coordinate systems that characterize the geometry of a BPM, shown in figure 5.10. These are:

- The coordinate system referring to the lab frame;
- the coordinate system with respect to the BPM; and
- the coordinate system describing the normal mode oscillations of the beam.

For the purposes of low emittance tuning, we shall find that the coordinate system defined by the normal modes is the most helpful.

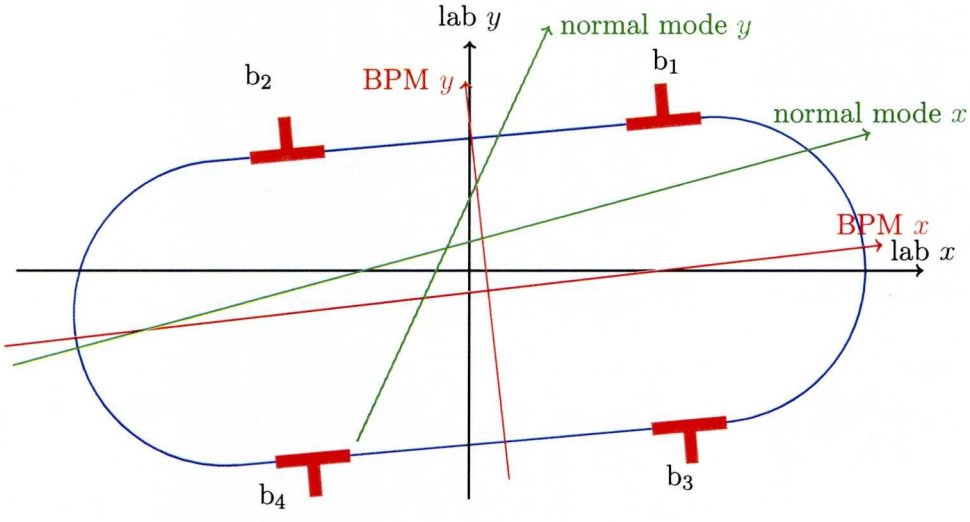

Figure 5.10: Schematic of a Beam Position Monitor (BPM).

If the dispersion is purely parallel to one normal mode, then emission of a photon will excite only that normal mode, illustrated in figure 5.11.

The basis for the technique relies on measurement of the response of the BPM buttons to excitation of the two transverse normal modes. In practice this can be done in different ways:

- observe turn-by-turn button signals following a "ping" to the beam;
- observe turn-by-turn button signals during resonant "shaking" of the beam;
- fitting phase and amplitude data; and

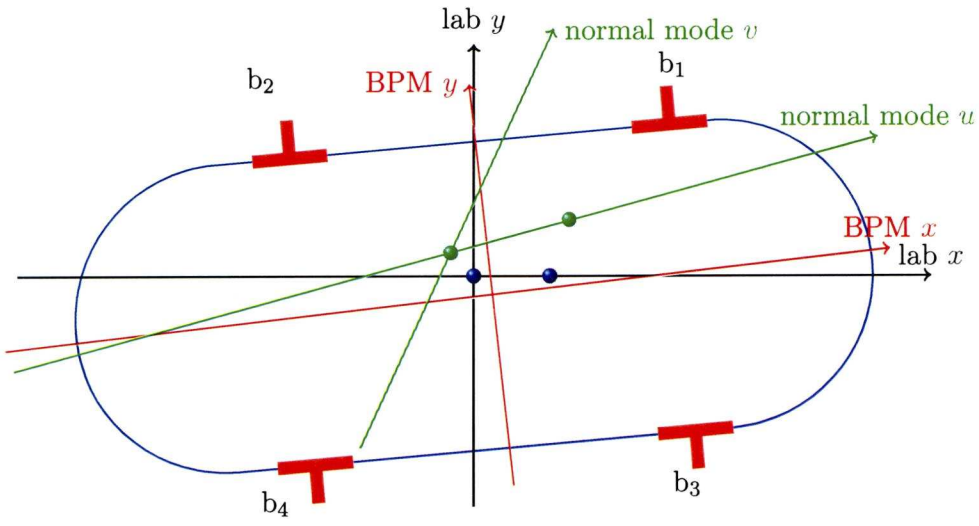

Figure 5.11: The important coordinate system for low emittance tuning is defined by the normal modes. If the dispersion is purely parallel to one normal mode, then emission of a photon will excite only that normal mode. The calibration of BPMs using normal mode excitation can help to minimise the normal mode II dispersion, consequently minimising mode II emittance. If a change in beam energy leads to a change in orbit along the x axis (blue dots), then the vertical (y) dispersion is zero; however if the normal mode axes are tilted with respect to the laboratory axes, then there will still be a quantum excitation of the mode II emittance, as a consequence of betatron coupling. However, if a change in beam energy leads to a change in orbit along the normal mode u axis (green dots), then there will be no quantum excitation of the mode II emittance.

- constructing a linear combination of the x and y BPM readings to minimize the presence of cross-plane signals.

5.2.2 Experimental Data

In this section we present data collected at CesrTA on 12/10/2009. To perform the calibration, we first need to determine the correlations between button signals following normal mode excitations. The relevant data are shown in figures 5.12 and 5.13: the possible combinations of correlations between the 4 buttons are illustrated (b_5 and b_6 indicate what the BPM system interprets as the x and y position, respectively).

The gradient of the button signal correlation plots give the elements of a matrix that relates the changes in button signals to changes in normal mode

coordinates as shown in equation (5.8):

$$\begin{aligned}
\begin{pmatrix} \Delta b_1 \\ \Delta b_2 \\ \Delta b_3 \\ \Delta b_4 \end{pmatrix} &= \begin{pmatrix} \frac{\partial b_1}{\partial u} & \frac{\partial b_1}{\partial v} \\ \frac{\partial b_2}{\partial u} & \frac{\partial b_2}{\partial v} \\ \frac{\partial b_3}{\partial u} & \frac{\partial b_3}{\partial v} \\ \frac{\partial b_4}{\partial u} & \frac{\partial b_4}{\partial v} \end{pmatrix} \cdot \begin{pmatrix} \Delta u \\ \Delta v \end{pmatrix} \\
&= \begin{pmatrix} 1 & 1 \\ \left(\frac{\partial b_2}{\partial b_1}\right)_v & \left(\frac{\partial b_2}{\partial b_1}\right)_u \\ \left(\frac{\partial b_3}{\partial b_1}\right)_v & \left(\frac{\partial b_3}{\partial b_1}\right)_u \\ \left(\frac{\partial b_4}{\partial b_1}\right)_v & \left(\frac{\partial b_4}{\partial b_1}\right)_u \end{pmatrix} \cdot \begin{pmatrix} \Delta u \frac{\partial b_1}{\partial u} \\ \Delta v \frac{\partial b_1}{\partial v} \end{pmatrix} \\
&= B \cdot \begin{pmatrix} \Delta u \frac{\partial b_1}{\partial u} \\ \Delta v \frac{\partial b_1}{\partial v} \end{pmatrix}
\end{aligned} \tag{5.8}$$

The 2×4 matrix B^{-1} defined by:

$$B^{-1} \cdot B = \begin{pmatrix} 1 & 0 \\ 0 & 1 \end{pmatrix}, \tag{5.9}$$

gives us the BPM calibration; it is then possible to determine changes in normal mode coordinates from changes in the button signals.

To test the accuracy of an attempted calibration we can compare the Fourier spectra of:

1. uncalibrated x and y turn by turn signals, and;

2. calibrated u and v turn by turn signals.

In general, an excitation in either transverse direction causes a disturbance in the other transverse direction also, and that is seen as two distinct peaks in the $x - y$ coordinate system of the lab frame. In the $u - v$ normal mode coordinate system though, excitation of the beam should disturb only the relevant direction, corresponding to one distinct peak. This expectation is verified as shown in figures 5.14. and 5.15 following the two normal mode excitations respectively.

5.2.3 Correction Using the BPM Calibration Technique

We have seen that in order to achieve an ultra-low vertical emittance, correction of the betatron coupling as well as the vertical dispersion is needed. However the "tilts" on the BPMs can lead to systematic errors in measurements of both betatron coupling and vertical dispersion. In chapter 3 we saw that although Orbit Response Matrix analysis provides a very good way of understanding the optics, it has not been very successful in tuning the ATF damping ring at the desired levels of vertical emittance. Here we investigate the effect of the BPM calibration technique on the standard correction routine applied at the ATF.

The simulations of the correction process were performed using the following set-up:

- Application of 150 μm vertical misalignment errors to all sextupoles.
- Application of 100 μm vertical misalignment errors to all quadrupoles.
- Implementation of a partial vertical orbit correction, leaving 300 μm rms vertical closed orbit distortion (to represent BPM alignment errors).
- Application of 3% random gain errors to each button of each BPM.
- Tracking of a bunch in each of the normal modes and collection of BPM measurements on each turn. Use of the turn-by-turn data to calibrate the BPMs.
- Make a dispersion measurement (by tracking a bunch with a longitudinal excitation).
- Application of a dispersion correction based on calibrated BPM dispersion measurements, using 34 skew quadrupoles (one family) in the damping ring.

The beam is excited sequentially in both the transverse normal modes and turn-by-turn data are collected. These data are analyzed to characterize the response of each BPM to beam motion in each normal mode. The dispersion calculations in the simulation are based on beam motion observation at the BPMs with respect to energy changes. Using the BPM characterization from the turn-by-turn data, the dispersion "parallel" to each normal

mode can be identified. The applied correction aims at the minimization of the dispersion "parallel" to the "vertical" normal mode. Should the dispersion parallel to one normal mode be zero, the quantum excitation of this mode will be zero; the emittance in this mode will be solely generated by the radiation opening angle.

It should be noted that this sequential orbit and dispersion correction is performed using response matrices calculated from the ideal model.

Figure 5.16 shows the final vertical emittance in the ATF for a number of different seeds, without BPM calibration.

Figure 5.17 shows the results for the same correction procedure as before, but now with the use of the "calibrated" BPMs.

It is evident that the correction in the last case shows significantly better results, since the majority of the seeds lead to a final vertical emittance under the 2 pm limit. In the case of the correction without the use of the BPM calibration, the final vertical emittance range of values is much larger and most of the seeds indicate a correction of vertical emittance to a level much worse than 2 pm.

Figures 5.18 and 5.19 show the dependence of the correction process on the BPM gain errors, with the blue lines showing the range of final vertical emittances for different random seeds. In the case of the calibrated BPMs, the correction is almost independent of the magnitude of the BPM gain errors and a constant vertical emittance correction is achieved; without BPM calibration, the correction rapidly degrades to the point of failure after a certain level of BPM gain error.

5.2.4 Implementation of the BPM Gain Analysis at the DCO4 Lattice

The combined orbit-dispersion correction simulations presented in chapter 4, showed that the performance of the correction is heavily dependent on the performance of the BPMs. Furthermore, the application of ORM analysis techniques, like LOCO, for a lattice the size of the ILC damping ring, raises computational issues since the matrices involved in the calculation become very big. Therefore it would be advantageous to investigate whether a correction using BPM gain analysis could correct the vertical emittance at the specified levels for the ILC damping rings.

For the following simulations the tolerances are relaxed compared to the

simulations in chapter 4, so that now the rms vertical misalignment errors on the quadrupoles and sextupoles are 100 μm and 150 μm respectively. Figures 5.20 and 5.21 show the results of the correction procedure described in 5.2.3, with a BPM gain error of 4%.

In the case of a 6 km ring like the ILC damping ring, the use of BPM calibration, is proven to be significant since it brings the final vertical emittance under the 2 pm threshold. When this calibration is not performed, the final vertical emittance increases, reaching tens of picometers.

The correction procedure using the BPM calibration technique is also not sensitive to the magnitude of the gain errors the BPMs exhibit, as shown in figure 5.22. If the calibration of the BPMs is ignored though, the correction gradually loses its effectiveness and for large values of BPM gain errors, the algorithm becomes unstable; the correction ends up increasing the vertical emittance (figure 5.23).

5.3 Conclusions

The characterization and measurement of betatron coupling is a key step in reducing the vertical emittance. Well-established techniques have been used in order to measure the betatron coupling, but have been shown to lack efficiency in time as well as localized applicability. On the other hand, having access to high quality BPM data for successful tuning of an accelerator system at the ultra low emittance level has been shown in previous chapters of this work to be of great importance. Therefore it is important to have some means of calibrating the BPMs in a rapid yet accurate way.

The "unifying" theme in both these aspects of low emittance tuning is the use of the normal mode excitation of the beam. Combined with the recent development and expanding availability of BPMs capable of recording tracking data on a turn-by-turn basis, it is possible to extract information that is very helpful in dealing with both of these issues.

The technique proposed, described in section 5.1, for characterisation of the coupled lattice functions has the advantage of time efficiency and offer the possibility of local betatron coupling correction. However, the results of the simulations indicate that it is too sensitive to BPM gain errors and this limits its practical usefulness. The accuracy of the fit relies also on having a good model of the lattice in which the technique is applied. It

may be possible to improve the reliability of the the fit by carrying out the fitting iteratively, e.g. once the lattice functions have been fitted at different locations around the ring, the quadrupole strengths leading to these lattice functions can be determined. There is the possibility of further improvement of the quality of the fit that can be achieved; for example, data from a larger number of BPMs could be used to provide additional constraints to the fit.

The calibration of BPMs appears to be a much more promising technique. This technique has been shown experimentally to provide accurate calibration of the BPMs in a consistent and rapid manner. The use of the calibrated BPMs in a correction scheme then has been shown in simulations to significantly improve the low emittance tuning attempts. Perhaps most importantly, this technique can be advantageous for low emittance tuning irrespective of ring size, bypassing the computation constraints of methods like ORM analysis, usually imposed in the case of large accelerator systems, like the ILC damping rings.

Hopefully, the normal mode calibration of the BPMs to assist with low emittance tuning can be tried in an existing storage ring like the ATF, once the necessary hardware upgrades have been completed.

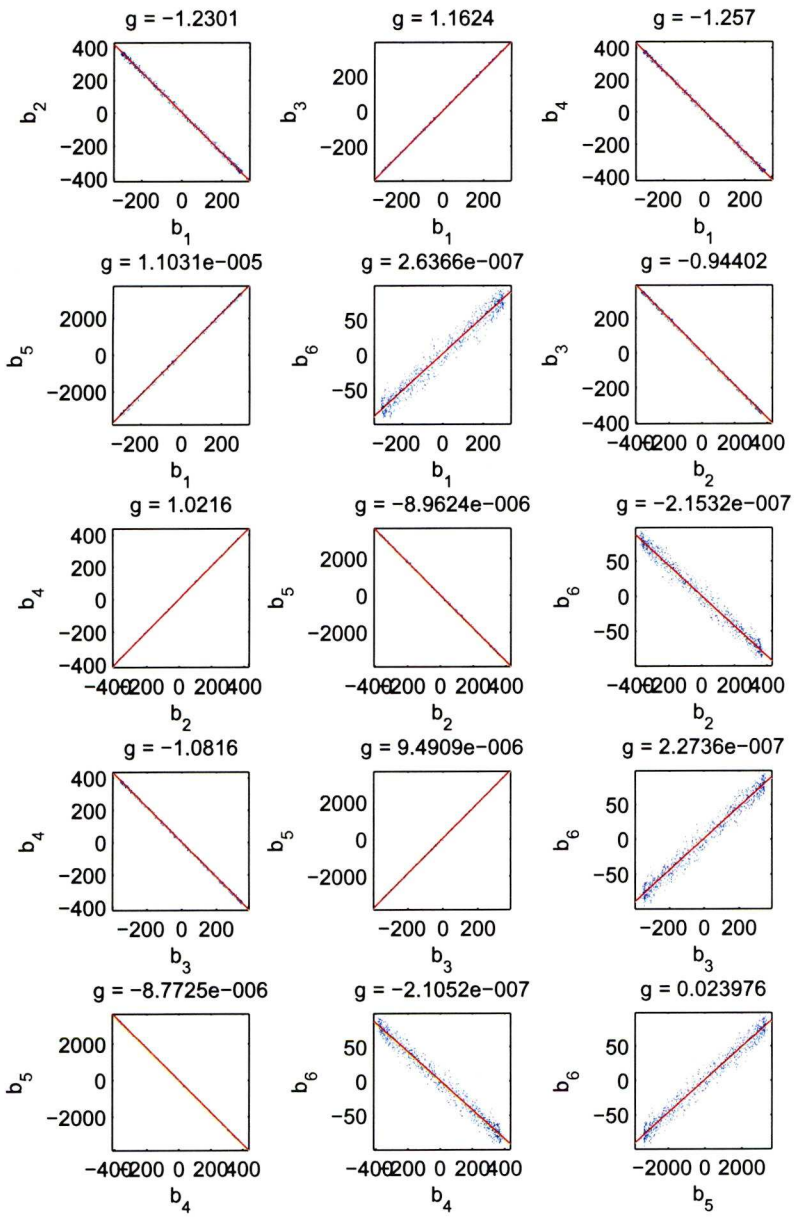

Figure 5.12: Correlations between button signals following a horizontal (mode I) excitation. For example, the final sub-plot in the figure (bottom right hand corner) shows a correlation between the y coordinate and the x coordinate of the beam as read by the BPM. This shows either the presence of coupling, or an inaccurate calibration of the BPM (to the Cartesian coordinates); it is not possible, using the data in the present plot to distinguish between them.

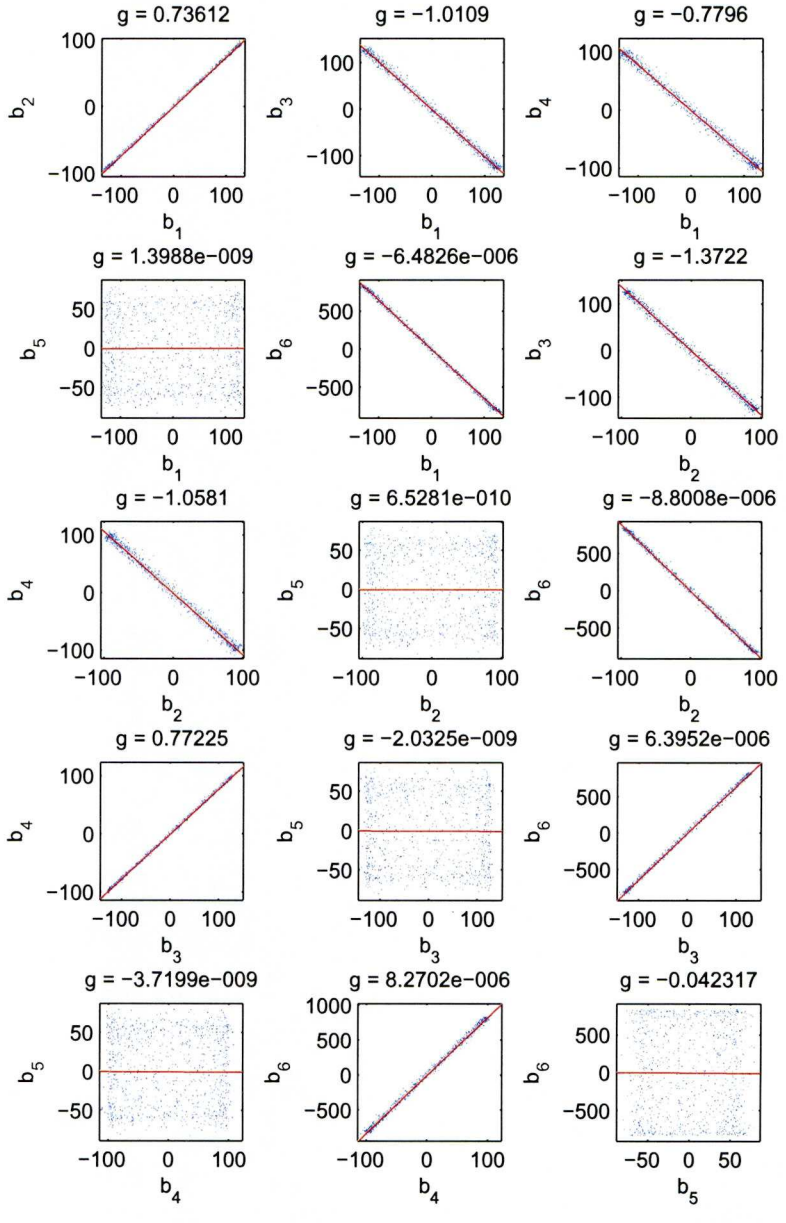

Figure 5.13: Correlations between button signals following a vertical (mode II) excitation. We now see that there is no correlation between signals b_5 and b_6 (bottom right hand corner). This means that the x value returned by the BPM (b_5) is orthogonal to the direction along which the beam oscillates when excited in normal mode II.

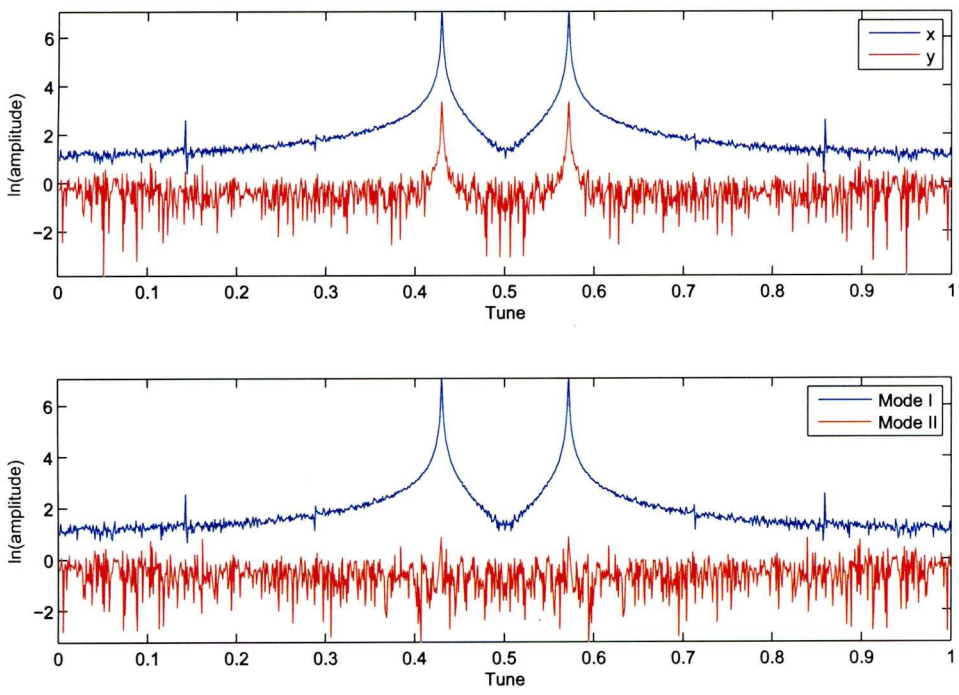

Figure 5.14: Fourier spectra of readings from a BPM with beam excitation at the Mode I resonant frequency. The horizontal axis shows the frequency of the Fourier mode (in machine tune units); the vertical axis shows the logarithm of the mode amplitude (in arbitrary units). Top: spectra of x and y BPM readings (nominal calibration). Bottom: spectra of u (Mode I coordinate) and v (Mode II coordinate) readings from a BPM calibrated using normal mode excitations. In the top plot, we see that the Mode I oscillation appears in both x and y BPM readings (peaks at the same frequency in the x and y coordinates). In the bottom plot, we see that an oscillation in Mode I appears only in the u (Mode I) coordinate.

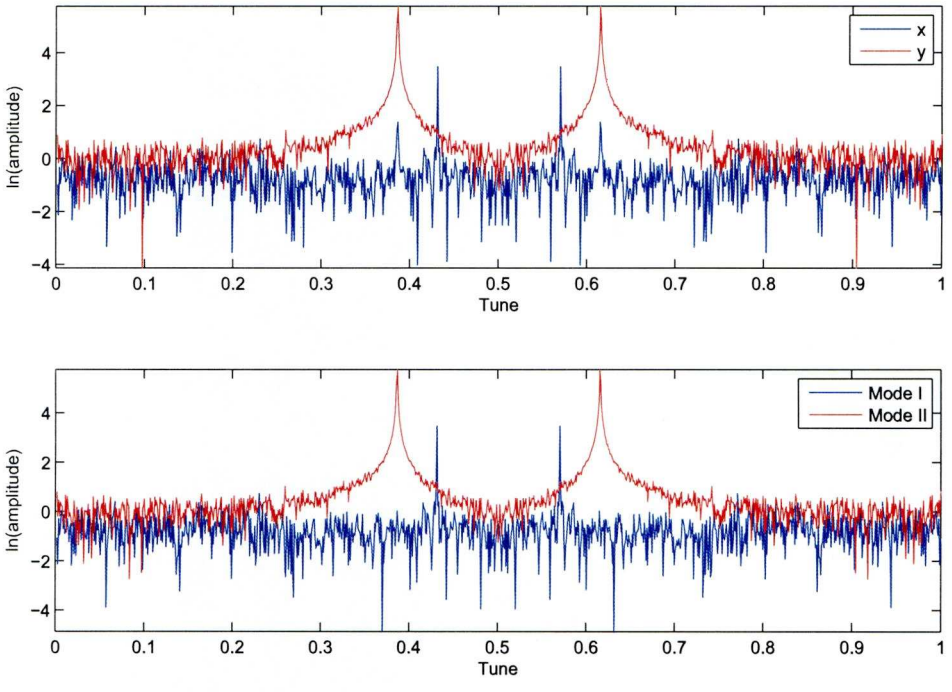

Figure 5.15: Fourier spectra of readings from a BPM with beam excitation at the Mode II resonant frequency. The horizontal axis shows the frequency of the Fourier mode (in machine tune units); the vertical axis shows the logarithm of the mode amplitude (in arbitrary units). Top: spectra of x and y BPM readings (nominal calibration). Bottom: spectra of u (Mode I coordinate) and v (Mode II coordinate) readings from a BPM calibrated using normal mode excitations. In the top plot, we see that the Mode II oscillation appears in both x and y BPM readings (peaks at the same frequency in the x and y coordinates). In the bottom plot, we see that an oscillation in Mode II appears only in the v (Mode II) coordinate. With the normal mode calibration (bottom plot), there remains a peak in the u (Mode I) coordinate, but it is at a different frequency from the peak in the v (Mode II) coordinate, and is likely from a different source of excitation.

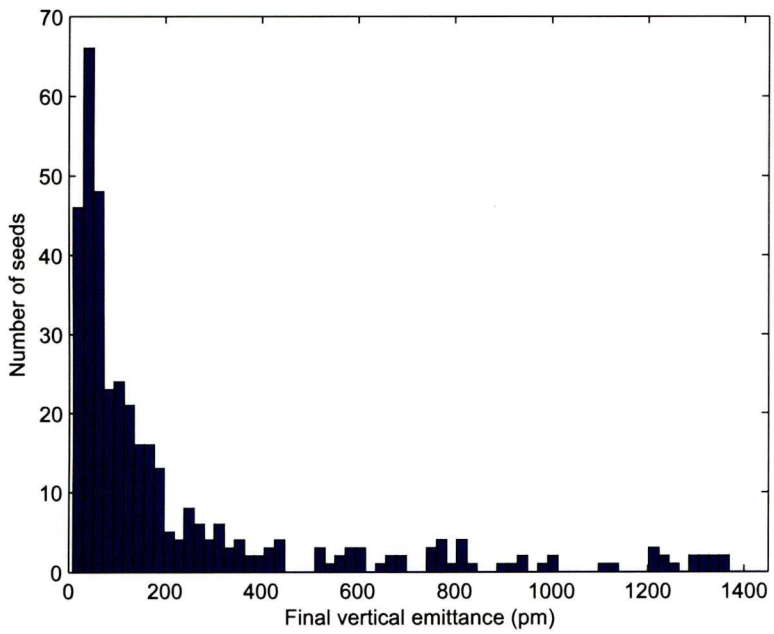

Figure 5.16: ATF Damping Ring, 3% BPM gain error: Final vertical emittance distribution for 400 seeds, no BPM calibration. The very broad range (reaching the nm scale) of results indicates that with this amount of BPM gain error, correction is not effective if no BPM calibration is applied.

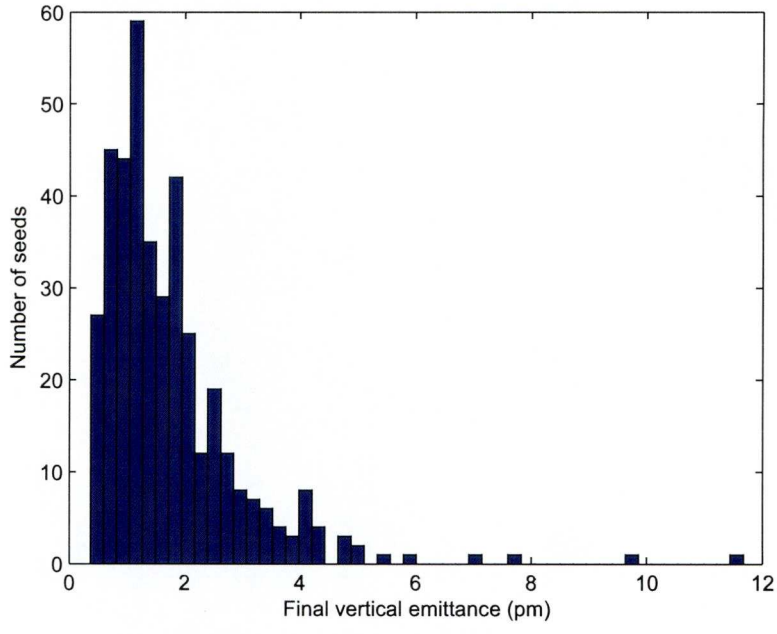

Figure 5.17: ATF Damping Ring, 3% BPM gain error: Final vertical emittance distribution for 400 seeds, BPM calibration. The calibration of the BPMs brings down the final vertical emittance to an average of less than 2 pm.

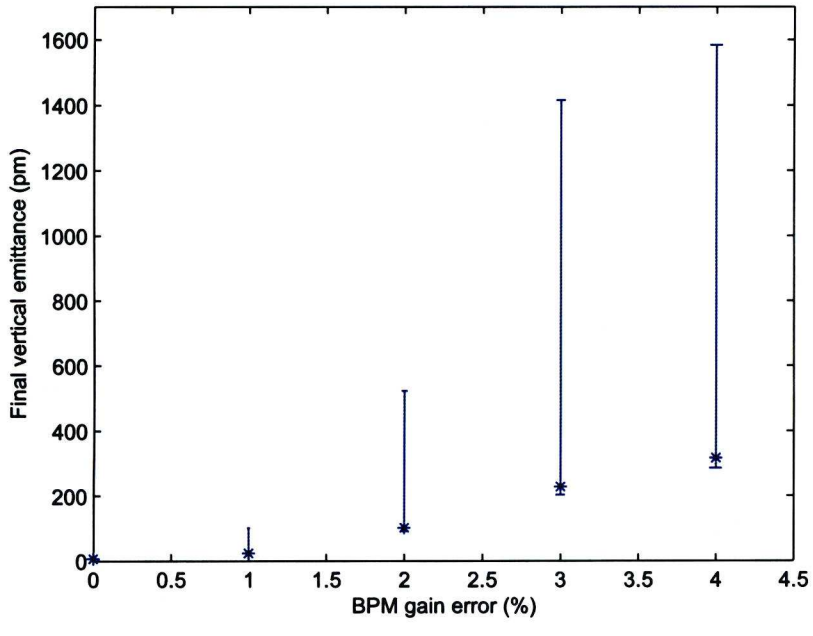

Figure 5.18: Dependence of correction scheme on BPM gain errors for the ATF Damping Ring; No BPM calibration. We observe that even at 2% BPM gain error, the correction is ineffective in bringing the emittance down to the desired levels.

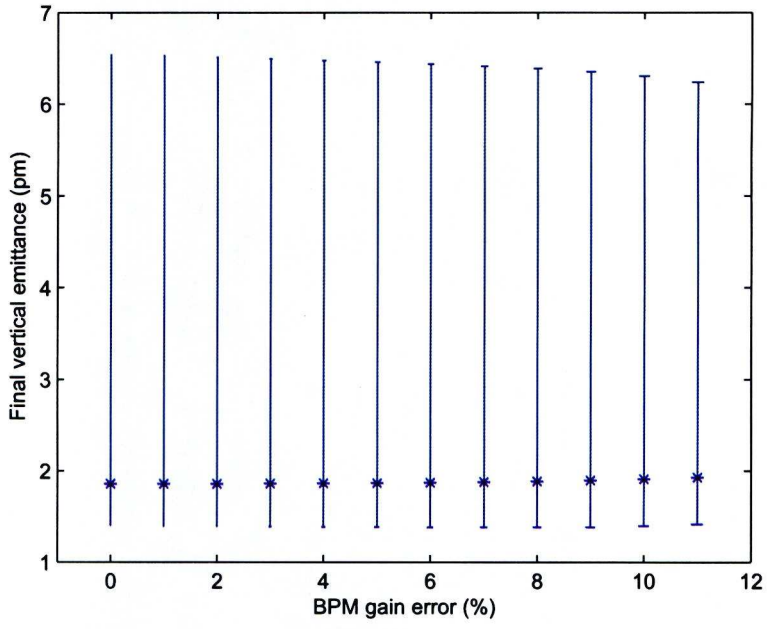

Figure 5.19: Dependence of correction scheme on BPM gain errors for the ATF Damping Ring; Calibrated BPMs. The calibration leads to a correction that is insensitive to the magnitude of BPM gain errors.

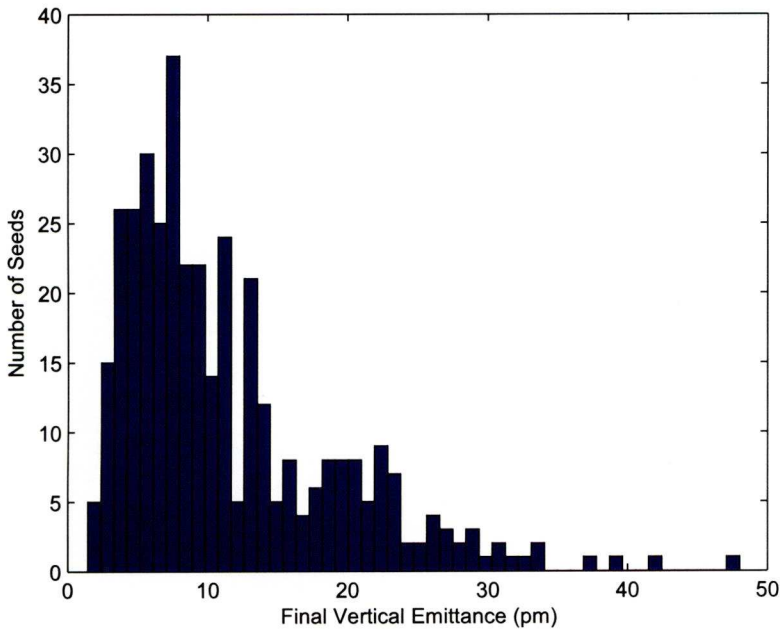

Figure 5.20: DCO4 Damping Ring, 4% BPM gain errors: Final vertical emittance distribution for 400 seeds, no BPM calibration. When this calibration is not performed, the final vertical emittance increases, reaching tens of picometers, far from the desired level of 2 pm.

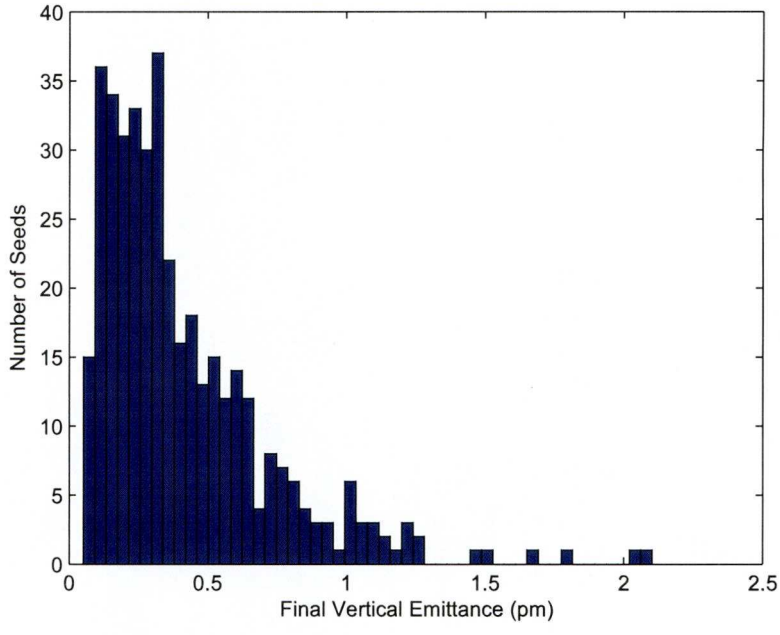

Figure 5.21: DCO4 Damping Ring, 4% BPM gain errors: Final vertical emittance distribution for 400 seeds, with BPM calibration. Calibrating the BPMs leads to effective correction, bringing the vertical emittance down to the specified level.

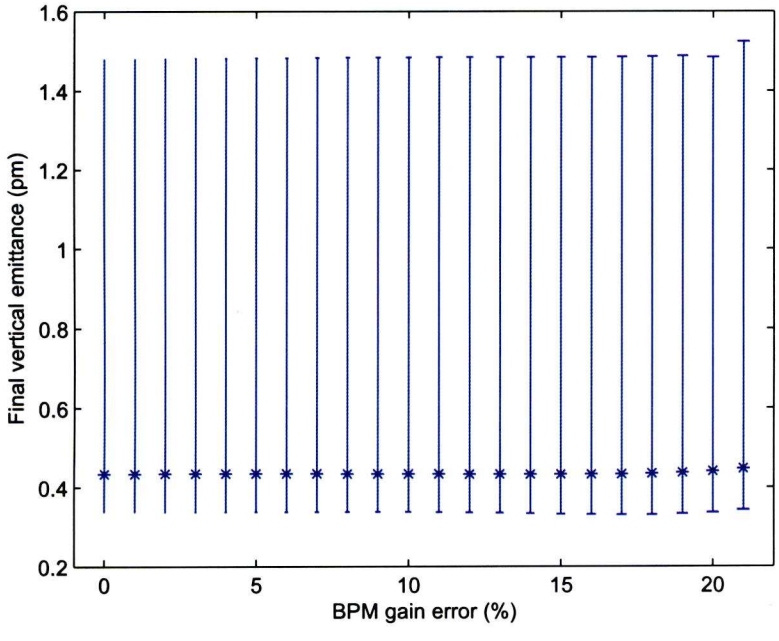

Figure 5.22: Final vertical emittance versus BPM gain errors for the DCO4 lattice; correction applied using calibrated BPMs. The correction procedure using the BPM calibration technique is not sensitive to the magnitude of the gain errors the BPMs exhibit, even at very high levels of gain error.

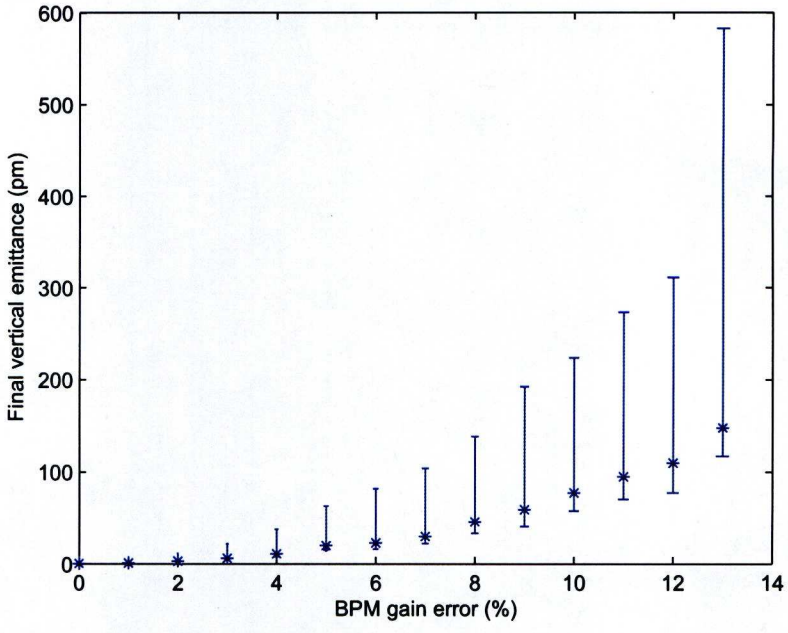

Figure 5.23: Final vertical emittance versus BPM gain errors for the DCO4 lattice; no calibration of the BPMs. Ignoring the BPM calibration, the correction gradually loses its effectiveness and for large values of BPM gain errors, the algorithm becomes unstable; the correction ends up increasing the vertical emittance.

Chapter 6

Conclusions

The work presented in this thesis deals with issues related to beam quality for future linear colliders. The need for increasingly high luminosity with every new machine is what ultimately drives the need for low-emittance tuning of accelerator systems. Our investigations focused on the International Linear Collider damping rings; we investigated the effectiveness of different correction procedures in view of various types of errors and identified possible limitations that arise in currently established low-emittance tuning techniques.

The Accelerator Test Facility at KEK is dedicated to the study of low-emittance beams. Orbit response matrix analysis at the ATF-KEK has not yet been proven experimentally to lower the vertical emittance to the levels required for the ILC damping rings. We investigated the effects of degeneracies in the LOCO algorithm; our simulations showed that there is no significant degeneracy between skew quadrupole strengths and corrector tilts. However, a degeneracy between skew quadrupole strengths and BPM couplings has been shown to exist, limiting the achievable vertical emittance using this technique to approximately 6 pm. Given that the simulations performed have not included all the errors that will exist in reality, it is reasonable to expect that, in the presence of more sources of errors, ORM analysis will not be sufficient to correct the vertical emittance to the level of 2 pm. On the other hand, this technique is still a very useful tool for providing information about the machine optics. Therefore, it would be useful to be able to implement it in a more rapid manner. Simulations have shown that ORM data can be collected using about half of the total number

of orbit correctors, without compromising the correction outcome.

It is also important to note that the application of LOCO to a machine the size of the ILC damping ring is likely to run into problems regarding computation and time efficiency. The ORM data of such a storage ring create matrices that are too big to handle for the current implementation of LOCO. There are of course options to be explored in order to overcome such difficulties. One option would be to implement parallelization of the code in order to speed up the computationally intensive routines used by the algorithm, such as the SVD least squares fitting; this of course would mean that the entire implementation of the algorithm would have to be rewritten. A different approach would be to try to apply the existing implementation to sections of the ring, thereby reducing the amount of ORM data needed.

We also investigated a combined orbit-dispersion correction routine on several different designs of the ILC damping rings. In the presence of quadrupole and sextupole vertical misalignments (the major expected sources of vertical emittance) simulations showed that it is possible to optimise the process so that a vertical emittance of a fraction of a pm can be achieved, even with reduced number of BPMs and correctors. However, BPM coupling compromises severely the reliability of the combined orbit-dispersion correction. Although it is still possible in idealised simulations to achieve the desired levels of vertical emittance, it is unlikely that such good results could be achieved in practice.

Having identified that BPM performance is critical for any low-emittance tuning attempt, we explored two novel tuning techniques that involve BPM gain analysis and Turn-By-Turn (TBT) data. The first of these techniques is aimed at characterising the betatron coupled lattice functions and performing a local betatron coupling correction. The proposed fitting procedures work reasonably well as long as the BPM gain errors are fairly small; the accuracy of the fit also depends on the quality of the model of the lattice. However, the accuracy with which the coupling can be determined appears to be sensitive to BPM coupling errors and this looks likely to limit the practical usefulness of the technique.

The second technique, dealing with BPM calibration using normal mode excitation and TBT data collection, appears to be much more promising. Simulations show a significant improvement of the correction outcome once the BPMs have been calibrated and the correction time is no longer "hin-

dered" by the size of the facility it is being applied to. With the upcoming upgrades of the BPM systems and correctors in both the ATF at KEK and the CesrTA at Cornell, it should be possible to test the proposed correction procedure using calibrated BPMs experimentally in the near future.

Appendix A

Singular-Value Decomposition (SVD)

M.I.T. Professor Gilbert Strang calls it "wonderful"[20], an "absolutely high point of linear algebra"[63] that *"...is not nearly as famous as it should be."*[51].

The Singular-Value Decomposition is a factorization method for rectangular real or complex matrices. It has many applications in signal processing and statistics, and can be used for matrix approximation, determining the rank, range and null space of a matrix. Here we concentrate on the applications of SVD most relevant to Low Emittance Tuning, namely the computation of the **pseudoinverse** and **least squares fitting** of data. We finally discuss briefly the subject of numerical calculation for the SVD method.

A.1 The Theorem

Suppose M is an $m \times n$ matrix whose entries come from the *field* K, which is either the field of real numbers or the field of complex numbers. For such a matrix M there exists a factorization that is of the form

$$M = U\Sigma V^* \tag{A.1}$$

where U is an $m \times m$ unitary matrix over K, the matrix Σ is an $m \times n$ diagonal matrix with non-negative real numbers on the diagonal and V^* is the conjugate transpose of V, an $n \times n$ unitary matrix over K. Such a factorization is called a singular-value decomposition.

A common convention is to order the diagonal entries Σ_{ij} in decreasing order. In this case the diagonal matrix Σ is uniquely determined by M (though the matrices U and V are not). The diagonal values of Σ are known as the *singular values* of M.

A.2 Singular Values

A non-negative real number σ is a **singular value** *for M if and only if there exist unit-length vectors u in K^m and v in K^n such that*

$$Mv = \sigma u \qquad and \qquad M^*u = \sigma v \tag{A.2}$$

The vectors u and v are called the **left-singular vector** and the **right-singular vector** of σ, respectively.

From equation A.1 the diagonal entries of Σ are necessarily equal to the singular values of M. The columns of U and V are, respectively, left- and right-singular vectors for the corresponding singular values. Consequently, the above theorem states that:

- An $m \times n$ matrix M has at least one and at most $\rho = min(m, \rho)$ distinct singular values.
- It is always possible to find a unitary basis for K^m consisting of left-singular vectors of M.
- It is always possible to find a unitary basis for K^n consisting of right-singular vectors of M.

A singular value which can produce two left- (or right-) singular vectors that are linearly independent is called *degenerate*. Non-degenerate singular values have always unique left and right singular values, up to multiplication by a unit phase factor $e^{i\phi}$. Consequently, if all singular values are non-degenerate and non-zero, then its singular-value decomposition is unique, up to multiplication of a column of U by a unit phase factor and simultaneous multiplication of the corresponding column of V by the same unit phase factor.

Degenerate singular values, by definition, have non-unique singular vectors. If u_1 and u_2 are two left-singular vectors which both correspond to the same singular value σ, then any normalized linear combination of the

two vectors is also a singular vector corresponding to the singular value σ. The similar statement is true for right-singular vectors. Consequently, if M has degenerate singular values, then its singular-value decomposition is not unique.

A.3 Pseudoinverse

Singular-value decomposition can be used to compute the pseudoinverse of a matrix. The pseudoinverse of the matrix M in A.1 is

$$M^{+} = V\Sigma^{+}U^{*} \tag{A.3}$$

where Σ^{+} is the pseudoinverse of Σ with every non-zero entry replaced by its reciprocal.

A.4 Total Least Squares Minimisation

A total least squares problem refers to determining the vector $\mathbf{x}$ which minimizes the 2-norm vector $\mathbf{Ax}$ under the constraint $\|\mathbf{x}\| = 1$. The solution turns out to be the right-singular vector of $\mathbf{A}$ corresponding to the smallest singular value.

A.5 Calculation of the SVD

It can be shown that U and V from equation (A.1) are the matrices composed by the eigenvectors of MM' and $M'M$. That singular value decomposition of a matrix M, then, is a fairly straightforward procedure:

- Form the products MM' and $M'M$.
- Find their eigenvectors and eigenvalues.

However, there is always a gap between mathematical theory and computational practice. Arithmetic operations carried out on real numbers do not have (as one would desire) infinite precision. Therefore, the results can only approximate with limited precision the real computation. Procedures that are simple and elegant can suffer dramatic flaws when described in a computational algorithm and the SVD is no exception to this rule. It turns

out that the computation of the product $M'M$ can be subject to serious loss of precision. Direct methods exist though, for calculating the SVD of M without having to resort to the formation of $M'M$.

The SVD of M is usually computed in two-steps. Firstly, M is reduced to a bidiagonal matrix using Householder transformations; then the computation of the SVD of the bidiagonal matrix is performed with iterative methods involving eigenvalue algorithms. In the case that $m \gg n$, then it is useful to first reduce M to a triangular matrix using QR decomposition and then use the Householder transformations to further reduce M into a bidiagonal form.

The calculation of the SVD in the second step was first described by Golub and Kahan [22] and its variant, described by Golub and Reinsch [23] is that most used today.

Appendix B

Accelerator Physics Codes

A multitude of accelerator physics codes is currently in use, with varying "popularity" and scope of purpose. Some of these codes can model a number of different phenomena related to beam dynamics in an accelerator system, while others are more specific. Here we give a brief description of the codes used for the simulations presented in this thesis: MAD, AT and Merlin.

B.1 Methodical Accelerator Design (MAD)

MAD is a widely used code, developed at CERN [58, 57]. It provides the tools for modeling charged-particle optics in alternating-gradient accelerators and beam lines and is often the software of choice for the initial design and configuration of new accelerator systems. Features include among others: linear lattice parameter calculation, linear lattice matching, transfer matrix matching, closed orbit correction and particle tracking.

The code is maintained and developed on a regular basis and extensive documentation and a manual are available. The syntax is fairly straightforward; a typical code sample defining ring and magnetic component parameters is the following:

```
! ILCDR FODO LATTICE "DCO4"

E0      := 5.0          ! nominal beam energy (GeV)

BLENGTH := 2.00         ! length of standard bending magnet
QLENGTH := 0.30         ! length of standard quadrupole
```

```
SLENGTH := 0.25          ! length of standard sextupole

ANGARCB := TWOPI/200     ! angle of arc
                         ! bending magnet (200 arc-fodo cells)

! Drift from quadrupole to beam position monitor

  LDBPM := 0.0
  DBPM:    DRIFT, L=LDBPM

! Beam position monitor

  BPMRNG:  MONITOR
  BPMDFT:          DRIFT, L=0

! Drift from orbit corrector to quadrupole

  LDCOR := 0.0
  DCOR:    DRIFT, L=LDCOR

! Orbit corrector

  LCOR  := 0.0
  CORRNG:  KICKER, L=LCOR, HKICK=0, VKICK=0
  DCORRNG: DRIFT, L=LCOR

! Skew quadrupole (coupling corrector)

  SKQRNG: QUADRUPOLE, L=0.2, K1=0.0, TILT

! Corrector, quad and BPM

  CQB(Q1): LINE=(CORRNG,DCOR,Q1,DBPM,BPMRNG)
```

Unfortunately, the data handling and post processing capabilities of MAD are not very flexible (because MAD has its own "command" language) and therefore the use of other software packages is often needed. At

the same time the code operates as a "black box", in the sense that the user does not have immediate and direct access to the subroutines (the physics) that perform the calculations (although the source code is available).

B.2 Accelerator Toolbox (AT)

The Accelerator Toolbox provides a collection of functions for modeling particle accelerators and beam transport lines [53]. The code was structured in a way that benefits from the functionality and simplicity of MATLAB [62]. The latter commercially available programming environment specializes in technical computing and visualization and therefore simplifies the data handling and analysis procedure.

Most of the AT is written in the MATLAB programming language. In order to avoid the speed drawback of interpreted programming languages (like MATLAB), computationally intensive routines have been written in C and compiled into MEX-files; binary code is therefore executable from within the MATLAB environment. The source code is available so that inspection and modifications (if necessary) can be made. An example using AT to find the orbit response matrix is the following :

```
%FINDRESPMDEMO response matrix demo
% This script illustrates the use of AT function FINDRESPM

spear2
% The most common RM is corrector-to-BPM
% In this demonstration we will not use the actual correctors
% to keep the lattice simple.

% We will use all focusing quadrupoles as correctors:
% In order to do this we need to use StrMPolesymplectic4 pass-method
% for them. This mehod looks at all terms of the polynomial
% expansion of transverse magnetic field.
% (QuadLinearPass only looks at field 'K')
% PolynomB(1) gives horizontal kick
% PolynomA(1) gives a vertical kick

% Find indexes of elements that belong to QF Q1 Q2 Q3 families
```

```
% We will use them as corrector elements
QFI = findcells(THERING,'FamName','QF');
Q1I = findcells(THERING,'FamName','Q1');
Q2I = findcells(THERING,'FamName','Q2');
Q3I = findcells(THERING,'FamName','Q3');
CORRINDEX = sort([ QFI Q1I Q2I Q3I]);
% Install the new pass-method 'StrMPoleSymplectic4Pass'
THERING = setcellstruct(THERING,'PassMethod',CORRINDEX,'StrMPoleSymplectic4Pass')

% We will use etrance points of all bending magnets as observation points (BPMs)
BPMINDEX = findcells(THERING,'BendingAngle');

NBPM = length(BPMINDEX);
NCOR = length(CORRINDEX);

% Prepare input parameters for FINDRESPM that will tell it, which
% parameters to use as orbit perturbations
% See help for FINDRESPM

% Set the size of a parameter change for numeric differentiation
KICKSIZE = 1e-5;

RX = findrespm(THERING,BPMINDEX ,CORRINDEX, KICKSIZE, 'PolynomB',1,1);
RY = findrespm(THERING,BPMINDEX ,CORRINDEX, KICKSIZE, 'PolynomA',1,1);
% Build the response matrix
% In the form
%
% | HH HV |
% | VH VV |
%
% HH - Horizontal BPM response to horizontal orbit kicks
% HV - Horizontal BPM response to vertical orbit kicks
% VH - vertical BPM response to horizontal orbit kicks
% VV - vertical BPM response to vertical orbit kicks
RespM_XY = [RX{1} RY{1}; RX{3} RY{3}];
figure(1);
```

```
mesh(RespM_XY);
colormap('copper');
xlabel('Corrector Number')
ylabel('BPM Number');
zlabel('Normalized Orbit Response');
title('Orbit Response Matrix - uncoupled lattice')

% Now we wish to introduce coupling:
QDI = findcells(THERING,'FamName','QD');
% Generate random rotations:
QDTILTS =   1*(pi/180)*randn(1,length(QDI));
% Put random values in the ring
settilt(QDI,QDTILTS);

% Generate the new response matrix for the lattice with errors
RX = findrespm(THERING,BPMINDEX ,CORRINDEX, KICKSIZE, 'PolynomB',1,1);
RY = findrespm(THERING,BPMINDEX ,CORRINDEX, KICKSIZE, 'PolynomA',1,1);

RespM_XY_Coupled = [RX{1} RY{1}; RX{3} RY{3}];
figure(2);
mesh(RespM_XY_Coupled);
colormap('copper');
title('Orbit Response Matrix - coupled lattice')
xlabel('Corrector Number')
ylabel('BPM Number');
zlabel('Normalized Orbit Response');
```

A lattice definition can be imported from a MAD lattice description file using an appropriate translation function. All plotting commands and other programming tasks, memory management and interactive graphics are built into MATLAB.

B.3 Merlin

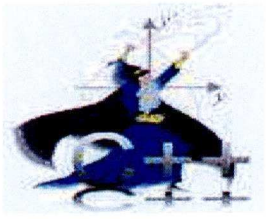

Merlin [61] is a C++ class library for performing charged particle accelerator simulations. Originally designed for simulations concerning linear collider beam dynamics, it has since been extended to include more traditional storage ring physics. The code greatly benefits from the object-oriented programming nature of C++.

An interface to a MAD optics listing is supported (class MADInterface), which reads a lattice file generated with the MAD OPTICS command. The following code example demonstrates the calculation of the closed orbit distortion, for a lattice with magnet alignment errors:

```
#include "NumericalUtils/PhysicalUnits.h"
#include "MADInterface/MADInterface.h"
#include "AcceleratorModel/Supports/MagnetMover.h"
#include "BeamDynamics/ParticleTracking/ParticleBunch.h"
#include "BeamDynamics/ParticleTracking/ParticleTracker.h"

#include "RingDynamics/ClosedOrbit.h"
#include "BPMVectorBuffer.h"

#define BEAMENERGY 5.0*GeV

typedef vector< MagnetMover* > MagnetMoverList;

using namespace PhysicalUnits;
using namespace ParticleTracking;
```

```
int main()
{
// Construct the AcceleratorModel
// from a lattice file produced by MAD
MADInterface madi("../lattices/MERLINFodo.lattice.txt", BEAMENERGY);

ofstream madlog("mad.log");
madi.SetLogFile(madlog);
madi.SetLoggingOn();

AcceleratorModel* theModel = madi.ConstructModel();

// Extract a list of magnet movers from the AcceleratorModel
// and translate the 20th mover 20 microns vertically
MagnetMoverList magnetMovers;
theModel->ExtractTypedElements(magnetMovers);
magnetMovers[20]->SetY(20.0e-6);


// Find the closed orbit in the ring.
ClosedOrbit theClosedOrbit(theModel,BEAMENERGY);
PSvector co(0);
theClosedOrbit.FindClosedOrbit(co);


// Construct a bunch of particles
// to track through the lattice.
// Here we just add a single particle on the closed orbit.
ParticleBunch* theBunch = new ParticleBunch(BEAMENERGY);
theBunch->AddParticle(co);


// Construct a ParticleTracker to perform the tracking
ParticleTracker tracker(theModel->GetBeamline(), theBunch);
```

```
// Construct a BPMBuffer to record the bunch centroid at each BPM
BPMVectorBuffer* bpmVecBuffer = new BPMVectorBuffer();
BPM::SetDefaultBuffer(bpmVecBuffer);

// Do the tracking
tracker.Run();


// Write the tracking results to a file
ofstream bpmLog("ClosedOrbit.dat");
vector<BPM::Data>& theBPMBuffer = bpmVecBuffer->BPMReading;
for(vector<BPM::Data>::iterator bpm_iter=theBPMBuffer.begin();
                    bpm_iter!=theBPMBuffer.end(); bpm_iter++)
 {
bpmLog<<std::setw(14)<<(bpm_iter->x).value;
bpmLog<<std::setw(14)<<(bpm_iter->x).error;
bpmLog<<std::setw(14)<<(bpm_iter->y).value;
bpmLog<<std::setw(14)<<(bpm_iter->y).error;
bpmLog<<endl;
 };

BPM::SetDefaultBuffer(0);
delete bpmVecBuffer;

delete theBunch;
delete theModel;

cout<<"Finished!"<<endl;

return 0;
}
```

Merlin has the very important advantage of flexibility regarding data generation and data handling, originating from generic C++ attributes. However, visualization and data (statistical) analysis routines are not built-in and can be cumbersome to code in C++. Furthermore, access to the source code of the provided classes allows direct inspection of the implemented

algorithms. Some documentation is available, however it is not complete.

Bibliography

[1] ICFA Beam Dynamics Newsletter #44, December 2007.

[2] A. Andersson, M. Böge, A. Lüdeke, V. Schlott, and A. Streun. Determination of a small vertical electron beam profile and emittance at the Swiss Light Source. *Nuclear Instruments and Methods in Physics Reasearch A*, (591):437–446, 2008.

[3] R. Assmann, P. Raimondi, G. Roy, and J. Wenninger. Emittance optimization with dispersion free steering at LEP. *Phys. Rev. ST Accel. Beams*, 3(12):121001, Dec 2000.

[4] R. Assmann, P. Raimondi, and J. Wenninger. A method for simultaneous optimisation of orbit and dispersion in storage rings. In *proceedings of EPAC*, Vienna, Austria, 2000.

[5] P.P. Bagley and D.L. Rubin. Correction of transverse coupling in a storage ring. In *proceedings of PAC*, pages 874–876, Chicago, IL, 1989.

[6] M. Bai, S. Peggs, T. Roser, T. Satogata, and D. Trbojevic. Measuring beta function and phase advance in RHIC with an AC dipole. In *proceedings of PAC*, pages 2204–2206, Portland, OR, 2003.

[7] M. Bai, F. Pilat, T. Satogata, R. Tomas, and F. Schmidt. Measurement of linear coupling resonance in RHIC. In *proceedings of PAC*, pages 2207–2209, Portland, OR, 2003.

[8] M.G. Billing, G. Dugan, R. Meller, M. Palmer, M. Rendina, N. Rider, J. Sikora, C. Strohman, and R.L. Holtzapple. Techniques for observation of beam dynamics in the presence of an electron cloud. In *proceedings of IPAC*, pages 1197–1199, Kyoto, Japan, 2010.

[9] H. Braun, J.P. Delahaye, A. De Roeck, and G. Geschonke. Clic here for the future. CERN Courier, September 2008.

[10] P.J. Bryant, P. Galbraith, J.P. Gourber, G. Guignard, and K. Takikawa. Measurement of the excitation of the coupling resonance $Q_h - Q_v = 0$. *Transactions on Nuclear Sceince*, 3(9):1440–1441, 1977.

[11] Yunhai Cai. Method of measuring the coupled lattice functions at the interaction point in $e + e-$ storage rings. *Phys. Rev. E*, 68(3):036501, Sep 2003.

[12] E. Cenni, M. Canetti, F. Gangini, L. Cassinari, J.-C. Denard, C. Herbeaux, and J.-L. Billaud. Construction and quality control of synchrotron soleil beam position monitors. In *proceedings of EPAC*, pages 487 – 489, Genoa, Italy, 2010.

[13] A.W. Chao. Evaluation of beam distribution parameters in an electron storage ring. *Journal of Applied Physics*, 50(2):595–598, 1979.

[14] A.W. Chao and M. Tigner, editors. *Handbook of Accelerator Physics and Engineering.* World Scientific, 1999.

[15] Y. Chung and E. Cahaha. Performance of the beam position monitor for the advanced photon source. In *proceedings of Conference on synchrotron radiation instrumentation*, Madison, Wisconsin, 1996.

[16] J.A. Clarke. *The Science and Technology of Undulators and Wigglers.* Oxford University Press, 2004.

[17] E.D. Courant and H.S. Snyder. Theory of the alternating-gradient synchrotron. *Annals of Physics*, 3(1-48), 1958.

[18] D.A. Edwards and L.C. Teng. Parametrization of linear coupled motion in periodic systems. *IEEE Trans. Nucl. Sci.*, 20:885–888, 1973.

[19] W. Fischer. Robust linear coupling correction with n-turn maps. *Phys. Rev. ST Accel. Beams*, 6(6):062801, Jun 2003.

[20] S. Gilbert. Bringing the SVD to life. *SIAM News*, 39(1), 2006.

[21] H. Goldstein, C. P. Poole, and J. L. Safko. *Classical Mechanics.* Addison Wesley, 3^{rd} edition, 2001.

[22] G. Golub and W. Kahan. Calculating the singular values and pseudo-inverse of a matrix. *SIAM Journal on Numerical Analysis*, 2(2):205–224, 1965.

[23] G.H. Golub and C. Reinsch. Singular value decomposition and least square solutions. *Numerische Mathematik*, 14:403–420, 1970.

[24] S. Guiducci. Damping rings towards ultra-low emittances. In *proceedings of EPAC*, Edinburgh, Scotland, 2006.

[25] M. Korostelev. RDR lattice update. `http://ilcagenda.linearcollider.org/contributionDisplay.py?contribId=105&sessionId=27&confId=3461`, August 2009. Linear Collider Workshop of the Americas, Albuquerque, New Mexico.

[26] M. Korostelev and A. Wolski. DCO4 lattice design for 6.4 km ILC damping rings. In *proceedings of IPAC*, pages 3575–3577, Kyoto, Japan, 2010.

[27] K. Kubo, C. Adolphsen, K.L.F. Bane, T.O. Raubenheimer, and K.A. Thompson. Alignment tolerance of accelerating structures and corrections for future linear colliders. In *proceedings of EPAC*, Barcelona, Spain, 1996.

[28] K. Kubo, M. Akemoto, S. Anderson, T. Aoki, S. Araki, K. L. F. Bane, P. Blum, J. Corlett, K. Dobashi, P. Emma, J. Frisch, M. Fukuda, Z. Guo, K. Hasegawa, H. Hayano, T. Higo, A. Higurashi, Y. Honda, T. Iimura, T. Imai, K. Jobe, S. Kamada, P. Karataev, S. Kashiwagi, E. Kim, T. Kobuki, T. Kotseroglou, Y. Kurihara, M. Kuriki, R. Kuroda, S. Kuroda, T. Lee, X. Luo, D. J. Mccormick, B. Mckee, T. Mimashi, M. Minty, T. Muto, Takashi Naito, G. Naumenko, J. Nelson, M. N. Nguyen, K Oide, T. Okugi, T. Omori, T. Oshima, G Pei, A Potylitsyn, Q. Qin, T. Raubenheimer, M. Ross, H. Sakai, I. Sakai, F. Schmidt, T. Slaton, H. Smith, S. Smith, T. Smith, Toshikazu Suzuki, M. Takano, Seishi Takeda, N. Terunuma, N. Toge, J. Turner, J. Urakawa, V. Vogel, M. Woodley, J. Yocky, A. Young, and F. Zimmermann. Extremely Low Vertical-Emittance Beam in the Accelerator Test Facility at KEK. *Physical Review Letters*, 88(19):4–7, 2002.

[29] Kiyoshi Kubo. Simulation study of low emittance tuning of the Accelerator Test Facility damping ring at KEK. *Phys. Rev. ST Accel. Beams*, 6(9):092801, Sep 2003.

[30] S.Y. Lee. *Accelerator Physics.* World Scientific, 2^{nd} edition, 2004.

[31] Y. Luo, M. Bai, F. Pilat, T. Satogata, and D. Trbojevic. Measurement of ir optics with linear coupling's action-angle parametrization. *Phys. Rev. ST Accel. Beams*, 8(8):084001, Aug 2005.

[32] Y. Luo, P. Cameron, A. Della Penna, J. Laster, R. Lee, A. Marusic, F. Pilat, T. Roser, D. Trbojevic, and J. Wei. Measurement of global betatron coupling with skew quadrupole modulation. *Phys. Rev. ST Accel. Beams*, 8(1):014001, Jan 2005.

[33] K. Ohmi, K. Hirata, and K. Oide. From the beam-envelope matrix to synchrotron-radiation integrals. *Phys. Rev. E*, 49(1):751–765, Jan 1994.

[34] Y. Ohnishi, K. Ohmi, H. Koiso, M. Masuzawa, A. Morita, K. Mori, K. Oide, Y. Seimiya, and D. Zhou. Measurement of chromatic $x - y$ coupling. *Phys. Rev. ST Accel. Beams*, 12(9):091002, Sep 2009.

[35] T. Okugi et al. Evaluation of extremely low emittance. *Phys. Rev. ST Accel. Beams*, 2(9):022801, Feb 1999.

[36] M.A. Palmer, M.G. Billing, R.E. Meller, M.C. Rendina, N.T. Rider, D.L. Rubin, J. Shanks, C.R. Strohman, and R.L. Holtzapple. Cesr beam position monitor system upgrade for cesrta and chess operations. In *proceedings of IPAC*, pages 1191–1193, Kyoto, Japan, 2010.

[37] K. Panagiotidis and A. Wolski. Alignment sensitivities in the ILC damping rings. In *proceedings of PAC*, Albuquerque, New Mexico, 2007.

[38] K. Panagiotidis and A. Wolski. Coupling correction for the ILC damping rings. In *proceedings of EPAC*, Genoa, Italy, 2008.

[39] K. Panagiotidis and A. Wolski. Possible limitations in coupling correction using Orbit Response Matrix analysis. In *proceedings of PAC*, pages 2 – 4, Vancouver, Canada, 2009.

[40] K. Panagiotidis, A. Wolski, and M. Korostelev. Low-Emittance Tuning simulations for the ILC damping rings. In *proceedings of IPAC*, pages 1 – 3, Kyoto, Japan, 2010.

[41] D. P. Peterson, J.P. Alexander, C. Conolly, N. Eggert, E. Fontes, W. Hopkins, B. Kries, A. Lyndaker, M. McDonald, M. Palmer, M. Rendina, P. Revesz, N. Rider, J. Savino, R. Seeley, and J.W. Flanagan. Cesrta x-ray beam size monitor operation. In *proceedings of IPAC*, pages 1194–1196, Kyoto, Japan, 2010.

[42] F. Pilat, J. Beebe-Wang, W. Fischer, V. Ptitsyn, and T. Satogata. Coupling Measurement and correction at RHIC. In *proceedings of EPAC*, pages 1178–1180, Paris, France, 2002.

[43] Tor O. Raubenheimer. *The generation and acceleration of low emittance flat beams for future linear colliders.* Slac- 387, Stanford, 1992.

[44] J.R. Rees. Symplecticity in beam dynamics: An introduction. SLAC-PUB-9939, June 2003.

[45] D. Robin, J. Safranek, G. Portmann, and H. Nishimura. Model calibration and symmetry restoration of the Advanced Light Source. In *proceedings of EPAC*, Barcelona, Spain, 1996.

[46] J. Safranek. Experimental determination of storage ring optics using orbit response measurements. *Nuclear Instruments and Methods in Physics Research A*, 388(3):27–36, 1996.

[47] D. Sagan, R. Meller, R. Littauer, and D. Rubin. Betatron phase and coupling measurements at the Cornell Electron/Positron Storage Ring. *Phys. Rev. ST Accel. Beams*, 3(9):092801, Sep 2000.

[48] D. Sagan and D. Rubin. Linear analysis of coupled lattices. *Phys. Rev. ST Accel. Beams*, 2(7):074001, Jul 1999.

[49] M.J Spencer, M.J. Boland, R.T. Dowd, G. LeBlanc, and Y.E. Tan. Loco at the australian sunchrotron. In *proceedings of PAC*, pages 3217–3219, Albuquerque, New Mexico, USA, 2007.

[50] C. Steier et al. Coupling correction and beam dynamics at ultra-low vertical emittance in the ALS. In *proceedings of PAC*, Portland, Oregon, 2003.

[51] G. Strang. *Linear Algebra and its Applications.* Academic Press, 2^{nd} edition, 1980.

[52] A. Terebilo. Accelerator modeling with Matlab accelerator toolbox. In *proceedings of PAC*, Chicago, IL, 1999.

[53] A. Terebilo. Accelerator toolbox for Matlab. SLAC-PUB-8732, February 2001.

[54] J.J. Thomson. Cathode rays. *Philosophical Magazine*, 44(293), 1897.

[55] M. Tigner. A possible apparatus for electron clashing-beam experiments. *Il Nuovo Cimento*, 37(3):1228–1231, 1965.

[56] `http://clic-study.web.cern.ch/CLIC-Study/intro.html`.

[57] `http://mad.home.cern.ch/mad`.

[58] `http://mad.home.cern.ch/mad/mad8web/mad8.html`.

[59] `http://ssrl.slac.stanford.edu/at`.

[60] `http://www-atf.kek.jp/atf/introduction/html`.

[61] `http://www.desy.de/~merlin`.

[62] `http://www.mathworks.com`.

[63] `http://www.uwlax.edu/faculty/will/svd/index.html`.

[64] N. Walker, A. Wolski, A. Seryi, and P. Tenenbaum. Physics and Technology of Linear Collider Facilities. USPAS, University of California, Santa Barbara, http::/www.desy.de/ñjwalker/uspas/, June 2003.

[65] H. Wiedemann. *Particle Accelerator Physics.* Springer, 3^{rd} edition, 2007.

[66] A. Wolski. Damping ring design and physics issues. Fourth International Accelerator School for Linear Colliders, Beijing, September 2009.

[67] A. Wolski, J. Gao, and S. Guiducci, editors. *Configuration Studies and Recomendations for the ILC Damping Rings.* LBNL-79449, 2006.

[68] A. Wolski, J. Nelson, M. Ross, M. Woodley, and M. Mishra. Analysis of KEK-ATF optics and coupling using orbit response matrix analysis. Technical Report 12156, SLAC-PUB, 2004.

[69] A. Wolski and K. Panagiotidis. Turn-By-Turn trajectory data in storage rings. In *proceedings of IPAC*, Kyoto, Japan, 2010.

[70] Andrzej Wolski. Alternative approach to general coupled linear optics. *Phys. Rev. ST Accel. Beams*, 9(2):024001, Feb 2006.

[71] A. Xiao and L. Emery. Characterization of a 6 km damping ring for the International Linear Collider. In *proceedings of PAC*, Knoxville, TN, 2005.

[72] A. Xiao and L. Emery. International Linear Collider damping ring lattice design. In *proceedings of PAC*, Albuquerque, New Mexico, 2007.

[73] K. Yokoga. Test facilities. Presentation at ILC PAC review, Korea, 2009.